IMPLICATIONS OF FOREST PRACTICES ON DOWNSTREAM FLOODING

Phase II Final Report

By

Pascal Storck
Dennis P. Lettenmaier
Brian A. Connelly
Terrance W. Cundy

TIMBER FISH &WILDLIFE

July 1, 1995

IMPLICATIONS OF FOREST PRACTICES ON DOWNSTREAM FLOODING

PHASE II FINAL REPORT

by

Pascal Storck [a]
Dennis P. Lettenmaier [a]
Brian A. Connelly[b]
Terrance W. Cundy [c]

to

Washington Forest Protection Association
King County Surface Water Management Division
Weyerhauser Co.
U.S. Forest Service
National Council of the Paper Industry for Air and Stream Improvement

University of Washington

July 1, 1995

[a] Department of Civil Engineering, Box 352700, University of Washington, Seattle, WA 98195
[b] College of Forest Resources, Box 352100, University of Washington, Seattle, WA 98195
(now at U.S. National Weather Service, North Central River Forecast Center, Minneapolis, MN)
[c] College of Forest Resources, Box 352100, University of Washington, Seattle, WA 98195
(now at Potlatch Corp., Lewiston, ID)

Abstract

Field studies have shown that substantial changes in snowmelt during rain-on-snow events can occur due to removal of forest cover. These changes are attributable to differences in snow accumulation as a result of canopy interception changes, and to differences in latent and sensible heat associated with increased wind at the snow surface when vegetation is removed. However, the field studies are of necessity point observations; at the watershed scale, the effects of vegetation changes on any particular flood are complicated by variations in antecedent snow accumulation, spatial differences in temperature and precipitation during the storm, and the area-elevation distribution of the watershed.

At the watershed scale, physically realistic computer simulation models offer the best hope for understanding the effects of forest harvesting on hydrologic response, and on flood peaks in particular. The Distributed Hydrology-Soils-Vegetation Model (DHSVM) was modified for the purposes of evaluating the effects of forest harvesting on flooding. Changes and enhancements to the model include: a) incorporation of a module to estimate topographic effects on precipitation, b) modification of the original single layer snow model to incorporate a thin surface layer, c) inclusion of a channel routing scheme, and d) certain changes to the representation of vegetation effects on aerodynamic resistance under the forest canopy.

Following testing of the modified version of DHSVM, it was applied to produce a 46 year simulation (1948-93) of the: Snoqualmie River at Carnation, with vegetation fixed at 1989 conditions. The residuals (difference between simulated and observed peak flows) were analyzed for trends. Because the residuals series is effectively adjusted for climatic variations that might have been associated with the specific storms associated with the floods, any trends should be the result of vegetation changes.

Based on the residuals analysis, the major conclusions of this study are:

1) No significant trend has occurred during the period of analysis in the annual maximum flood series, while the smaller floods in the peaks over threshold series (less than 650 cms) showed statistically significant increases;

2) The amount of forest harvesting that has actually occurred in the Snoqualmie River watershed is not enough to explain the observed trend in the smaller floods in the peaks-over-

threshold series;

3) Land use effects not represented by DHSVM, such as forest roads, may have a greater effect than ROS physics, which are represented by the model;

4) The largest changes in peak streamflows were found to occur from spring peak flows, most of which are significantly smaller than bankfull capacity. While this result is not of practical significance in terms of flood changes in the Snoqualmie basin, it may have important implications for changes in flood peaks resulting from forest harvesting in eastside catchments, where spring snowmelt peaks dominate the flood series;

5) Observed changes in the smaller floods of the peaks-over-threshold series are much larger than those predicted given the magnitude of historical land use changes. This result suggests that some mechanism other than changes in ROS runoff is the cause.

A sensitivity analysis was conducted of changes in selected events in the peaks-over-threshold series that would have occurred for three alternative harvest strategies, with harvested areas distributed spatially based on visual impact considerations. The three strategies resulted in 10 percent of the basin being cut at elevations below 300 m, between 300 and 900 m, and above 900 m, respectively. The peaks-over- threshold for the period 1948-55 with the alternative strategies, and for prescribed complete forest cover, were compared using DHSVM. Increases in the peaks-over-threshold were predicted to be small, averaging under 2 percent (maximum 10 percent) for harvest below 300 m, about 2 percent (maximum 5 percent) for harvest between 300-900 m. Even smaller changes were predicted when the harvest was concentrated above 900 m.

Table of Contents

List of Figures

List of Tables

Chapter 1. Introduction

1.1 Background

Most major floods in western Washington occur in late fall and early winter as the result of intense warm rainfall, accompanied by melting of at least part of the accumulated snowpack. A recent example of such an event was the flood of late November 1990, when the arrival of a Pacific warm front followed an extended period of cool, wet weather. The freezing level in the Cascade and Olympic Mountains rapidly rose from about 500 to over 2500 meters. This change was accompanied by as much as fifteen inches of rain in a 48 hour period. As a result, a significant portion of the accumulated snowpack below 2500 meters melted. The combination of the heavy rain and an additional 75 mm of snowmelt (expressed as a water equivalent) resulted in extensive flooding in many western Washington rivers. Many of the major rivers which drain the west central Cascades experienced flood peaks with recurrence intervals exceeding 100 years. The estimated flood damage in King County alone exceeded $20 million. A similar event occurred at about the same time of year in 1986, and also caused major flooding and extensive damage in Western Washington. During late December 1994, record flows occurred in streams draining the southern Olympic Range, especially the Skokomish River. Extensive flooding in January 1995 in western Oregon and Northern California was also caused in part by rain-on-snow events.

The severity and frequency of these recent floods has focused attention on logging practices as a possible cause. The effects of timber harvesting on streamflow have been well documented (e.g., Harr, 1986). In fact, the U.S. Forest Service has advocated clearcutting of coniferous forests to increase water yields in Colorado and Arizona (Brown, 1969; Hoover, 1967). More recently, some researchers have focused on differences in snow pack dynamics between forested and open sites as a major contributor to increased runoff during rain-on-snow events (Berris and Harr, 1987; Berg, et al., 1991; Kattelmann, 1987). These studies all found that snow accumulation, snow melt, and runoff are significantly greater in clear cut areas than in adjacent forested areas.

It is worthwhile to examine briefly one of the best known of these studies to gain insight into the magnitude of the differences between clear-cut and forested areas and the mechanisms which cause them. Berris and Harr (1987) investigated snow dynamics during rain-on-snow (ROS) events for two similar plots in the transient snow zone (900 m elevation) of the western

Cascade range in Oregon. One of the plots was clear-cut in 198 1 and the other contained old growth forest. Observations showed that the snowpack water equivalent of the clear-cut plot averaged about twice that of the forest plot over the two year study period. The difference was attributed to interception of snow by the forest canopy and differences in energy fluxes at the snow surface. Snow held in the canopy has a greater surface area per unit volume exposed to surface energy transfer than does snow on the ground. Moreover, due to higher wind speed, the latent and sensible heat transfer is greater in the canopy than on the ground. These two factors combine to increase the melt rate of snow in the canopy, which limits the snowpack accumulation under the trees. Also, during ROS events, the forest canopy partially shelters the snowpack under the forest (due to reduced wind) from the large latent and sensible heat fluxes that contribute to melt in open areas. Although these effects are somewhat counteracted by reduced net solar radiation under trees relative to clearings, which tends to reduce the accumulation of snow in clearings relative to forested areas, this effect is most important during the melt season under clear and nearly clear sky conditions, which are uncommon in the Pacific Northwest during the period when most ROS events occur. The consensus of the various studies that have compared melt processes in clearings and forested areas is that removal of the forest canopy can increase snow accumulation and snow melt, especially during ROS events.

1.2 Study History

Although the evidence from the small plot studies indicates the potential for cause-effect relationships between logging and changes in the hydrologic response of forested watersheds, little is known about the importance of these effects at the watershed scale, especially for watersheds with large ranges in elevation. Given that a number of studies suggest that clearcutting increases runoff generation on small plots, the next logical step is to determine whether or not these local increases translate to increased peak discharge at the watershed scale (e.g., hundreds to thousands of km'). Phase 1 of this project (Connelly, et al., 1993) presented preliminary results of an investigation of ROS events at the watershed scale. The main contributions and results from Phase 1 are briefly summarized here.

Initially, a statistical analysis of the annual peak discharge records of nine Western Washington watersheds with lengthy (continuous records (1932 to 1989) was conducted to determine whether there was evidence of long term trends. Two of the nine catchments (the North **Fork** Stil-

laguamish and the Satsop River)' showed upward trends in peak discharge over time at the 0.05 significance level. More sophisticated tests were then applied to these two catchments, for which the magnitude and location of forest harvesting over the past 50 years was well documented, to isolate the effect of land-use changes from climate variability. The results showed that, after accounting for climate variability, only the North Fork Stillaguamish River showed an increase in annual peak discharge. The basin of particular interest to this study, the Snoqualmie, showed no significant trend in either the climate-adjusted or the unadjusted annual peak discharge series. The paradox in these results is that the Snoqualmie River basin has undergone more harvesting in the transient snow zone during the period of analysis than the North Fork Stillaguamish.

These results contrast with those reported by Jones and Grant (1996). In their work, paired comparisons of peaks-over-threshold series for five watershed pairings (two small catchment pairs in the H.J. Andrews Experimental Watershed and three much larger western Oregon watersheds pairs) were performed. They showed that on a storm-by-storm basis, the flood peaks in those catchments and watersheds with the greatest harvesting had increased relative to those in the unharvested. (or less harvested) ones. Although these results seem to be in contradiction to those we obtained for western Washington rivers, one possible explanation is that Jones and Grant used a threshold that resulted in inclusion of an average of three to four floods per year in their analysis, whereas ours used the annual flood series (largest flood each year). Therefore, their analysis was dominated by smaller floods than ours and suggests that the effects of vegetation changes are most pronounced on smaller floods.

To provide more insight into the mechanisms related to forest harvesting that affect flood response, a physically based modeling approach was used to model explicitly the effects of soils, vegetation, terrain, and snow physics on runoff production. The Distributed Hydrology-Soils-Vegetation Model (DHSVM) of Wigmosta et al. (I 994) was adapted for this purpose. DHSVM was originally developed and applied to the Middle Fork Flathead River watershed, Montana; preliminary testing of the model on the Snoqualmie River watershed indicated several aspects of the model and/or assumptions that required modification to produce satisfactory simulations. These included a) incorporation of a module to estimate topographic effects on precipitation, b) modification of the original single layer snow model to incorporate a thin surface layer, c) inclusion of a channel routing scheme, and d) certain changes to the representation of vegetation effects on aerodynamic resistance under the forest canopy. In Phase I (Connelly et al., 1993), a

point version of DHSVM was used to model snow accumulation and melt at a single point (specifically, for simulation of the data reported by Berris, 1984). The model results were compared to observations in both a clearing and a forested location. The predicted snowpack outflow agreed reasonably well with observations, especially for the clearing. The uncalibrated model was then applied to the entire Snoqualmie watershed (drainage area 1559 km^2) using a pixel size of 100 m, and the hydrograph of the Snoqualmie River at Carnation was simulated during the ROS event of December 2-6, 1982. This application showed that the spatial patterns of snow accumulation, melt, and runoff generation, were plausible. However, this initial simulation overpredicted the observed peak streamflow, the predicted peak occurred sooner than observed, and the recession limb of the hydrograph decayed to base levels too rapidly.

This report describes the extension, testing, and calibration of DHSVM for the Snoqualmie River watershed. Attention is focused on a) those changes that have been made to DHSVM for application to the Snoqualmie River; b) the performance of the model during selected calibration events; c) analysis of residuals from a 46 year simulation (1948-1993) of observed peak flows; and d) an assessment of the sensitivity of Snoqualmie River floods to alternative harvest patterns.

1.3 Objectives

The objectives of the work reported herein are:

1) To calibrate and validate the extended version of DHSVM against selected major Snoqualmie River flood events and determine the model's parameter sensitivity;

2. To conduct a retrospective analysis of the annual flood peak series by simulation of the entire period of record (1948-93) and to test the residuals of the model predictions and observed flood peaks for trends;

3. Use DHSVM to predict the effects of alternative forest harvesting strategies on peak streamflow events.

1.4 Report Organization

Chapter 3 briefly describes the base version of DHSVM as originally developed by Wigmosta et al. (1994), and discusses the extensions made to DHSVM and the testing of those extensions as applied to the Snoqualmie watershed. Chapter 4 summarizes the data required by DHSVM and the sources of these data for the Snoqualmie basin study. Chapter 5 describes the calibration of the extended DHSVM for the Snoqualmie basin. Chapter 6 presents the results of the retrospective analysis of flood peaks during the period from 1948 to 1993. Chapter 7 describes the effect of various harvest strategies on peak streamflows. Chapter 8 summarizes the main conclusions of this report.

Chapter 2. The Role of DHSVM in Watershed Analysis

Prior to about 1950, the focus of forest land management was on timber yield, with minimal concern for the ancillary effects on a watershed's physical and biological characteristics. This emphasis has changed over the last decades, with restrictions on logging due to Endangered Species Act (ESA) listings of species such as the spotted owl, marbled murelet, and certain salmonid fish. Nonetheless, the residual effects of past forest practices are now evident in degraded quality of many forested watersheds in the Pacific Northwest (FEMAT, 1993).

One outgrowth of concerns over watershed degradation has been the concept of watershed analysis. Watershed analysis is (essentially a systems analysis approach for extracting timber while preserving, to a certain extent, the watersheds ecosystem functions and protecting local communities from hazards such as flooding that may be exacerbated by land management. Figure 2.1 (adapted from Montgomery et al., 1995) shows how the regional and watershed scale aspects of watershed analysis interact. At the regional scale, management objectives and constraints are identified. The regional scale might be defined as a state or part thereof (e.g., western Washington) or a larger geographic region (e.g., the Columbia river basin). At the smaller, watershed scale (typically tens to hundreds of km^2), these objectives and constraints are addressed within the context of the watershed analysis paradigm, which identifies the interaction between key physical and biological processes and the effects of land management.

A relatively straightforward example serves to illustrate these points. Forest harvesting in upland watersheds has removed the source of much of the large woody debris that historically has played a major role in determining the hydraulic characteristics of Northwest streams and rivers, Once the old debris is washed out of the channel or removed by channel cleaning operations, the channel can convey more water before flooding. While this effect can have a short-term, local benefit to landowners adjacent to the channel, it can have disastrous consequences for fish habitat. If the supply of sediment to the channel is not altered, the channel will incise into its bed and remove the gravel used by many species of fish as spawning beds and habitat. In addition, the conveyance capacity of downstream channels may be constricted due to enhancement of bedload.

Even for this simple example, the best course of action is not immediately obvious, since

forest managers, residential and recreational homeowners, and fisheries managers all have different objectives, different metrics of watershed quality, and different 'optimal' plans of action. In a sense, one person's objective function is another's constraint. For instance, the forest manager might tend to optimize timber yield, subject to environmental constraints (such as sediment yield, and/or surrogates such as buffer strip location and size). On the other hand, the fisheries manager would tend to view any negative impacts of logging on stream habitat as undesirable. while residential property owners would focus more on the aesthetic impacts of logging. A further complicating factor is that population growth will bring increasing pressure for floodplain development,

Figure 2.1. Watershed Management Paradigm: A. schematic illustrating the context for watershed analysis. (After Montgomery et al., 1995)

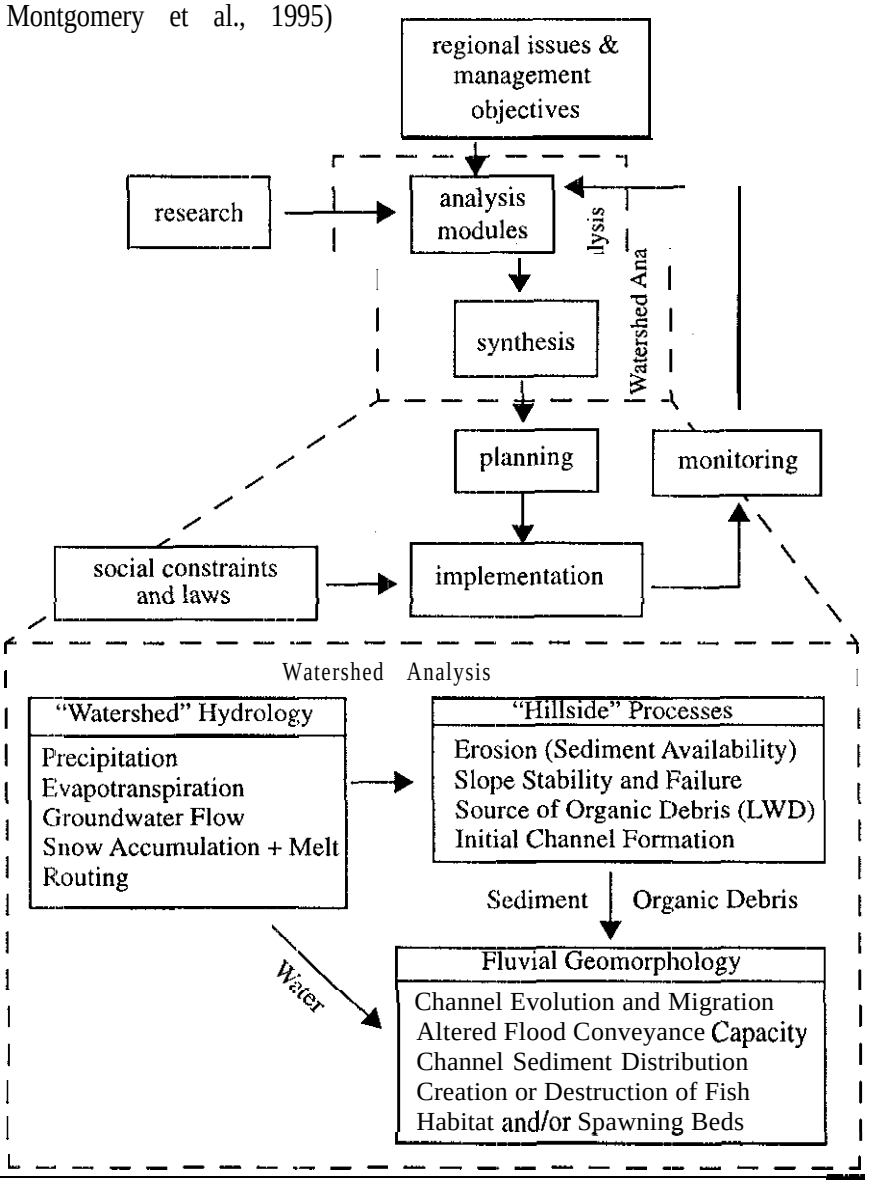

thus increasing the potential for downstream flood damage. None of these concerns can be ignored, but each suggests alternate courses of action.

To be effective, watershed analysis must first clearly define its objectives, and then strike a balance among the competing requirements of resource extraction and watershed health and viability. Striking this balance, at least in terms of the effects of forest harvesting on flooding, and other hydrologic issues such as watershed yield, can be greatly enhanced by predictive models that allow the assessment of the likely hydrologic consequences of timber harvesting. DHSVM has been designed specifically to address such issues.

As envisioned by the Washington Forest Practice Board (WFPB, 1993; see also Montgomery et al., 1995), watershed analysis is intended to develop an understanding of the effects of land management actions on watersheds with typical sizes of several hundred square kilometers. Watershed resource assessments include:

Mass Wasting
Surface Erosion
Hydrology
Riparian Vegetation
Stream Channels
Fish Habitat
Water Supply/Public Works

Based on these assessments, prescriptions are developed to mitigate impacts from forest management activities.

It is well accepted that the hydrologic function of a watershed is one of the key aspects affecting all the other resources listed above. Therefore, it is imperative that the hydrologic assessment be capable of diagnosing past interactions with other resources. Furthermore, it must also be able to predict and evaluate the consequences of future management alternatives.

DHSVM meets the criteria above. In several important respects, DHSVM is an improvement over the current hydrology assessment procedure. First, it is capable of portraying hydrologic processes continuously in space and time. This allows the evaluation of management impacts at any spatial scale within the watershed, ranging from stand scale to small watershed to

the entire basin. Second, and most importantly, the model is general so it can portray hydrologic processes occurring over their full range.

Of special concern in the: Pacific Northwest is snowmelt. DHSVM is capable of simulating snow accumulation and melt over hourly, daily and seasonal times scales. Therefore, it can be applied where rain-on-snow is the principal concern, and it is equally applicable where springtime, seasonal snowmelt is dominant.

In relation to mass wasting, DHSVM evaluates and portrays soil saturation in both space and time and incorporates the effects of vegetation manipulation on soil saturation. Therefore, it directly integrates topography, soils, vegetation and hydrology for the evaluation of mass wasting.

A final feature of DHSVM that is relevant to other aspects of the watershed analysis is that hydrographs can be estimated at any point in the channel system. ‘This flow information is relevant to stream channel and fish habitat assessments.

Chapter 3. The Distributed Soil-Hydrology-Vegetation Model

3.1 Model Description

The original form of DHSVM is described in detail in Wigmosta et al. (1994), who applied it to the Middle Fork Flathead River, Montana at a daily time step for a two-year period. The validation of this initial model application focused on reproduction of the seasonal hydrograph (which, in the Middle Fork Flathead, is dominated by spring snowmelt runoff) and the simulation of snow area1 extent during the spring melt period. Simulation of ROS floods is a somewhat more demanding application and required a number of enhancements to the model, as described later in this chapter. First, the original form of the model applied by Wigmosta et al. to the Middle Fork Flathead is described briefly, as it is the starting point for the subsequent changes and enhancements made to the model for application to the Snoqualmie River. For more details, the reader is referred to Wigmosta et al. (1994).

DHSVM provides a dynamic (one day or shorter time step) representation of the spatial distribution of soil moisture, evapotranspiration, and runoff production. It consists of a two-layer canopy representation for evapotranspiration, a single layer energy-balance model for snow accumulation and melt, a two-layer unsaturated soil model, and a saturated subsurface flow model. Model inputs are near-surface meteorology (precipitation, temperature, wind, humidity) and incoming short- and longwave radiation. Digital elevation data are used to model topographic controls on incoming shortwave radiation, precipitation, air temperature, and downslope water movement. Surface land cover and soil properties are assigned to each digital elevation model (DEM) grid cell. The DEM resolution is arbitrary, but usually is on the order of 90 m.

In each grid cell, the modeled land surface may be composed of overstory vegetation, understory vegetation, and soil. The overstory may cover all or a prescribed fraction of the land surface. The understory, if present, covers the entire ground surface. The model allows land surface representations ranging from a closed two-story forest, to sparse low-lying natural vegetation or crops, to bare soil. Although the model can run at any fixed time step; most testing to date has used either a daily or three-hour time step. As part of this work, we modified DHSVM to run with a variable time step so that evolving processes, such as the summer drydown, can be simulated at a daily time step, while faster processes, such as floods, can be simulated at a shorter, e.g. hourly, time step. Meteorological conditions (precipitation, air temperature, solar radiation, wind speed, vapor pressure) are prescribed at a specified distance above the overstory.

The overstory is allowed to remove water from both the upper and lower soil zones, while the understory can remove water only from the upper zone. Solar radiation and wind speed are attenuated through the two canopies, providing different values for the overstory, understory, and soil. Stomata1 resistance is calculated for each story based on air temperature, the vapor pressure deficit, soil moisture conditions, and the photosynthetically active radiation flux. Soil water evaporation is dependent on the climatic demand modulated by the soil's ability to supply water.

Snow accumulation and melt are simulated using a single-layer energy-balance model that explicitly incorporates the effects of topography and vegetation cover on energy exchange at the snow surface. Unsaturated moisture movement through the two soil layers is calculated using Darcy's law. This downward moisture flux recharges the grid cell water table. Each grid cell exchanges saturated zone water with adjacent neighbors as a function of water table depth and local topography, resulting in a transient, three-dimensional representation of saturated subsurface flow. Return flow and saturation overland flow are generated in locations where grid cell water tables intersect the ground surface.

Evaporation of intercepted water from the surfaces of wet vegetation is assumed to occur at the potential rate, which is determined in part by calculating the aerodynamic resistance while assuming no canopy resistance. Transpiration from dry vegetative surfaces is calculated using a Penman-Monteith approach. The model calculates evaporation and transpiration independently for each story in a stepwise fashion. First, intercepted water is evaporated at the potential rate. Transpiration from dry vegetation is then calculated in a manner that allows the vegetation surface to go from wet to dry during a time step (i.e., evaporation followed by transpiration). The model uses a soil physics-based approach to calculate soil evaporation (Entekhabi and Eagleson, 1989).

Separate shortwave and llongwave radiation budgets are developed for the overstory, understory, and ground surface. The amount of shortwave radiation captured by the overstory is dependent on its leaf area index, fractional ground cover, reflectance coefficient, and transparency to shortwave radiation. Back-reflection from the understory is also considered. Separate budgets pertain when snow cover is present.

The model uses a physics-based representation of snow accumulation and melt, similar to that described by Anderson (1968). During melting conditions the snowpack is assumed isothermal at $0^{o}C$. The model accounts, for the energy advected by rain, as well as net radiation, sensible and latent heat. Precipitation occurring below a threshold temperature is assumed to be snow, and

its moisture content adds to the water equivalent of the pack. The model accounts for the cold content of the snowpack, which must be satisfied before melt can occur.

Dynamics of unsaturated moisture movement are simulated using a two-layer model. The thickness of the upper zone is equal to the average rooting depth of the understory vegetation. The lower zone: extends to the average overstory rooting depth. The understory can extract water only from the upper zone, while the overstory can remove water from both zones. The fraction of overstory roots in the upper zone is specified, which, along with soil moisture, determines the relative amount of transpiration from the two zones. Soil evaporation is restricted to the upper zone.

The mode1 accounts explicitly for subsurface redistribution of moisture. Each DEM grid cell exchanges saturated subsurface flow with its eight adjacent neighbors. Assuming the local hydraulic gradient is equal to the local ground surface, a given cell will receive water from upslope neighbors and discharge to adjacent downslope cells. A topographic peak will discharge to all eight neighbors, while a depression receives subsurface flow from all of its neighbors.

3.2 DHSVM Extensions

DHSVM was specifically developed for use in mountainous areas. However, some portions of DHSVM as applied by Wigmosta et al (1994) to the middle fork Flathead River do not realistically mode1 hydrologic processes in maritime mountainous watersheds, such as the Snoqualmie River. The original version of DHSVM: (1) ignores all but the most basic of orographic controls on precipitation by distributing precipitation over the watershed via a simple elevation lapse model, (2) assumes that all surface runoff exits the watershed during the time interval it is generated (i.e. no surface routing), (3) does not distinguish between rain and snow interception and does not mode1 snow melt or release from the canopy, and (4) represents the snowpack as a single layer.

Each of these limitations was removed to make DHSVM more applicable to mountainous marine watersheds. An orographic precipitation mode1 (Rhea, 1978) was implemented, which explicitly models the effects of orographic enhancement and rain shadowing. A distributed-velocity routing model (Maidment et al., 1996) was added to route surface flow to the outlet. The snow mode1 was generalized to more accurately predict snow melt from the ground snowpack. A representation of snow interception and subsequent melt and/or mass release from the canopy was also added. In addition, the two-stream radiation mode1 of Dubayah (1990), which was incorporated in DHSVM by Arola (1993), was used to predict the effects of topography on incoming solar radiation. The development, implementation and testing of each improvement for the Snoqualmie watershed is discussed in this chapter.

Orographic Precipitation Model

DHSVM, as originally implemented by Wigmosta et al. (1994), made use of a simple station-based precipitation algorithm that scaled precipitation based on elevation. This approach cannot account for the complex effects of topography (such as rain shadowing) on the distribution of precipitation in mountainous areas since it does not attempt to mode1 the physics that control precipitation. To overcome this limitation, we implemented a variation of Rhea's (1978) orographic precipitation model which follows parcels of air through topographically induced moist adiabatic ascents and descents. The parcel trajectories are limited to simple two-dimensional flow (in the longitudinal and vertical directions) over the terrain, oriented in the direction of the upper-atmospheric wind direction. Mass balances of liquid water and water vapor are calculated by allowing a fixed fraction of the total cloud water content (local condensation and upstream

imported moisture) to precipitate (hence be removed from the column) while carrying the remainder downstream where it is available for precipitation.

Since the orographic model is based on air flow over topography, its implementation requires knowledge of the topographic features encountered by air crossing the model domain in the direction of the upper atmospheric flow (at 850 mb in our implementation). To this end, the topography, as represented by a digital elevation model (DEM), was resampled to a coarse mesh aligned with the 850 mb flow as shown in Figure 3.1. In our implementation, each grid cell is square with dimensions of 0.5 km while the wind directions are taken in multiples of 22.5 degrees from 0 to 360 degrees. These dimensions and restrictions were chosen to limit the computational requirements of the model while allowing adequate representation of varying storm paths and precipitation distributions. Each row of grid elements in the longitudinal direction is considered one transect of the model domain. Air parcels are advected over the topography along each transect independent of the air flow and water balances of the neighboring transects. Each grid element encountered along a transect represents a single crass-section. Mass balances are performed for each cross-secti.on along a transect. Given this representation of the topographic mesh, the basic

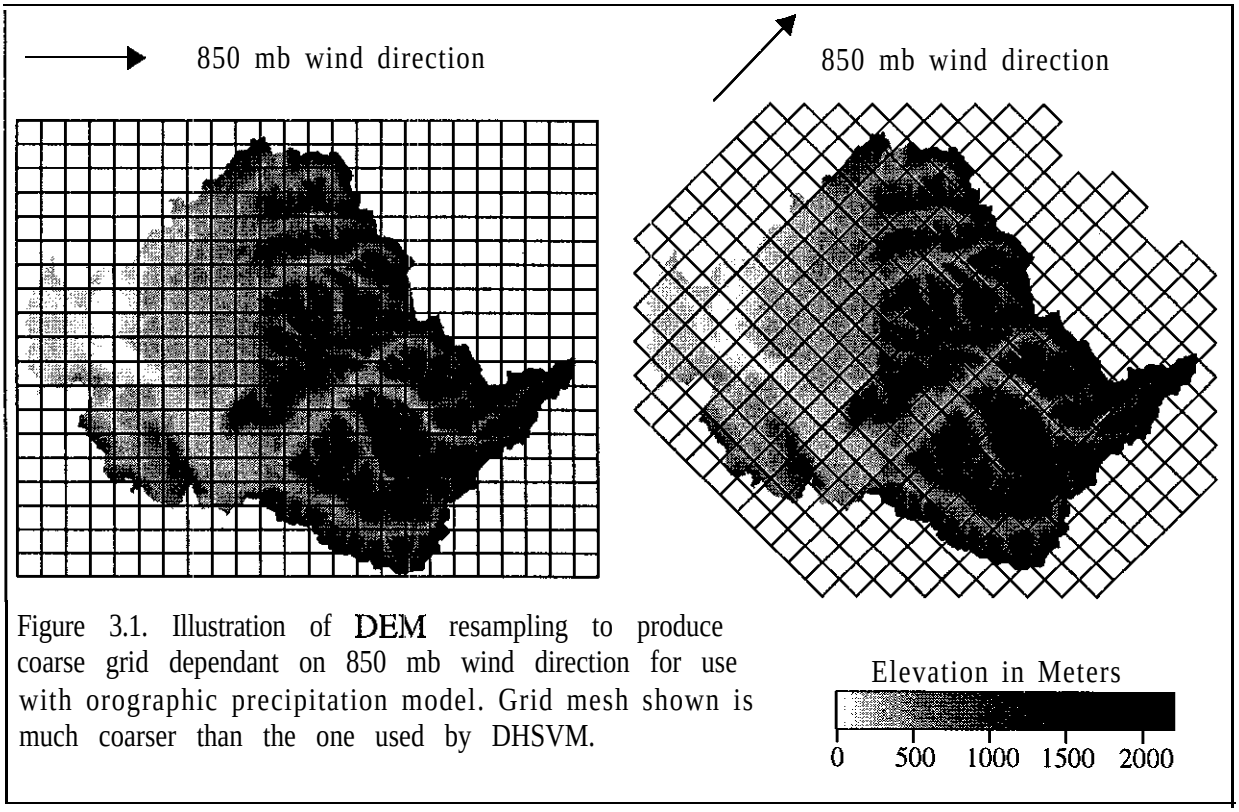

Figure 3.1. Illustration of DEM resampling to produce coarse grid dependant on 850 mb wind direction for use with orographic precipitation model. Grid mesh shown is much coarser than the one used by DHSVM.

form of the orographic precipitation model is described by

$$R_i = \frac{EV\Delta P}{\rho_w g \Delta x}(Q_i + \Delta C_i) \tag{3.1}$$

where

R_i = precipitation rate over cross section i

V = the mid-layer horizontal wind speed at cross section i

AP = pressure thickness of the layer over cross section i

E = precipitation efficiency

Q_i = cloud water content advected into i from downstream

ΔC_i = condensation (or evaporation) due to vertical motion in i

Ax = cross section length

ρ_w = density of water

g = gravitational constant

The term $(Q_i+\Delta C_i)$ is the total available liquid water available for precipitation above each cross-section. The orographic model developed by Rhea (1978) uses Eq. 3.1 for a number of vertical layers in the atmosphere and allows for the evaporation of precipitation produced at higher elevation layers as the droplets fall through lower, unsaturated layers of the atmosphere. This implementation, requires nearby atmospheric soundings of temperature and humidity at a number of atmospheric pressure levels. Unfortunately, profile data that would be representative of the Snoqualmie watershed are not available. Rhea's model was therefore simplified to represent the atmosphere as a single layer. The model is forced with local pressure, temperature, and precipitation from the Stampede Pass weather station, which is located just outside the watershed. Upper atmospheric wind direction and magnitude are interpolated to Stampede Pass from the National Meteorological Center grid point data set. Since the orographic model is implemented only when precipitation is occurring at the station, the relative humidity at the station is assumed to be 100 percent.

The liquid cloud water content at the beginning of each transect is estimated from Stampede Pass observations as follows. The initial liquid water (Q_1) at the first (upstream) cross section of each slice is determined by first calculating the total cloud water available for precipitation

above Stampede Pass. From Eq. 3.1,

$$(Q_{sta} + \Delta C_{sta}) = \frac{R_{sta}}{\left(\frac{EV\Delta P}{\rho_w g \Delta x}\right)} \tag{3.2}$$

Since the total cloud water above the station includes both Q_{sta} and ΔC_{sta}, Q_{sta} is calculated as a fixed fraction (0.75 in this application) of the right-hand-side of Equation 3.2. The value of Q_{sta} is then scaled by the ratio between the saturation mixing ratio (W_s= mass of water vapor / mass of dry air per unit volume) at the elevation of the first cross section and the saturation mixing ratio at Stampede Pass to obtain Q_1 :

$$Q_1 = Q_{sta}\left(\frac{w_{s1}}{w_{ssta}}\right) \tag{3.3}$$

where the saturation mixing ratio is given by

$$w_s = 0.622\frac{e_s}{P} \tag{3.4}$$

where e_s is the saturation vapor pressure (solely a function of air temperature) and P is the atmospheric pressure. The distribution of pressure is assumed to be hydrostatic while the temperature distribution is assumed to follow the moist adiabatic lapse rate.

The precipitation rate at section 1 is determined by application of Eq. 3.1 by setting AC to zero. Orographic effects in the first cross-section are ignored because no upstream information on topography is available. The liquid water (Q) remaining above section 1 is then advected to section 2. The saturation mixing ratio is calculated over cross-section 2 based on its temperature and pressure. Once again the temperature profile is assumed to follow the moist adiabatic lapse rate. The amount of condensation of water vapor or evaporation of liquid water is given by

$$\Delta C_1 = (w_{s1} - w_{s2})\,E_2 \tag{3.5}$$

where E_2 is a condensation-evaporation parameter which limits the rate at which water can evaporate or condense (Peck and Schaake, 1990). If w_{s1} exceeds w_{s2} then the mass of water vapor decreases and thus the mass of liquid water increases from the previous cross-section. Eq. 3.1 is then used to determine the precipitation rate over the cross-section and any remaining liquid water is advected to the next cross-section and the process is repeated. The precipitation on each element of the coarser resampled grid is then mapped back to the finer grid used by the remainder of

DHSVM.

One further constraint must be imposed on the model as a result of its single layer formulation. Since liquid water is removed above each cross-section, the total available water for precipitation will decrease rapidly along each longitudinal slice. If the model were multilayer, this decrease in available atmospheric water in the lowest layer would be replenished by precipitation from upper layers which evaporates in the lower layers. To avoid this problem without implementing a multilayer model, we assume that any precipitation from upper layers is sufficient to replenish any advected cloud water content (Q) which might precipitate over a cross-section. Thus the advected cloud water content is updated from one cross section to the next as follows:

$$Q_{I+1} = Q_I + (1 - E)\,\Delta C_I \frac{|\Delta P_{(I+1)} - I|}{|\Delta P_{sta} - 850mb|} \qquad (3.6)$$

The orographic precipitation model was applied to the Snoqualmie watershed for the period March 1, 1983 through November 30, 1986 at a daily time increment. The model was forced with local and regional climatic variables as described above and was calibrated to observations at low level elevations. These observation are shown in Table 3.1.

Table 3.1:: Observed Precipitation at Various Stations in and near the Snoqualmie Watershed from March 1, 1983 to November 30, 1986

Station	Elevation (meters)	Observed Precipitation (meters)
Stampede Pass	1206	7.24
Snoqualmie Falls	134	5.43
Cedar Lake	474	8.35
Tolt Reservoir	610	8.40

During this period Stampede Pass recorded a total precipitation of 7.24 meters. Discharge from the basin as observed by the USGS stream gauge on the Snoqualmie River near Carnation was 7.12. meters, suggesting that the long term discharge from the basin is approximately equal to the precipitation at Stampede Pass. Therefore, the average precipitation over the basin must be greater than that observed at Stampede Pass to account for evapotranspiration losses, which typically average about 500 - 600 mm per year or 2.0 to 2.5 meters over the four growing seasons modeled in the calibration simulation. A rough estimate of average precipitation over the basin is approximately 9.6 meters over the observation period. A further consideration used in

calibrating the orographic model is the observation that the maximum annual precipitation at high elevations in the Cascade Range: is approximately 5000 mm per year (Staubitz, 1994).

The results of the calibration are summarized in Figures 3.2a and 3.2b which show the total amounts of precipitation for the entire calibration period averaged over 100 meter elevation bands. The legend for each precipitation vs. elevation curve also contains information on the average precipitation over the basin as well as the predicted minimum and maximum precipitation which fell on any individual pixels.

Figure 3.2a clearly shows that if all of the atmospheric water available above Stampede Pass (as calculated by Eq. 3.2) is used as the initial condition for each transect, the model either overpredicts precipitation over the basin or cannot realistically model the increase in precipitation with elevation. The model overpredicts the observed precipitation with large values of the precipitation efficiency factor (E). When the precipitation efficiency factor is decreased to the point where the average amount of precipitation over the basin is approximately correct, the model can't replicate the orographic effect.

However, if only 75% of the available atmospheric water at Stampede Pass is used as an initial condition for each transect, a wide range of realistic precipitation distributions can be obtained. As precipitation efficiency increases, the average precipitation over the basin also increases but not as much as when the condensation efficiency parameter (E_2) is increased. Increasing E from 0.25 to 0.5 while E_2 is 0.1 increases the average precipitation from 9.3 1 to 9.95 meters while increasing the maximum observed precipitation from 19.5 to only 23.19 meters. However, increasing E_2 from 0.1 to 0.2 while E is 0.25 increases average precipitation from 9.31 to 11.41 meters while increasing the maximum observed precipitation from 19.5 to 3 1.23 meters. Further simulations (not shown) confirm that minor changes in E_2 have a large impact on the magnitude of the orographic effect. The best fit with the observed data used $E=0.25$ and $E_2=0.12$. With these values, the average precipitation over the watershed was 9.67 meters and the maximum observed precipitation was 21.6 meters, while the average upper elevation precipitation was approximately 17 meters over the simulation period. Furthermore, these values of E and E_2 predict a total precipitation during the simulation period at Snoqualmie Falls of 6.4 m, at Tolt reservoir of 8.5 1 m, and at Cedar Lake of 6.91 m, all of which are consistent with observations, as noted in Table 3.1.

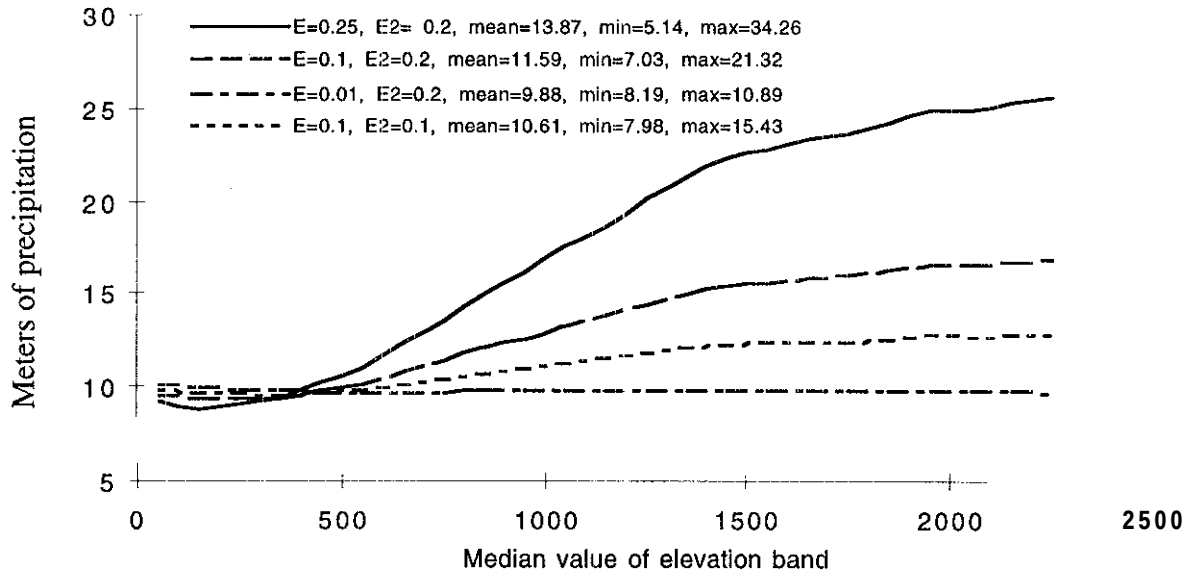

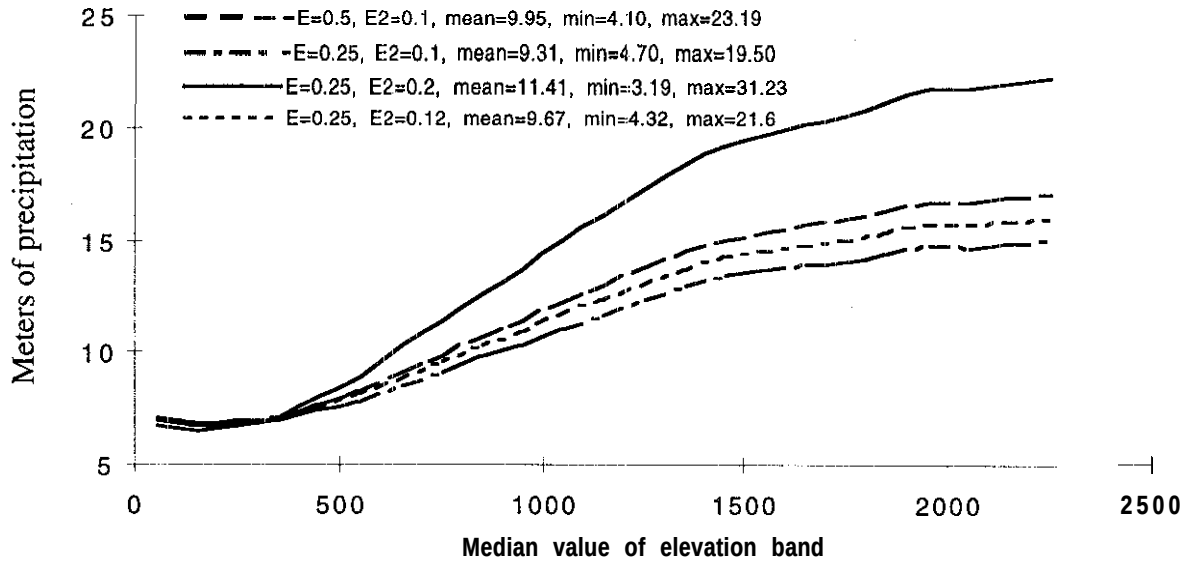

Figure 3.2a (top) and 3.2b. Results of orographic model calibration showing sensitivity of the model results to the pararneters E and E_2: a) 100% of Stampede Pass water available for initialization, b) 75% of Stampede Pass water available for initialization.

Figure 3.3 shows the distribution of precipitation over the watershed predicted with the calibrated orographic model for the entire simulation period and selected events. Note that the distribution for the entire simulation period closely follows the DEM. High elevations receive the most precipitation, upper river valleys receive less, and the Snoqualmie River floodplain receives the least. The event based images also show the effect of rain shadowing as it varies with the upper atmospheric wind direction.

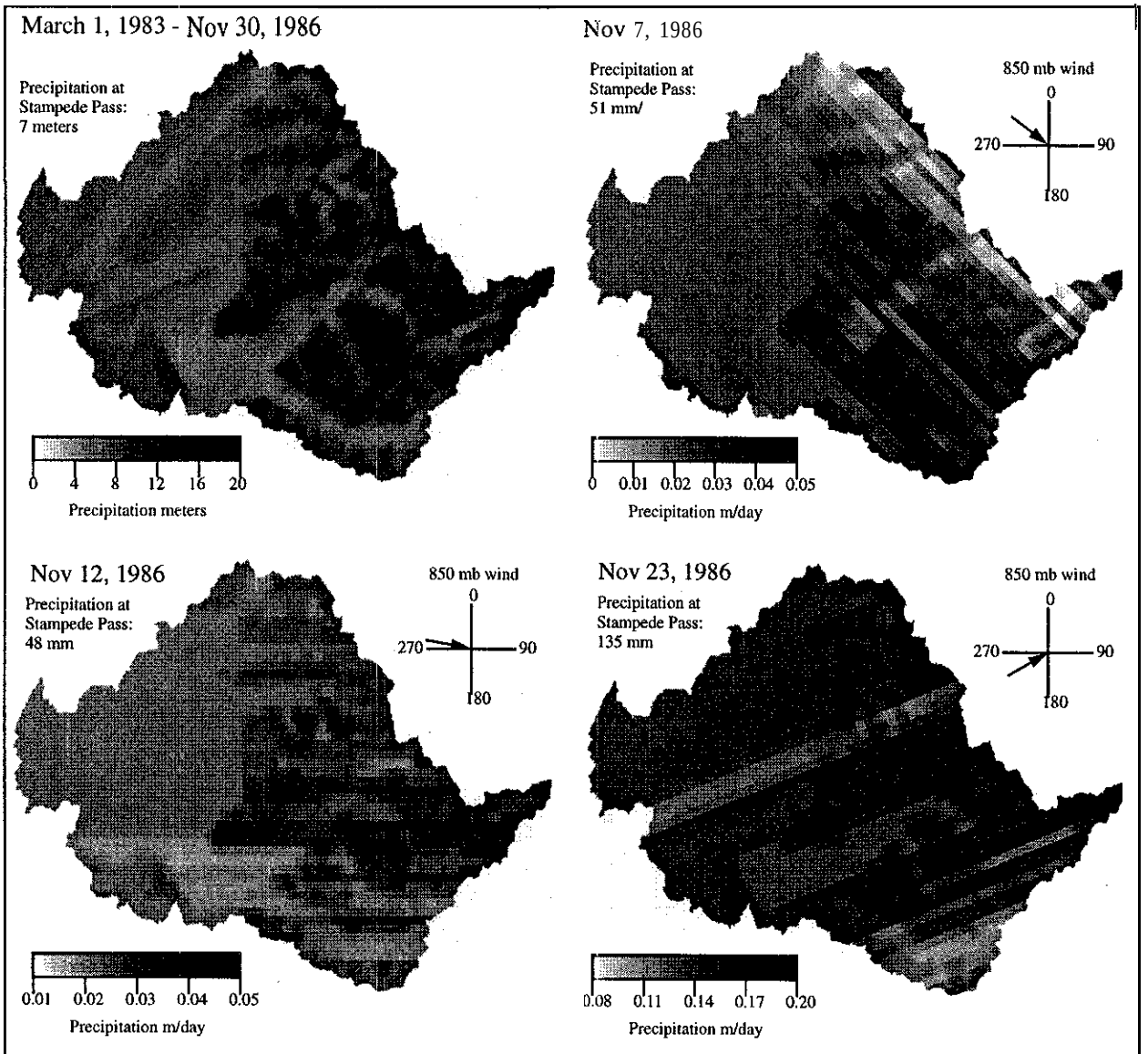

Figure 3.3. Orographic precipitation images for entire calibration period and selected 24 hour events. 850 mb wind direction is shown along with observed precipitation at Stampede Pass,

Surface Flow Routing Model

A distributed-velocity surface routing model was implemented which calculates the time required for runoff generated at a given pixel to travel to the basin outlet. The response function from each pixel is a function of this travel time and can consist of both a linear translation component and a linear storage component. The routing model was developed by Maidment et al. (1996) specifically for application to spatially distributed hydrologic models, and is ideally suited for inclusion in DHSVM.

Given a DEM, the total time for runoff produced at a given pixel to travel to the outlet is determined by the length of the path to the outlet and the local velocity along its path. Figure 3.4 illustrates how the flow path through the watershed is determined. Flow generated inside each pixel in the DEM can move in one of eight directions. For our implementation of the routing model, the flow is forced to move in the direction of the steepest downward slope. This approach is similar to the D8 method (O'Callaghan and Mark, 1984) and works well for steep terrain. For more gentle topography, an alternative approach such as the DEMON method of Costa-Cabral and Burges (1994), which routes flow as a two-dimensional sheet, could be used; this refinement is not necessary in the relatively steep Snoqualmie basin. If more than one pixel is in the direction of steepest descent, one direction is chosen at random and all other flow traveling through or generated by that pixel is then routed in the same direction. In the case that a pixel is a local minimum (i.e. a pool in which water collects), our method determines the flow paths out of these pools in the DEM by finding the lowest pixel which can be considered the edge of the pool and then orienting all the flow paths from pixels contained in the pool toward this exit pixel. Surface runoff which is generated in or enters these depressions is routed to the outlet of the depression and then

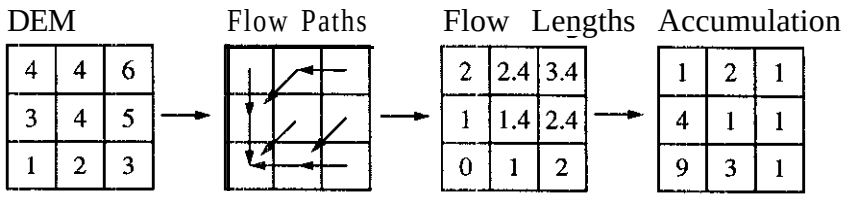

Figure 3.4. DEM based flow paths in the direction of steepest descent assuming square pixels of dimension 1. Flow lengths to the outlet and accumulation are also shown.

on to the basin outlet.

Once the local flow directions are known, the flow length to the outlet is determined by summing all of the distances traversed in each pixel over the entire flow path. If the flow path is oriented along a diagonal then the distance traversed while in that pixel is 1.414 times the pixel side dimension (assuming square pixels).

The local velocity of the flow in each pixel is determined by:

$$V = V_m \frac{S^b A^c}{\overline{S^b A^c}} \tag{3.7}$$

where V is the local velocity assigned to a cell whose local slope in the drainage direction is S and whose upstream drainage area is A. The upstream accumulated drainage area for any pixel is simply the total number of pixels whose flow travels through that pixel. If the pixel drains only itself then it is assigned an accumulated drainage area of one pixel. The exponents b and c are taken as 0.5 each (Maidment et al., 1996). The denominator in Eq. 3.7 is the average slope-accumulation term over the entire watershed and V_m is the average velocity over the watershed. This average velocity can either be used as a calibration parameter; alternatively, it can be estimated by dividing the average path length to the outlet by the typical lag time between the time of concentration of precipitation and the time of concentration of the hydrograph. This scheme of assigning local velocities based on the accumulated area and the local slope allows the velocity to increase as the drainage area increases while also allowing regions with steep gradients to retain realistically larger velocities. Implementation of Eq. 3.7 requires the further restriction of limiting the minimum and maximum velocities to predetermined values to avoid unrealistic velocities.

The time required for water generated in a pixel to flow to the outlet is then given by:

$$T_i = \sum_{i=1}^{n} \frac{L_i}{V_i} \tag{3.8}$$

where L_i is the distance traveled1 in pixel i and n is the total number of pixels through which water must travel to reach the outlet.

The simplest use of the travel time from Eq. 3.8 is to implement a pure translation routing model which implies that all the runoff generated at pixel i at time T will appear at the outlet at time $T + T_i$. While conceptually simple, this model does not allow for either local (land surface) or channel storage effects. To this end, we adopted the approach presented in Maidment et al.

which considers the travel time along the path to the outlet from each pixel to have associated with it both a translation and a storage component, the magnitudes of which are in fixed proportions. Thus, flow with a total travel time of T_i (as determined by Eq. 3.8) first enters a linear storage reservoir with average residence time T_r and then enters a linear channel with a translation time of T_s. These translation and reservoir times are related as follows:

$$T_i = T_r + T_s \tag{3.9}$$

$$\beta = \frac{T_r}{T_i} \tag{3.10}$$

where β is the ratio between the average time spent in the reservoir to the total travel time to the outlet, For simplicity, we assume β is a constant for all pixels, although this assumption can be easily removed from the routing model if more information about the storage properties of the watershed is available.

Given the total travel time (T_i) and β, T_r and T_s can be calculated from Eq. 3.9 and 3.10. The response at the outlet of the watershed due to a unit pulse of duration At (taken as the model timestep) of surface runoff generation at a given pixel is then given by:

$$h(t) = 0 \qquad t < T_s \tag{3.11a}$$

$$h(t) = \frac{1}{\Delta t}\left[1 - \exp\left(-\left(\frac{t - T_s}{T_r}\right)\right)\right] \qquad T_s \le t \le T_s + \Delta t \tag{3.11b}$$

$$h(t) = \frac{1}{\Delta t}\exp\left(-\left(\frac{t - T_s}{T_r}\right)\right)\left(\exp\left(\frac{\Delta t}{T_r}\right) - 1\right) \qquad t > T_s + \Delta t \tag{3.11c}$$

It is important to note that the routing model does not actually move the basin's surface flow from pixel to pixel. While a pixel-to-pixel method is physically realistic and would also allow straightforward calculation of sub-basin hydrographs, it is computationally infeasible. Instead, our implementation of the routing model groups all pixels with the same travel time together and transfers all water generated during a time step to the basin outlet via Eqs. 3.11.

Since the integral of Eq. 3.11 from t = 0 to t = ∞ is equal to unity, it can be used to predict the fraction of water generated at a pixel at time T which will reach the outlet during time steps T, T + At., T + $2\Delta t$, etc. The fractional distribution over time is the response function of each pixel to a unit pulse input and is estimated by:

$$R(T) = \frac{h(0) + h(T)}{2}, \quad R(T+\Delta t) = \frac{h(T) + h(T+\Delta t)}{2}, \quad . \tag{3.12}$$

Therefore, the travel time distribution of water from a pixel to the outlet can be entirely specified by its total travel time to the outlet (translation plus storage), the model time step, and β. If the model time step and β do not change, then Eqs. 3.9 to 3.12 can be implemented once for each travel time. The values of R(T) for each unique total travel time in the basin are used as input to DHSVM.

Since DHSVM is capable of using a variable time step, a slightly more complex implementation of the above method must be used to preserve continuity in the routing model. This involves restricting the time step used in the prediction of the response function to the smallest DHSVM time step (chosen as Δt=1 hour). Eqs. 3.9 to 3.12 are then implemented as described above to predict the response function for pulses with durations of 3 and 24 hours (assuming that 3 and 24 hours are the coarse and tine timesteps for the simulation). The routing model then distributes the water to the outlet based on the correct hourly response function for each pixel's travel time and the current DHSVM time step. Streamflow is obtained by advancing the hourly routing model by the number of hours in the current DHSVM time step. This procedure correctly transforms the variable time domain of DHSVM to match the fixed time domain of the routing model without a loss of continuity. An example of this method is shown in Figure 3.5. Note that inclusion of a linear storage reservoir allows some runoff to be routed to the outlet sooner than does a pure translation. model, and also extends the tail of the unit hydrograph from an individual pixel.

To implement the routing model for the Snoqualmie watershed, a FORTRAN program was written to determine the accumulation, slope, length, velocity and total travel time for a DEM. Alternatively, most widelly used GIS packages such as GRASS or ARC-INFO can be used to determine these values as well. The DEM for the Snoqualmie Watershed as well as its accumulation values and the total travel time from each pixel are shown in Figure 3.6. The locations of the major tributaries in the Snoqualmie basin are clearly shown in the accumulation image (as regions of high accumulation) and compare well with area1 photographs of the region. However, some of the confluences between rivers are not correctly located by the model. The most obvious errors are where the South Forkjoins the main-stem Snoqualmie and where the Tolt River merges with the Snoqualmie. Fortunately, these errors do not significantly alter the travel time to the outlet, and overall the model provides a good approximation of channel locations.

The value of V,, the average flow velocity in the watershed, was determined by calculating the average flow path in the watershed and dividing by the lag between the time of concentration of precipitation and the time of concentration of the hydrograph for two major events (see Figure 3.7). The average path length is 44 kilometers while the lag time is 24 hours, corresponding to an average flow velocity in the watershed of 0.5 m/sec. This value is lower than physically realistic channel velocities, especially for mountainous watersheds, since its calculation considers local and channel storage effects. However, it is significantly higher than the average velocity (0.15 m/sec) suggested by Maidrnent et al. for watersheds in the United States. Given a V_m of 0.5 m/sec, V_{min} and V_{max} were (chosen as 0.2 and 1 .O m/sec respectively. These values were chosen such that the average travel time predicted by the distributed velocity routing was similar to

Figure 3.5. Example of routing model implementation with a variable time step for one pixel generating 1 mm of runoff in a 3 hour time step, and then 1 mm of runoff in a consecutive 6 hour time step. Each position in the response function (R) corresponds to the fraction of water which exits the basin at each hour after it is generated.

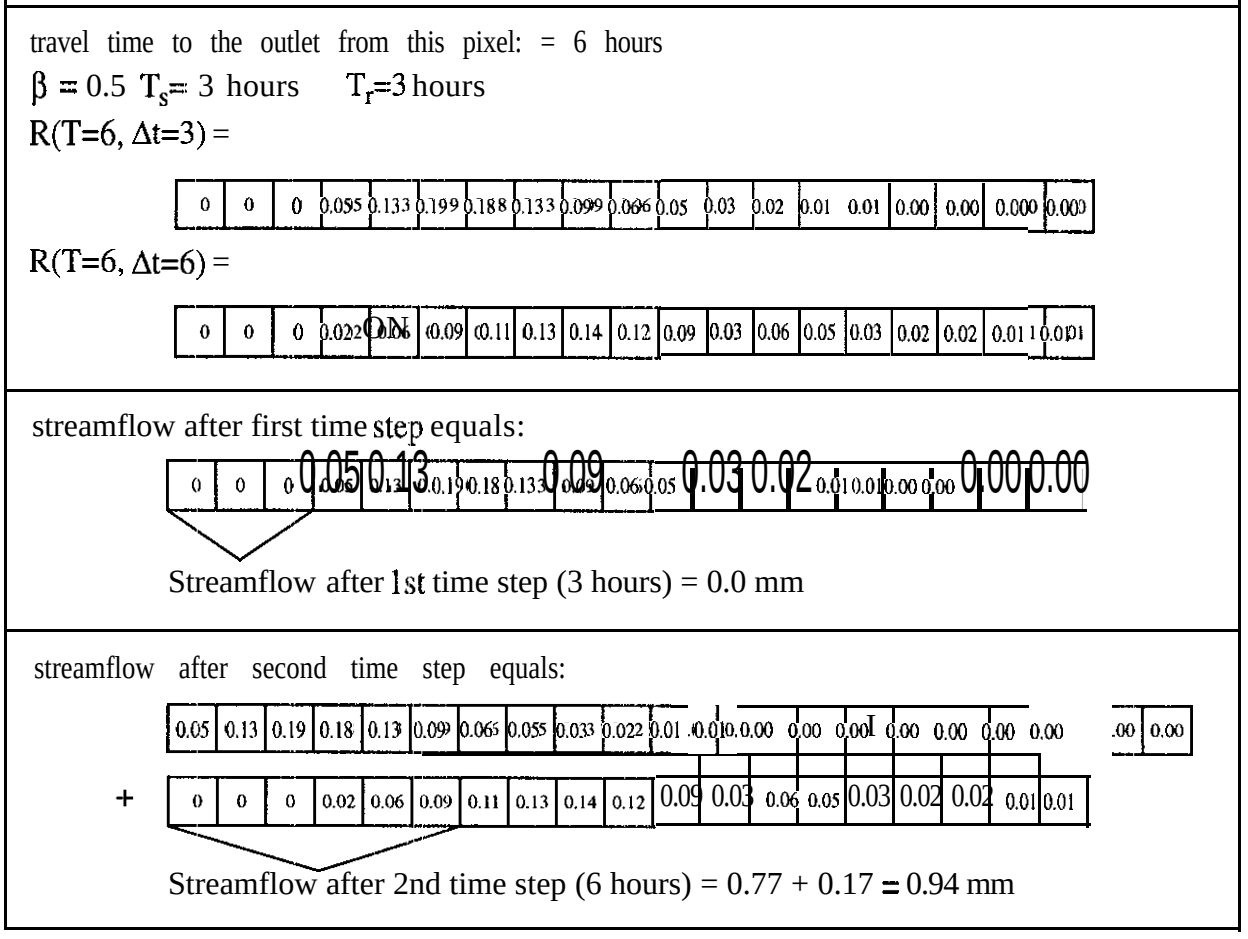

Figure 3.6. Digital elevation model, accumulation, and travel time to outlet images for the Snoqualmie watershed.

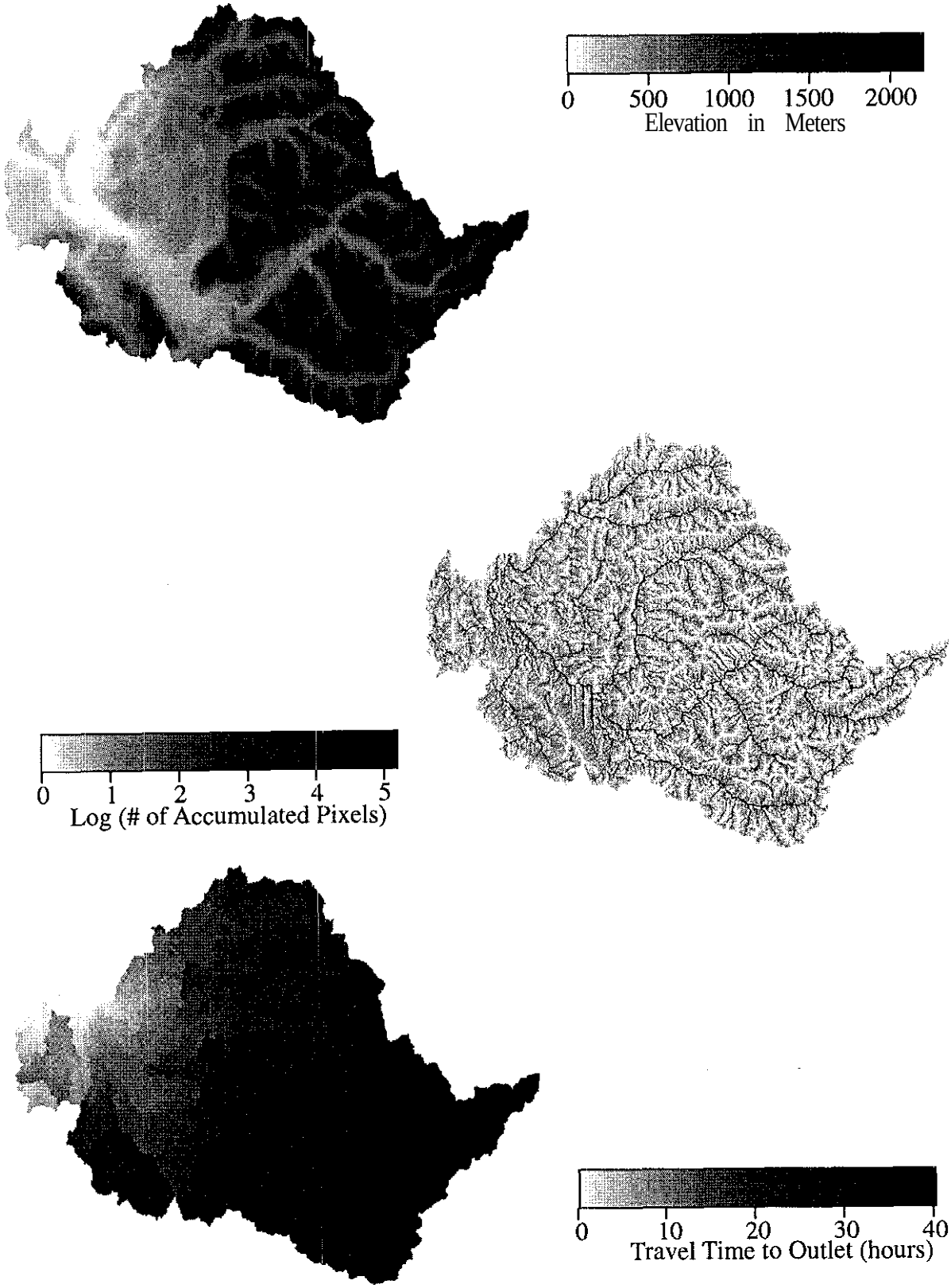

the calculated value of 24 hours. The magnitude of β was determined by calibration.

The routing model was calibrated against the November 1986 event and then verified against the November 1990 event. These storms were chosen because they were major rain-on-snow events in which the hydrographs were dominated by surface flow and routing. Since V_m, V_{min}, and V_{max} are used to calculate the travel time to the outlet, the sensitivity of the model to these parameters was determined by examining their effects on the travel time distribution of the

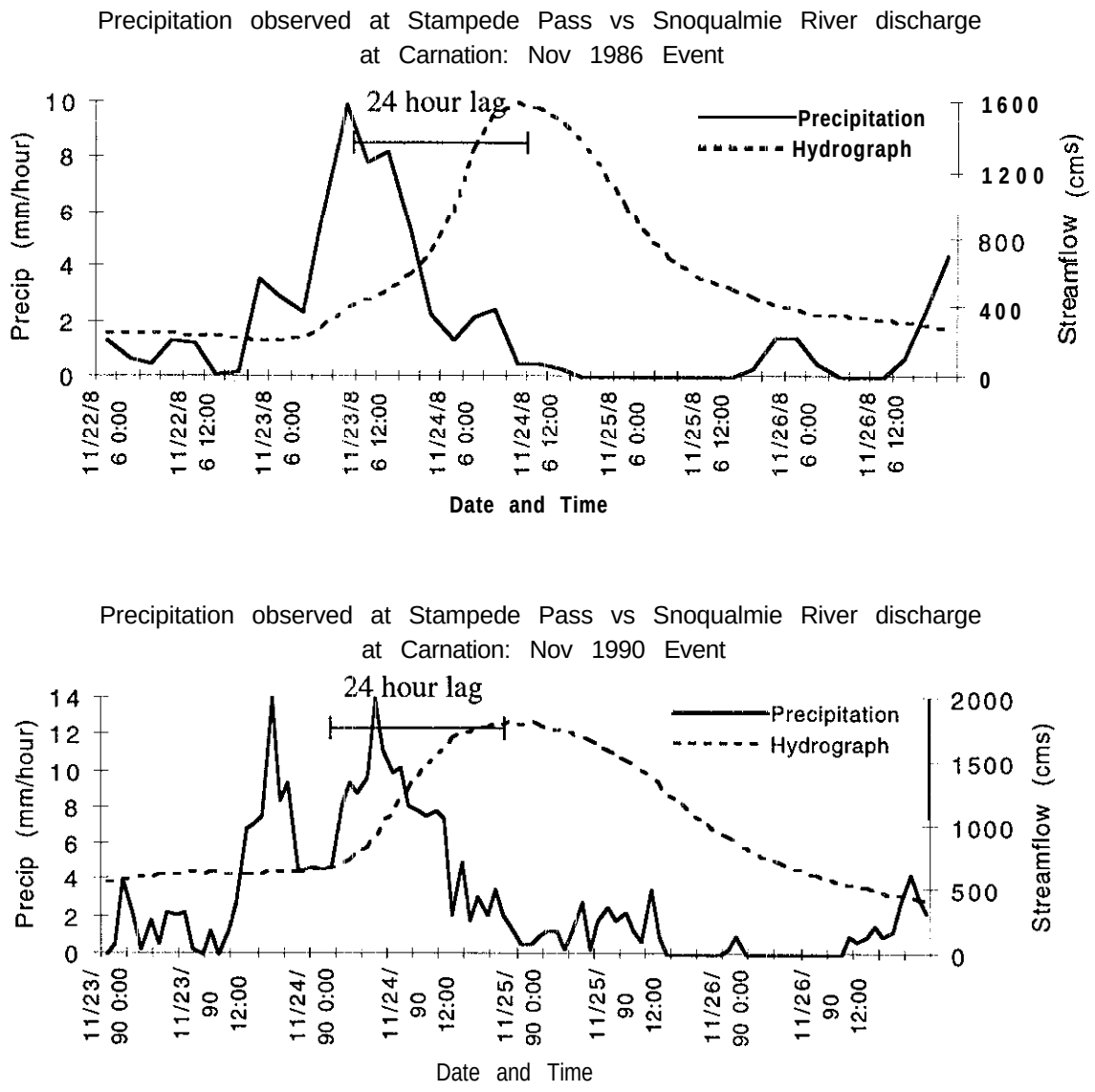

Figure 3.7. Lag time between peak precipitation and peak streamflow for Nov 1986 and 1990 events

watershed. The value of V_{max} was varied from 0.6 to 4.0 m/sec and was found to have almost no impact on the travel time distribution. However, the value of V_{min} greatly affects the travel times, so that even a rninor change away from the base value of 0.2 m/sec produces unrealistic travel-time distributions (i.e. the average travel time to the outlet does not agree with the predicted lag time calculated above). The critical value used to shape the predicted hydrograph and calibrate the routing model is β. Figure 3.8 shows the predicted vs. the observed hydrograph for the November 1984 event simulated with a 3 hour time step. The predictions are from DHSVM: (1) as originally developed without a routing model, (2) with a purely translational routing model, (3) with a translational and storage model with β=0.4, (4) with a translational and storage model with β=0.6.

Figure 3.8 clearly shows that without a routing model, DHSVM cannot adequately predict either the magnitude or timing of hydrograph peaks on an hourly time scale. The peak is overes-timated and occurs approximately 24 hours too soon. (This phase error is expected considering the lag time is approximately 24 hours). If a pure translation routing model is used, the hydrograph's peak is well timed but the recession occurs much too quickly. When the full storage and translation routing model is used both the timing and magnitude of the peak and the hydrograph recession are well predicted. However, as the value of β increases, the magnitude of the peak decreases due to the increased storage in the watershed. When β equals 0.6, the match between the observed and predicted hydrographs is best. Coincidentally, a value of β = 0.6 was suggested by Maidment et al. based on experience with a number of U.S. watersheds.

The routing model was then verified against the November 1990 event. Figure 3.8 shows the predicted vs. observed hydrograph for this verification event.

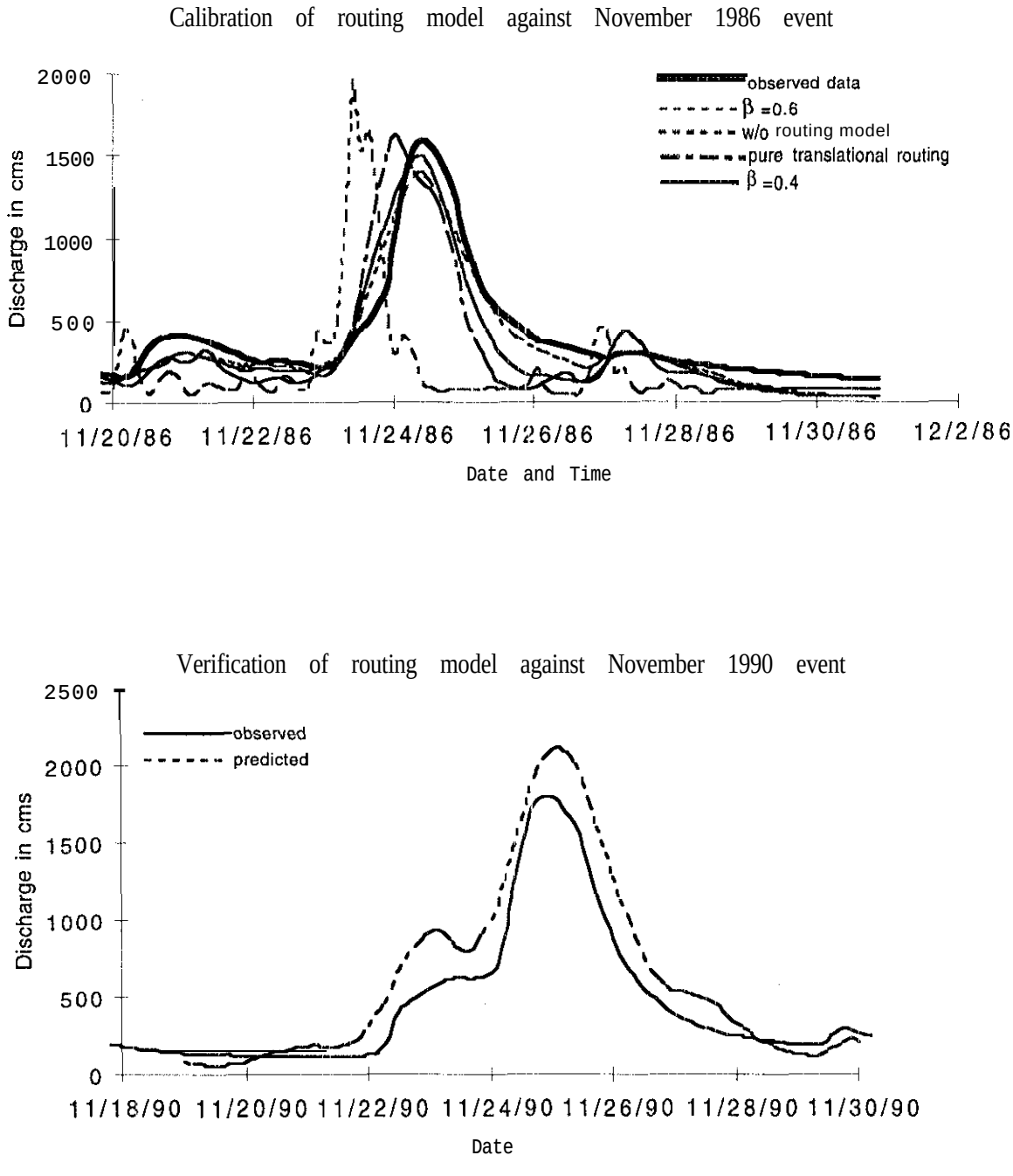

Figure 3.8. Calibration and verification of distributed routing model.

Two-layer Snow Melt Model

The original version of DHSVM implemented a single layer snow melt model based on the energy balance approach given in Anderson (1968). However, since the energy exchange between the atmosphere, canopy, and snowpack occurs at the snow surface: modeling the snowpack as a single layer is unrealistic, especially for deep snowpacks. Furthermore, the original version of DHSVM did not explicitly solve for the snowpack temperature based on the pack energy balance. Instead, the initial snow temperature at the beginning of a time step was used to calculate the terms in the energy balance. The net energy flux was then applied to the snowpack and the snowpack temperature at the end of the time step was calculated as a function of the final snowpack cold content. This approach was found to cause instability in the calculated snowpack temperature during the accumulation season, especially for thin snowpacks. To resolve these problems, DHSVM was extended to include a two-layer snow accumulation and ablation model which explicitly solves for the final snowpack surface temperature based on the energy balance at each model time step.

In the extended version of DHSVM, the snowpack is divided into two layers; a thin surface layer and the pack layer. Energy exchange between the atmosphere, forest canopy and snowpack occurs to and from the surface layer. Energy exchange between the surface layer and the pack layer occurs via melt water which percolates from the surface layer into the pack. In our implementation, the snow surface layer is the minimum of the entire pack water equivalent or 0.125 meters.

The energy balance applied at the surface layer is

$$c_s W \frac{dT_s}{dt} = Q_r + Q_s + Q_e + Q_p + Q_m \qquad (3.13)$$

where c_s is the specific heat of ice, W is the water equivalent of the snowpack surface layer, T_s is' the temperature: of the surface layer, t is time, Q_r is the net radiative flux, Q_s is the sensible heat flux, Q_e is the latent heat flux, Q_p is the energy advected to the snowpack via rain, and Q_m is the energy lost by the snowpack when a portion melts or gained by the pack when its liquid water refreezes. Note that each term in Eq. 3.13 (except for Q,) depends on the snowpack surface temperature. This (energy balance is identical to that used in the original version of DHSVM. Eq. 3.13 simply states that the net energy advected to the pack from the environment, plus any energy

gained by the pack in refreezing water (or lost by the pack during snow melt), is balanced by a change in temperature of the snowpack (change in cold content). The cold content is the amount of heat which, when added to the snowpack, will raise its temperature to 0°C; it is calculated directly from the snow temperature by

$$C = \min\ (c_s TW, 0) \tag{3.14}$$

where c_s, T , and W are the specific heat, temperature, and water equivalent of the snowpack's ice fraction.

Eq. 3.13 is solved as follows. At the beginning of each time step, the cold content, snow water equivalent, liquid water content, and ice fraction of both the surface layer and the pack layer are known. If a snowpack is present at the first timestep, then its temperature is initially set to 0^oC. The cold content and water equivalent of any freshly fallen snow is added to the surface layer and any rain is added to the liquid water content of the surface layer. If the snow water equivalent of the surface layer is greater than 0.125 meters, the excess water equivalent and its cold content are added to the pack layer. This transfer of cold content to the pack layer under accumulation conditions is the only mechanism in the model by which the temperature of the pack layer can decrease. The liquid water in the surface layer is then refrozen until the heat released is sufficient to satisfy the cold content of the surface layer. If the energy released from refreezing this water is not enough to satisfy the surface layer cold content, then all the water is frozen and the cold content and surface temperature are adjusted. If the heat released by freezing satisfies the cold content, then the surface temperature of the pack is increased to 0^oC and the liquid water of the: surface layer is reduced to that amount which did not freeze. For example, if the cold content is zero then the snow surface temperalnre is also 0°C and no liquid water can be refrozen (i.e. the cold content is immediately satisfied).

Next, each term in Eq. 3.13 is calculated assuming that the final snow surface temperature is 0^oC. If the equality condition of Eq. 3.13 is met then the energy balance is satisfied and the initial assumption was correct. If the energy balance is not satisfied, the final snow surface temperature is not 0^oC and the actual final temperature is estimated via a numerical scheme which iterates on the surface temperature until the energy balance is satisfied within a given tolerance. For example, an actively melting isothermal snowpack at 0^oC will satisfy the energy balance on the

first iteration. Since the change in cold content is zero, any input of energy from the environment must be used to melt part of the surface snowpack. For a surface snowpack slightly below 0^oC, any input of energy from the environment will quickly satisfy the cold content thereby raising the temperature to 0^oC and allowing any additional energy input to melt a portion of the snowpack. Once again the energy balance will be satisfied on the first iteration. Only during accumulation periods, when the snow surface temperature remains below 0^oC (or falls below 0^oC after a melt period) is the iterative scheme used to predict the final snow surface temperature of the snowpack.

Other mechanisms which can alter the mass of the surface layer are sublimation and condensation. The vapor flux (V) from the snowpack is driven by the vapor pressure difference between the air above the pack and the surface layer and is calculated as

$$V = \rho_a c_a \frac{0.622}{P} (e, - e_s) \tag{3.15}$$

where ρ_a is the air density, P is the atmospheric pressure, e_a is the vapor pressure of the air above the snowpack, e_s is the saturated vapor pressure of the snowpack itself and c_a is the aerodynamic conductance above the snowpack as defined by Wigmosta et al. (1994). Vapor flux can be either to or from the surface layer.

Melt water from the surface layer is then added to the liquid water content of the surface layer. If the liquid water of the surface layer exceeds its liquid water holding capacity, then all the excess liquid water is allowed to drain immediately to the pack layer. In the pack layer, the liquid water is refrozen until the cold content is satisfied. Energy exchange via conduction and diffusion between the lower layer and the surface layer and the soil are small relative to other inputs and are ignored (USCOE, 1956). Any liquid water remaining in the pack layer above its holding capacity is then released as snowpack outflow. The liquid water-holding capacity of both snow layers is assumed to be 0.03 times the ice fraction of the snow water equivalent.

Previous validation of the two layer snow accumulation and ablation model suggests that the model can accurately predict both short-term event-driven snow melt and long-term ablation of the pack. Connelly et al. (1993) verified the two layer snow melt model against observed daily snowpack outflow and snow water equivalent for a single accumulation and ROS event, November 27 to December 10, 1983 (Berris, 1984). Their results show that the two layer model can accurately predict snowpack outflow and water equivalent in forested and open sites. However,

the predicted outflow more closely matched the observed outflow in the open site. This difference in performance was attributed to the location of the lysimeter directly underneath the canopy in a heavy drip zone. Drip from the canopy will increase the observed outflow and decrease the observed snow water equivalent. Connelly et al. (1993) also verified the snow melt model against daily snow water equivalent measurements obtained at a Soil Conservation Service SNOTEL snow pillow site located at Stampede Pass for water years 1983, 1987 and 1988. Results showed good agreement between predicted and observed values of seasonal snow water equivalent especially during the accumulation season.

To further validate the snow model, it was applied to observed snowpack outflow data collected during one ROS event in the Umpqua National Forest near Tokatee, Oregon. The field data at this site were collected by Wetherbee (1995). The study site is located at the 4000 foot elevation in the Cascade Range, approximately 30 miles NNW of Crater Lake. Data from two snow melt lysimeters (Sites l-l and 1-2) approximately 100 meters apart were used to validate the model. Each lysimeter was placed in a forested site in which the forest canopy coverage ranged from approximately 60 to 90 percent. (No quantitative representative measurements of forest canopy density are available.) The lysimeter (approximately 3 feet by 6 feet) placement spanned the drip zone of the canopy, and rain/snow gauges were placed under the canopy as close to the lysimeters as possible. Lysimeter outflow was measured with tipping-bucket gages. In addition to rain/drip from the canopy, other meteorological data collected at the site include hourly observations of windspeed, short wave radiation, relative humidity and air temperature. Cloud cover was assumed to be 100 percent during the ROS event. Except for rain/drip which was collected at both sites, all meteorological data were collected at site l-l only. No meteorological observations in an open area were recorded during this event.

DHSVM was used to simulate the outflow from these lysimeters by running the model in point mode and directly forcing it with the observed meteorological variables. Long wave radiation under fully cloudy conditions was estimated using an emissivity of unity and assuming that the cloud temperature was equal to the dewpoint temperature. Vegetation was specified as 50 m. Douglas fir with a forest canopy coverage of 90 percent. Initial snow water equivalent was assumed to be 0.5 meters. However, since the ROS event did not completely melt the snowpack, the predicted outflow is not sensitive to the initial depth of the pack. Since DHSVM requires a specification of windspeed above the canopy, the observed value (at 2 meters) was used to

4.3 Distributed Soil and Vegetation Data

DHSVM also requires information about the soil and vegetation properties of each pixel including vertical hydraulic conductivity, soil depth, soil porosity, overstory leaf area index (LAI), understory LAI, overstory albedo, and many others. However, instead of specifying a value of each soil and vegetation parameter for each DHSVM pixel (which would lead to large data storage requirements), DHSVM uses only the dominant soil and vegetation type of each pixel. All pixels with identical soil classifications are then assigned one set of soil-dependent hydraulic parameters; all pixels with identical vegetation classifications are similarly assigned one set of vegetation-dependent hydraulic parameters. In other words, DHSVM fully describes all soil and vegetation parameters at a given pixel 'by a soil or vegetation class and a lookup table of parameters which is indexed by class.

The distribution of soil classes over the Snoqualmie watershed was obtained from GIS based vector maps of the watershed provided by the Mount Baker-Snoqualmie National Forest USFS station and the Washington Department of National Resources. Both agencies provided data in DLG-3 format which were converted into a 'pixel' based format consistent with the base DEM. This transformation produced an intermediate map from both sources that referenced each DHSVM pixel to a soil index number. These index numbers can in turn be referenced to a num-

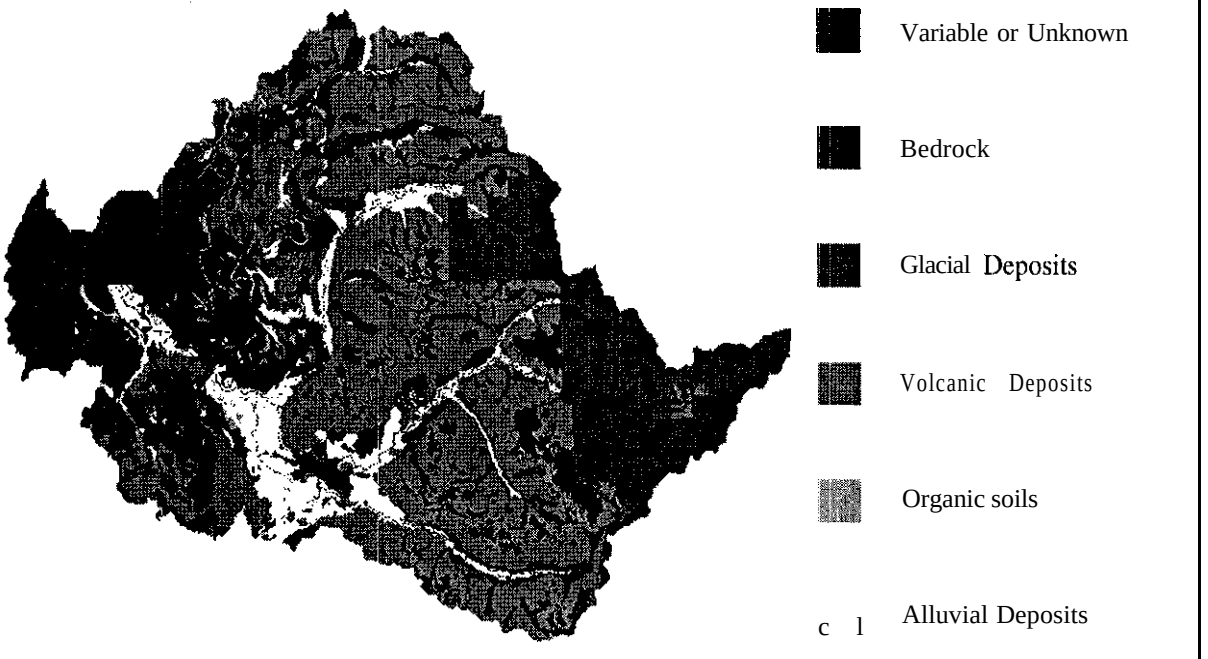

Figure 4.2. Major soil parent materials for the Snoqualmie watershed.

Predicted. vs. observed snow pack outflow at Umpqua Site l-1 during ROS event.

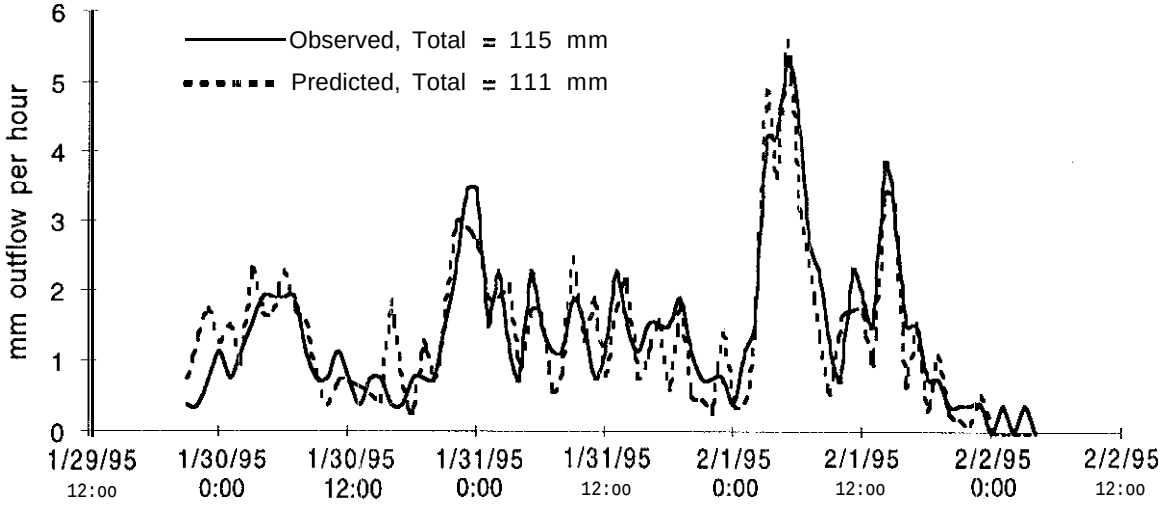

Predicted vs. observed snow pack outflow at Umpqua Site l-2 during ROS event.

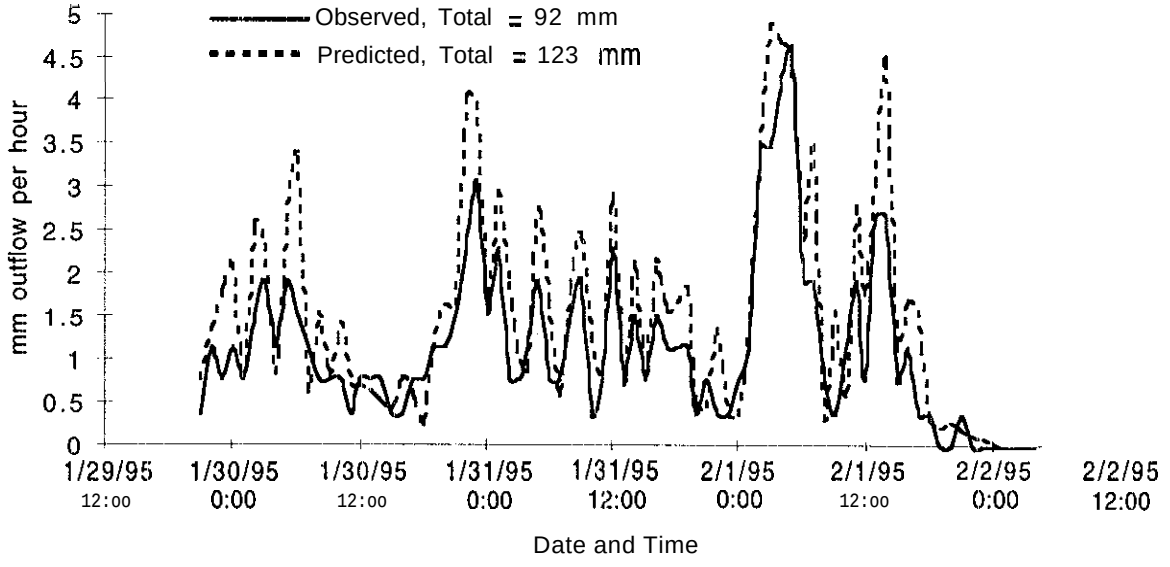

Figure 3.9. Verification of two layer snowmelt model at Umpqua National Forest site.

Snow Interception Model

The original version of DHSVM (Wigmosta et al. 1994) modeled intercepted rain and snow identically. Any intercepted precipitation was stored on the overstory until the maximum liquid water interception storage capacity was reached. Additional precipitation passed through the canopy as tbroughfall. Intercepted water could be removed only by evaporation, which was calculated at the potential rate. While this treatment may be acceptable for relatively cold, dry continental climates, where snow interception by the canopy is either minimal or short-lived, it is not valid for marine mountainous watersheds where interception storage of snowfall can play an important role in seasonal snow accumulation. Therefore, DHSVM was extended to include a snow interception model which explicitly models canopy snowmelt and mass release.

During each time step, snowfall is intercepted in the canopy according to Eq. 3.16 which was suggested by Calder (1990) based on gamma ray attenuation measurements of intercepted snow.

$$I = \left(1 - \frac{C_s}{B}\right)S \tag{3.16}$$

where I is the water equivalent of snow intercepted during a time step, C_s is the initial amount of intercepted snow in the canopy, 13 is the maximum interception capacity of the canopy, and S is the snowfall rate. The maximum interception capacity (B) is given by Kobayashi (1986) based on his experiments with snow interception on narrow boards which suggest that intercepted snow is a function of both air temperature and the area onto which the snow falls:

$$B = L_r LAI \tag{3.17}$$

where LAI is the projected leaf area index of the canopy and L_r is a leaf area ratio which is a function of temperature given by

$$L_r = 0.0005 \qquad T < -3 \tag{3.18a}$$

$$L_r = 0.002 \qquad T > -1 \tag{3.18b}$$

$$L_r = 0.0005\ (1.5T + 5.5) \qquad -3 \le T \le -1 \tag{3.18c}$$

where T is the air temperature in ^{o}C.

Wind can also reduce the intercepted snow. However, wind during snowfall plays a more significant role in canopy interception than wind redistribution after storms, especially if the air

temperature is below -3 °C (Schmidt and Troendle, 1992). The amount of newly intercepted snow blown off the canopy (R) is given by

$$R = \max(5.6e^{-5}UI, I) \quad (3.19)$$

where U is the windspeed above the canopy in meters per hour and I is given by Eq. 3.16 above.

Once the amount of newly intercepted snow is calculated, its snow water equivalent and cold content are added to the intercepted snowpack. The liquid water content of any rain is added to the liquid water content of the intercepted snowpack. The amount of snowmelt (if any) is calculated as for the two-layer snow melt mode1 except that the intercepted snow consists of only a single surface layer and the energy fluxes calculated are applicable to the overstory. Snowmelt can either cause liquid water to drip from the canopy or initiate mass release of snow from the canopy. If the amount of snowmelt plus initial liquid water storage is greater than the liquid water holding capacity but less than a threshold mass release initiation value, then the excess liquid water is allowed to drip out of the canopy. If the amount of snowmelt plus initial liquid water storage is greater than a threshold mass release initiation value then mass release of snow from the canopy is assumed to occur. The threshold liquid water content to trigger mass release is taken as 10 percent of the intercepted snow water equivalent, following Bunnell et al. (1985) and Calder (1990). The mass release mechanism operates by first allowing the threshold liquid water amount which triggered. mass release to drip from the canopy. A set fraction of the intercepted snow water equivalent is then continuously released from the canopy until the liquid water content of the remaining intercepted snow falls below the threshold value or the total amount of intercepted snow falls below a minimum value. For our implementation, the fixed fraction of release is 17 percent and the minimum snow water equivalent below which no mass release can occur (but drip can still occur) is 5 mm.

Solar Radiation Model

Topography exerts an important control on the distribution of solar radiation over a watershed due to the effects of shading and reflection from surrounding terrain, the magnitude of which depends on the time of year and time of day. These topographic controls on solar radiation can play an important role in determining the rate and location of snowmelt in mountainous areas. Prior to running DHSVM, clear-sky solar radiation is calculated for each pixel using the mode1 of Dubayah et al. (1990) as coded in Image Processing Workbench (IPW) routines (Frew, 1990;

Longley, 1992). This method was originally developed by Arola (1993) and was used by Wigmosta et al. (1994) in their application of DHSVM to the Middle Fork Flathead River.

The model of Dubayah et al. computes clear-sky radiation which is then partitioned into direct beam and diffuse radiation using IPW routines following Arola (1993). Together, these methods account for the date, time of day, pixel location, slope, aspect, and the effects of shading or reflection of shortwave radiation from surrounding terrain. Implementation of this method is briefly described below.

IPW is used to compute direct and diffuse beam solar radiation for each three-hour interval for the solar midpoint of each month for every pixel. For each three-hour interval, the time whose instantaneous radiation equals the interval average is as specified by Arola (1993). The predicted solar radiation distribution for the midpoint of each month is then used to represent the entire month. The midpoints of each month are January 17th, February 16th, March 16th, April 15th, May 15th, June llth, July 17th, August 16th, September 15th, October 15th, November 14th, and December 10th (Klein, 1976). For each month, the beam and diffuse components are partitioned into ten classes of the probability distributions over all pixels in the watershed with cumulative probability levels of 0.05, 0.15, 0.25, 0.35, 0.45, 0.55, 0.65, 0.75, 0.85, and 0.95. These classes are then indexed from 0 to 9 and each pixel is assigned a class for both direct beam and diffuse radiation for each time interval in the day and each month. The classes for each daily time interval for a given month are then stored in a file, which DHSVM can use in conjunction with a look-up table which contains the radiation levels for each probability class. This manner of representing incoming solar radiation provides an effective means of characterizing topographic controls on radiation while limiting computational expense. For example, instead of requiring an image of incoming direct beam and diffuse solar radiation (2 images) for each time step in the solar day (4 timesteps of 3 hours each) for all 12 months (total of 96 images at approximately 1.5 Mbytes per image) the incoming; solar radiation can be characterized with only 24 images of class values and 24 lookup tables containing only 10 values for each timestep.

The class images and lookup tables function as follows. For a given month, each pixel has one number which defines its incoming direct beam or diffuse radiation for each time step in the solar day. For example, assuming a solar day of 12 hours or 4 time steps, this number could be 2645, where the first number represents the direct beam class for solar timestep 1, the second number represents the direct beam class for time step 2, etc. The class information is then used to

access the lookup table for each month. For example, 2 would specify a pixel with clear sky direct beam radiation from the cumulative probability level of 0.25 (class 2 of 0 to 9).

The clear sky direct beam radiation is then adjusted for observed cloud cover by (Bras, 1990):

$$I_s = (1 - 0.65N^2) I_c \tag{3.20}$$

where I, is the corrected beam radiation, I, is the clear sky beam radiation, and N is the opaque cloud cover fraction. Diffuse radiation is assumed to be unaffected by cloud cover.

Chapter 4. DHSVM Inputs and Parameters

This chapter describes the input files and parameters required to implement DHSVM. Much of these data were previously generated for the Snoqualmie Watershed by Connelly et al. (1993), and are presented here as a foundation for the model calibration discussed in Chapter 5. Parameter sensitivity is also discussed in Chapter 5.

The input data for DHSVM fall into five main categories: (1) meteorological; (2) topography, as specified by a DEM; (3) land cover and soils; (4) basinwide constant parameters; and (5) initial hydrological state variables for each pixel. Each of these input requirements is discussed in more detail below using examples from the Snoqualmie watershed application. Data storage, manipulation and display for the: project used the U.S. Army Corps of Engineers' GRASS GIS software, but the data required by DHSVM are not dependent on any particular GIS platform.

4.1 Meteorological Data

The simulation period used in the retrospective analysis is from 1948 through 1993. To model the hydrologic response of a watershed accurately, DHSVM must be forced with meteorological data that represent the inputs to the watershed during this period. For the Snoqualmie basin we used meteorological data from the Stampede Pass weather station, which lies just south of the watershed on the Cascade Crest (elevation 1206 m.). Station data required by DHSVM include: air and dewpoint temperatures, cloud cover, incoming shortwave radiation, incoming (above canopy) longwave radiation, windspeed at a reference height above the canopy, and precipitation. Hourly measurements of these data were taken from the NOAA surface airways data base for Stampede Pass and any missing periods were estimated from measurements taken at Sea-Tac International Airport. The local observations of air and dewpoint temperatures were distributed over the watershed via a simple lapse rate method. Local observed values for cloud cover and calculated values of incoming long wave radiation were assumed to be uniform over the watershed. The: distribution of precipitation and short wave radiation were determined by the orographic and solar radiation sub-models as described in Chapter 3. The following additional data are needed to drive the orographic precipitation model: upper atmospheric (850 mb level) windspeed and direction and station (e.g. Stampede Pass) atmospheric pressure. Upper-atmospheric wind direction and magnitude were interpolated to Stampede Pass from the National Meteorological Center grid point data set. Local above-canopy wind speed was not required since the above

canopy wind speed was determined at each pixel based on the upper atmospheric wind speed.

4.2 Digital Elevation Models

Digital elevation data are required to describe the topography of the watershed. The DEM is the fundamental foundation on which DHSVM, and all of its distributed parameters are based. The DEM for the Snoquahnie River watershed and the surrounding area (shown in Figure 4.1) was obtained from the U.S. Geological Survey at a resolution of 3 arc-seconds. Because the 3 arc-second data result in pixel:? that are approximately rectangular (N-S dimension greater than E-W), we resampled the DEM to square pixels of 100 by 100 meters. The watershed was delineated to include: all pixels that eventually drain to the USGS gauge on the Snoquahnie River near Carnation. The delineated basin contained 157,722 pixels or 1,577 km^2, which agrees well with the 156 1 km^2 drainage area reported by the USGS for that gauge.

The orographic precipitation model requires that the base DEM be resampled to a coarser grid resolution (due to computational limitations) which is oriented with the upper atmospheric wind direction (during a particular precipitation event. This resampling (see Chapter 3, Fig. 3.3) was performed for each of 16 wind directions from 0 to 360 degrees at multiples of 22.5 degrees. The resampling produced 16 DEMs for use by the orographic model and 16 slice and cross section description files which map the high resolution DEM onto the orographic model's DEMs.

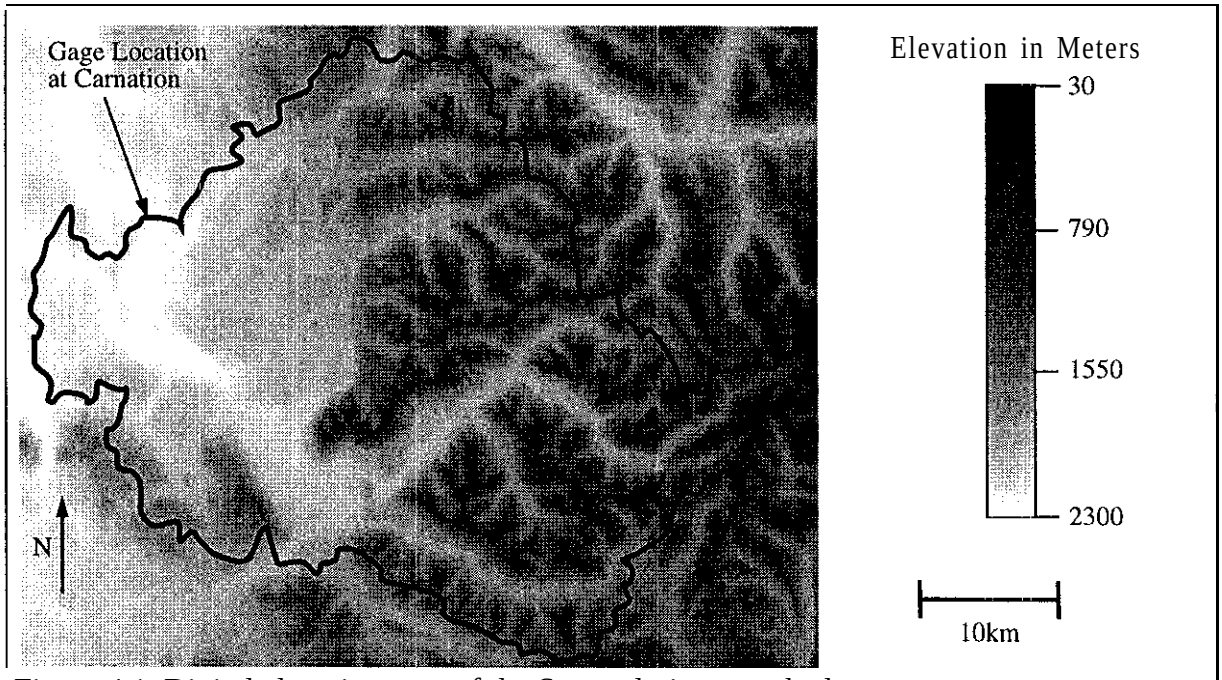

Figure 4.1. Digital elevation map of the Snoqualmie watershed and surrounding area

4.3 Distributed Soil and Vegetation Data

DHSVM also requires information about the soil and vegetation properties of each pixel including vertical hydraulic conductivity, soil depth, soil porosity, overstory leaf area index (LAI), understory LAI, overstory albedo, and many others. However, instead of specifying a value of each soil and vegetation parameter for each DHSVM pixel (which would lead to large data storage requirements), DHSVM uses only the dominant soil and vegetation type of each pixel. All pixels with identical soil classifications are then assigned one set of soil-dependent hydraulic parameters; all pixels with identical vegetation classifications are similarly assigned one set of vegetation-dependent hydraulic parameters. In other words, DHSVM fully describes all soil and vegetation parameters at a given pixel 'by a soil or vegetation class and a lookup table of parameters which is indexed by class.

The distribution of soil classes over the Snoqualmie watershed was obtained from GIS based vector maps of the watershed provided by the Mount Baker-Snoqualmie National Forest USFS station and the Washington Department of National Resources. Both agencies provided data in DLG-3 format which were converted into a 'pixel' based format consistent with the base DEM. This transformation produced an intermediate map from both sources that referenced each DHSVM pixel to a soil index number. These index numbers can in turn be referenced to a num-

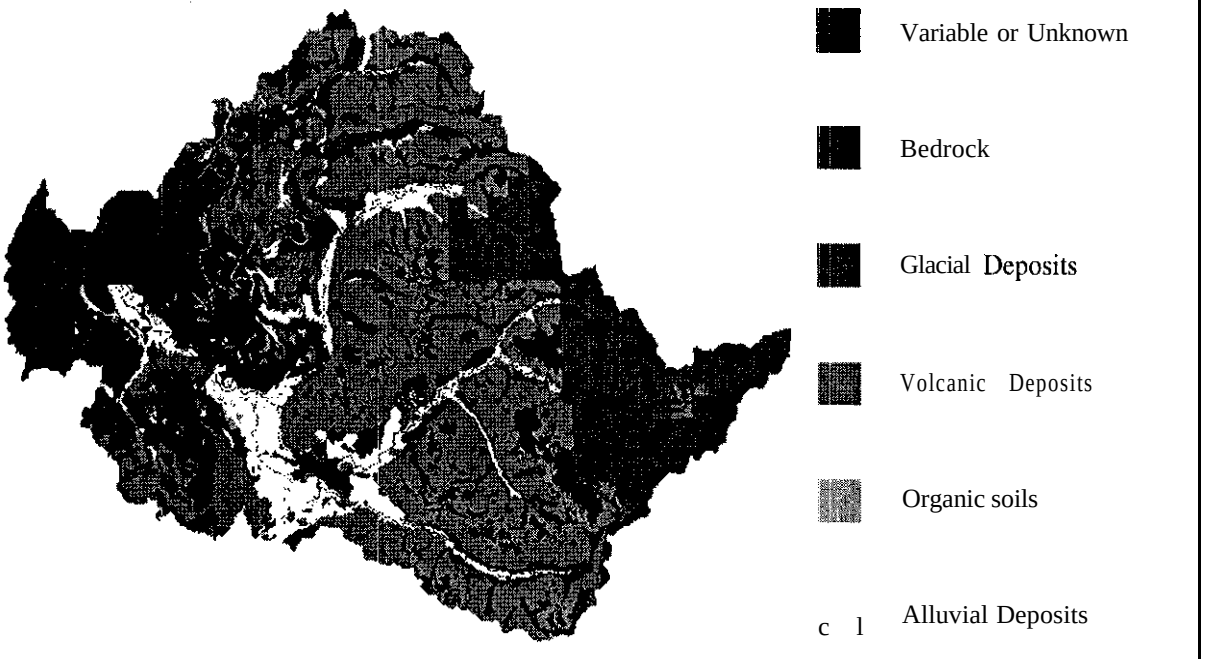

Figure 4.2. Major soil parent materials for the Snoqualmie watershed.

ber of physical soil characteristics including hydrologic class, field capacity and rooting zone depth. However, since the soil index classification schemes used by DNR and USFS were slightly different, we referenced each index number instead to the most consistent basis available, the soil parent material. The resulting map is shown in Figure 4.2. The physical soil parameters belonging to each soil class are listed in Table 4.1.

Table 4.1. Soil parameters for each soil category: Base values for the Snoqualmie Watershed

Parameter	Soil Source					
	bedrock	glacial	volcanic	organic	alluvial	variable
upper zone depth (m)	0.75	0.75	0.75	0.75	0.75	0.75
lower zone depth (m)	0.75	0.75	0.75	0.75	0.75	0.75
porosity	0.49	0.49	0.49	0.49	0.49	0.49
field capacity	0.25	0.25	0.25	0.25	0.25	0.25
wilting point	0.12	0.12	0.10	0.06	0.12	0.12
bubbling pressure (m of water)	0.76	0.52	0.35	0.04	0.76	0.76
vertical hydraulic conductivity (m/hr)	0.030	0.030	0.030	0.030	0.030	0.015
horizontal hydraulic conductivity exponent	0.19	0.19	0.19	0.23	0.19	0.19

The distribution of vegetation classes over the Snoqualmie Watershed was also obtained from GIS based vector maps provided by the USFS, DNR, and the Weyerhauser Corporation. Again, the DLG-3 data were transformed via GRASS into a format compatible with the base DEM. Each DHSVM pixel was then referenced by a stand number from each source data base. The stand reference number was then used to determine each pixel's dominant overstory species and the year it was last cut via attribute tables provided by each source. The dominant overstory vegetation in the Snoqualmie watershed is shown in Figure 4.3 and the parameters related to each overstory class are listed in Table 4.2 . The parameters list in Table 4.2 was compiled from a large number of sources. (Gholz, 1979; Monteith, 1976; Peterson et al., 1987, Gholz et al., 1976; Grier and Running, 1977; Waring et all., 1978; Franklin and Waring, 1980).

For the Snoqualmie basin implementation of DHSVM, each vegetation class was assumed

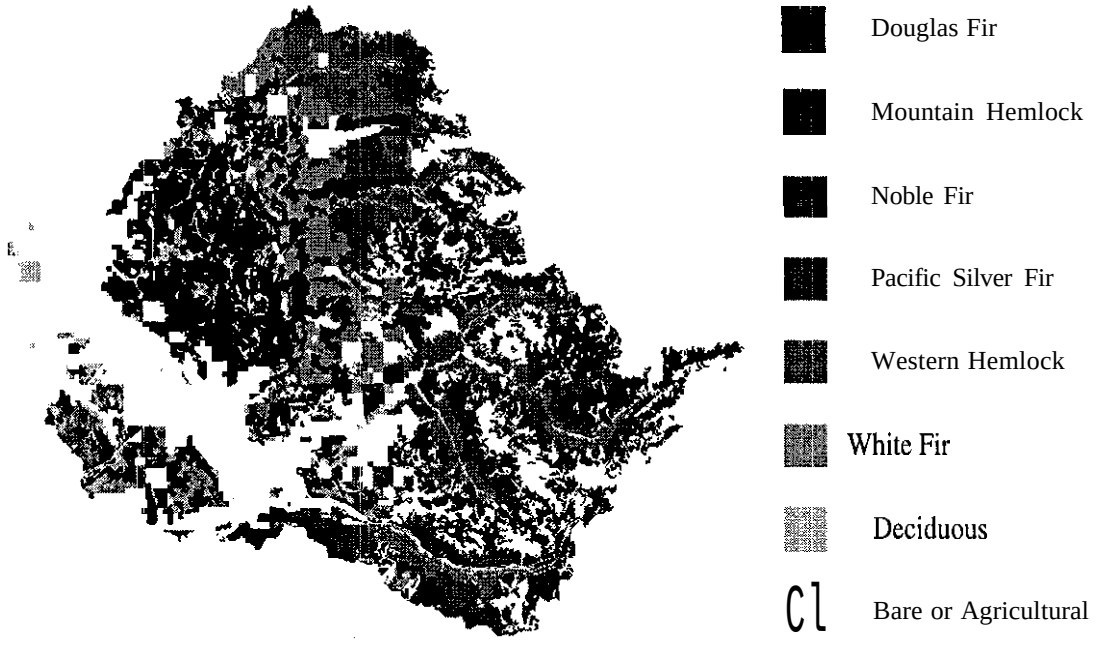

Figure 4.3. Major overstory vegetation categories of the Snoqualmie watershed

to contain an identical understory consisting of a constant LAI of 3.0, an albedo of 0.2, understory height of 0.5 meters, maximum stomatal conductance of 14.4 m/hr, minimum stomata1 conductance of 0.72 m/hr and a critical soil moisture for conductance of 0.13. For each, overstory vegetation class, bare ground was assumed to have an albedo of 0. 1 and a roughness length of 0.0 1 meters. However, DHSVM is not limited to such a simple representation of the understory. Each overstory vegetation class can have associated with it a distinct classification of understory.

In this application of DHSVM it is important to know the age of the overstory on each pixel. The vegetation data provided by each of the three sources specify the year each pixel was last cut. This information was extracted as part of the stand reference numbers and attribute tables. Assuming that each pixel was immediately replanted or seeded after it was cut, the age of the overstory on any pixel which was cut prior to the current simulation year can be estimated. Because the data only specify the last year the pixel was cut, we also assumed that prior to cutting, each pixel contained mature growth. This is equivalent to assuming that any secondary growth was hydrologically equivalent to old growth before it was cut. Therefore, if the pixel was clearcut after the current simulation year, then the pixel is assumed to contain mature growth.

Table 4.2. Overstory parameters for each vegetation category: Base values for the Snoquahnie watershed.

	Douglas. fir	MOW-tain hem-lock	Noble fir	Pacific silver fir	Western hemlock	White fir	Decidu-ous	Bare or agricul-tural
canopy attenuation coefficient.	0.5	0.5	0.5	0.5	0.5	0.5	0.5	0.5
summer overstory LAI (2-sided)	18.0	16.8	22.x	32.1	25.4	25.4	14.4	3.0
winter overstory LAI (Z-sided)	18.0	16.8	22.8	32.1	25.4	25.4	3.0	3.0
age when overstory LAI = maximum	20.0	20.0	20.0	20.0	20.0	20.0	20.0	0.0
overstory albedo	0.18	Cl.18	0.18	0.18	0.18	0.18	0.18	0.18
overstory height	75.0	35.0	50.0	50.0	60.0	50.0	30.0	1.0
age when overstory height = maximum	80.0	80.0	80.0	80.0	80.0	80.0	80.0	0.0
exponential wind-speed decay coeffi-cient	1.5	1.5	1.5	1.5	1.5	1.5	1.5	1.5
displacement height ratio (d/b)	0.63	0.63	0.63	0.63	0.63	0.63	0.63	0.63
roughness length ratio (z/h)	0.13	0.13	0.13	0.13	0.13	0.13	0.13	0.13
maximum overstory fractional coverage	0.9	0.9	0.9	0.9	0.9	0.9	0.9	0.9
age when coverage = maximum	20.0	2:0.0	20.0	20.0	20.0	20.0	20.0	0.0
overstory maximum stomata1 conduc-tance (m/hr)	10.8	10.8	10.8	10.8	10.8	10.8	10.8	10.8
overstory minimum stomatal conduc-tance (m/hr)	3.6	3.6	3.6	3.6	3.6	3.6	3.6	3.6
critical soil moisture content for overstory conductance	0.33	0.33	0.33	0.33	0.33	0.33	0.33	0.33
overstory light level	0.108	0.108	0.108	0.108	0.108	0.108	0.108	0.108
fraction of over. roots in upper soil layer	0.5	0.5	0.5	0.5	0.5	0.5	0.5	0.5

The distribution of most recent cut dates is shown in Figure 4.4a.

Figures 4.4b and 4.4c show the calculated age of the overstory for each pixel in the watershed for years 1948 and 1989. Note that some regions are represented as 0 years old in both images. These regions represent bare areas that were either never reforested after they were cut

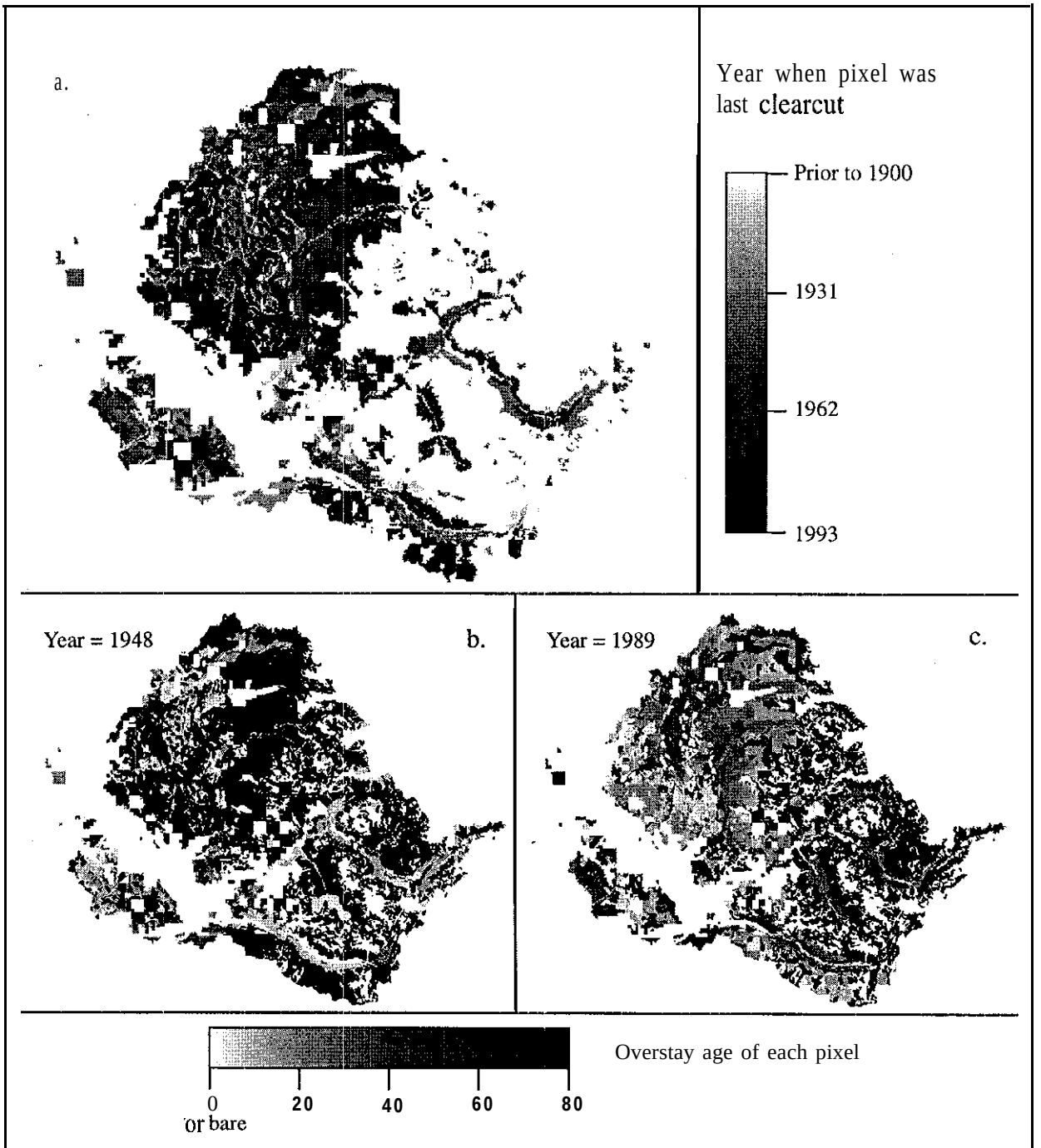

Figure 4.4. Year of Origin file used by DHSVM to predict overstory age. Examples shown for 1948 and 1989.

(e.g. the Snoqualmie valley between Snoqualmie and Carnation), or were always bare. Comparison of the 1948 and 1989 images shows that there was significant harvesting in the northwest portion of the watershed during this, period. A time trend analysis of the Snoqualmie watershed harvest history is presented in Chapter 6 (see e.g. Fig. 6.1) in the context of a retrospective analysis of trends in peak flows.

4.4 Constant Parameters

In its current form, not all of DHSVM's parameters are distributed. These parameters along with the base values used for the Snoqualmie Watershed application are presented in Table 4.3. This limitation could easily be removed if the application warranted.

Table 4.3. DHSVM Basinwide Constant Parameters: Base Values for the Snoqualmie Watersbed

Parameter	Value
Saturated horizontal hydraulic conductivity	0.1 m/hr
Edge length of square grid cell (pixel size)	100 m
Saturated hydraulic conductivity exponential decay coefficient	1.0
Snow roughness length	0.015 m
Wind measurement height (must be greater than maximum overstory height, not used if orographic precipitation model is active)	80 m
Vapor pressure deficit causing stomatal closure	4mb
Visible light fraction of total short wave radiation	0.5
Base meteorological station elevation (i.e. Stampede Pass elevation)	1125 m
Temperature lapse rate	0.006 C/m
Dewpoint lapse rate	0.00125 C/m
Temperature below which all precipitation is snow	0 C
Temperature above which all precipitation is rain	3.3 C
Maximum snow pack surface layer water equivalent	0.125 m
Depth of soil below the rooting zones	1.5 m

4.5 Initial Hydrologic State Variables

DHSVM calculates a number of hydrologic state variables at each pixel for every time step. Initialization of these variables must be provided at the start of the simulation. These include the distribution of soil moisture in both rooting zones, depth to the water table, snow

water equivalent on the ground and intercepted in the canopy, liquid water depth stored by both the overstory and understory. Also, DHSVM must be supplied with an initial set of flags (O-l variables) which specify whether or not each pixel contains: (1) any snow on the ground; (2) any snow in the canopy; and (3) an understory.

4.5 Distributed Routing Model Parameters

The distributed routing model used by DHSVM is based on a travel time, distribution to the outlet from each pixel as described in Chapter 3. To use this model, an input file must be constructed which contains the average travel time (in integer hours) to the outlet from each pixel. Furthermore, a file describing the shape of the unit hydrograph for each possible value of travel times and model timesteps must be made available to DHSVM. For this application, two FOR.. TRAN programs were written to generate these files for DHSVM. One program generates the travel time file given the base DEM and values of average, minimum and maximum channel velocities. The other generates the unit hydrographs for each travel time given a value of the routing storage parameter, the possible model time steps (DHSVM can use variable time steps in a simulation) and the maximum travel time to the outlet.

Chapter 5. DHSVM Snoqualmie Watershed Calibration

Even though DHSVM is physically based, which in theory should preclude calibration, some calibration is required since there is considerable uncertainty in many of the required parameters, This chapter discusses estimation of the following distributed and fixed parameters for the Snoqualmie watershed (1) leaf area index (LAI), (2) stomata1 conductance, (3) horizontal saturated hydraulic conductivity!, (4) vertical saturated hydraulic conductivity, and (5) depth of the top rooting zone soil layer. (Calibration of the orographic precipitation model, distributed routing model and verification of the snow melt model are discussed in Chapter 3.)

5.1 Selection of Calibration Period

DHSVM was implemented with base parameters (described in Chapter 4) for the period March 1, 1983 to November 30, 1986 at a daily timestep. The mean daily observed flow of the Snoqualmie river as measured b,y the USGS gaging station near Carnation (#12149000) is shown in Figure 5.1. The period of record for this gage begins in 1928 and contains no significant diversions except during water year 1985 in which the Seattle Water Department diverted an average daily discharge of 2 cms upstream from the gage for municipal use. Several smaller diversions occurred upstream of the gage for irrigation or domestic use. Low flow diversions also occurred for operation of the Snoqualmie powerplant, but water is returned to river upstream of gage. Overall, 'USGS rates the records for this gage as good, and for the purposes of our analysis, the diversions are negligible.

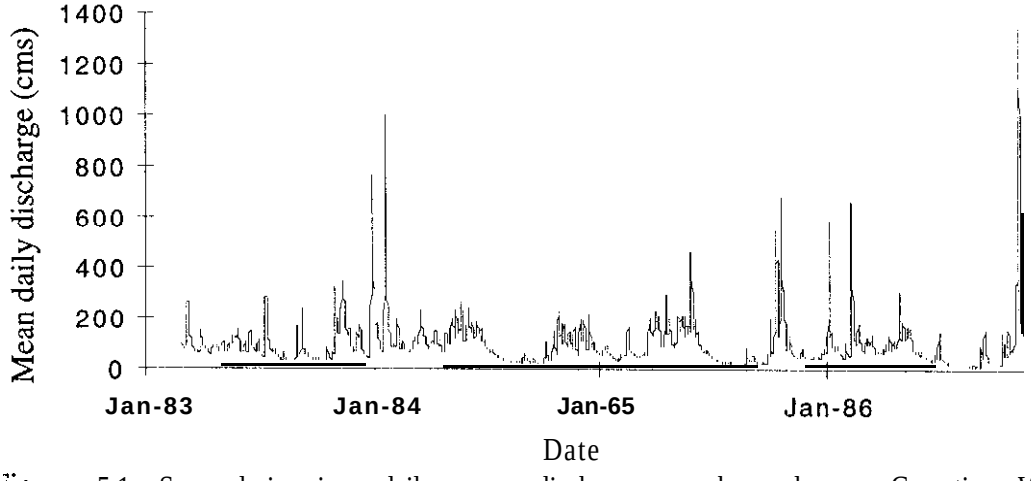

Figure 5.1. Snoqualmie river daily mean discharge as observed near Carnation WA between March 1 1983 and November 30 1986.

The calibration period contains a number of interesting rain-on-snow events, including the flood of November 1986 (instantaneous peak observed discharge of 1617 cms) which was the third largest flood recorded at the gage. The ROS events of January 1984 (instantaneous peak of 1206 cms) and February 1986 (instantaneous peak of 816 cms) occurred with wet initial conditions whereas the November 1986 storm occurred with relatively dry initial conditions. This calibration period also contained a single large summer event (524 cms) during June 1985. This range of initial conditions and event timing provides a good testing series for DHSVM. Although the flood of November, 1990 (the second largest recorded, at an instantaneous peak of 1846 cms) was not included in the calibration period, it was used to verify the performance of the model after the calibration was complete.

Initial hydrological conditions on March 1, 1983 were specified as follows for all calibration runs: snow water equivalent was set to a uniform value of 0.5 meters with no snow or water intercepted in the canopy or understory; saturation deficit was set to zero meters over the entire basin and the soil water content of both soil layers was set to saturation over the watershed; each pixel was forced to contain an understory. These initial values are appropriate estimates of actual conditions for the first of March,. Land cover was adjusted to represent forest conditions as observed in 1986.

5.2 DHSVM with Base Parameters

The mean predicted daily discharge with base parameters and the mean observed daily discharge for the entire calibration period are compared in Figure 5.2. The total predicted precipitation input during this simulation was 9953 mm. The total predicted discharge (6752 mm) is slightly less than that observed (‘7115 mm). While most events are well represented, the large rain on snow streamflows of January 1984 and February 1986 are overestimated while the November 1986 flood is underestimated. However, the summer event of 1985 is well estimated. The overprediction followed by an immediate underprediction during this summer event (and several other events during the calibration series) is caused by the inaccuracy of the routing model in simulating a twenty-four hour time step. When these events are simulated at a three hour time step, the accuracy of the predictions improves.

Examination of some other variables calculated by DHSVM during this simulation period allows for a more thorough evaluation of the base parameters. Figure 5.3 shows average soil

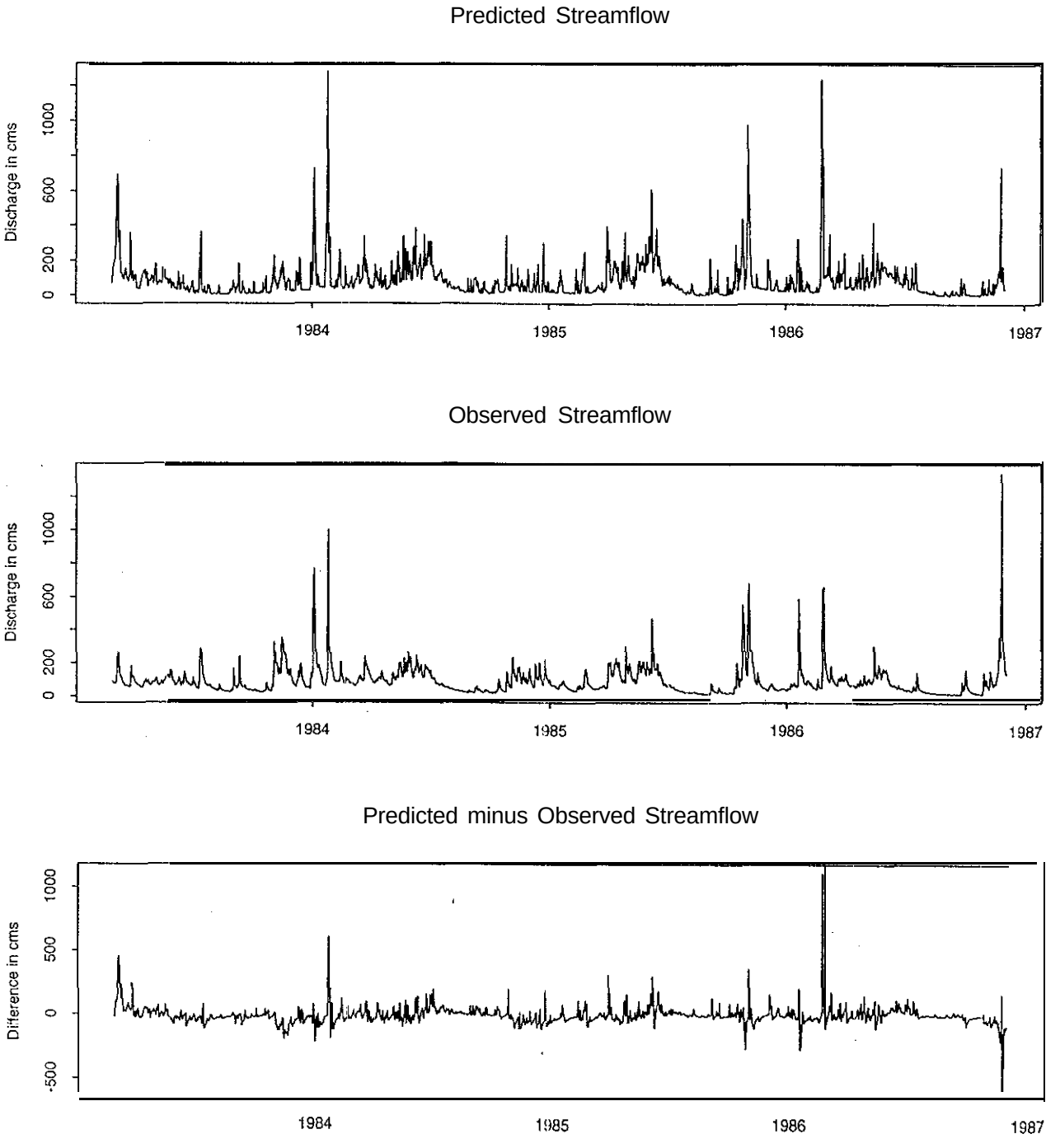

Figure 5.2. Comparison of observed vs. predicted discharge during the calibration period for DHSVM with base parameters.,

moisture in both soil layers over the entire watershed and the average saturated deficit in the watershed. The: annual cycle in soil moisture is clearly present; the watershed dries out during the summer months and becomes wet during the winter months as expected. Furthermore, the absence of long-term trends, such as the soil moisture decreasing continuously without sufficient recovery in the winter months, is indicative that DHSVM is behaving properly.

The daily average basinwide evapotranspiration during the simulation is shown in Figure 5.4. The seasonal cycle is clearly shown with most evapotranspiration occurring during the summer months and little evapotranspiration occurring in the winter months. However, the total amount of evapotranspiration predicted with the base parameters is too high. A total of 3,350 mm of evapotranspiration are predicted over the four growing seasons simulated (approx. 800 mm/year) with maximum basinwide averages above 10 mm/day. Expected yearly amounts of evapotranspiration in the Snoqualmie watershed are closer to 500 mm/year while the maximum observed daily evapotranspiration from a mature Douglas Fir is approximately 5 mm/day (Fritschen et al., 1973). These simulation errors called into question our estimates of LAI and stomatal conductances.

5.3 LAI and Stomatal Conductance

The base values of LAI were obtained from references which based their measurements of LAI on an empirical equation which relates LAI to the tree diameter at breast height for a number of different species (Gholz, 1976). However, Marshall and Waring (1986) have shown that LAI estimates based on tree diameter for such large species as Douglas fir can overestimate LAI by nearly 100 percent. Published Douglas fir LAI estimates based on tree diameter range between 9.3 (Gholz, 1982) and 21.8 (Waring et al., 1978) while estimates based on sapwood diameter measurements (which Marshall and ‘Waring suggest are more reliable) range from 7.3 (Waring et al. 1980) to 12.0 (Waring et al., 1981). (All measurements in these references were made in the Oregon Cascade Range.)

The values of LAI used as base parameters are all two-sided. However, the Penman-Monteith equation was originally developed for use witb one-sided estimates of LAI. For example, Monteith (1975) gave estimates for LAI of coniferous forests between 2 and 5. Therefore, the two sided estimates of LAI were converted to one-sided values by dividing by 2.3 before using the values to estimate evapotranspiration. To bring our elevated two-sided LAI values into

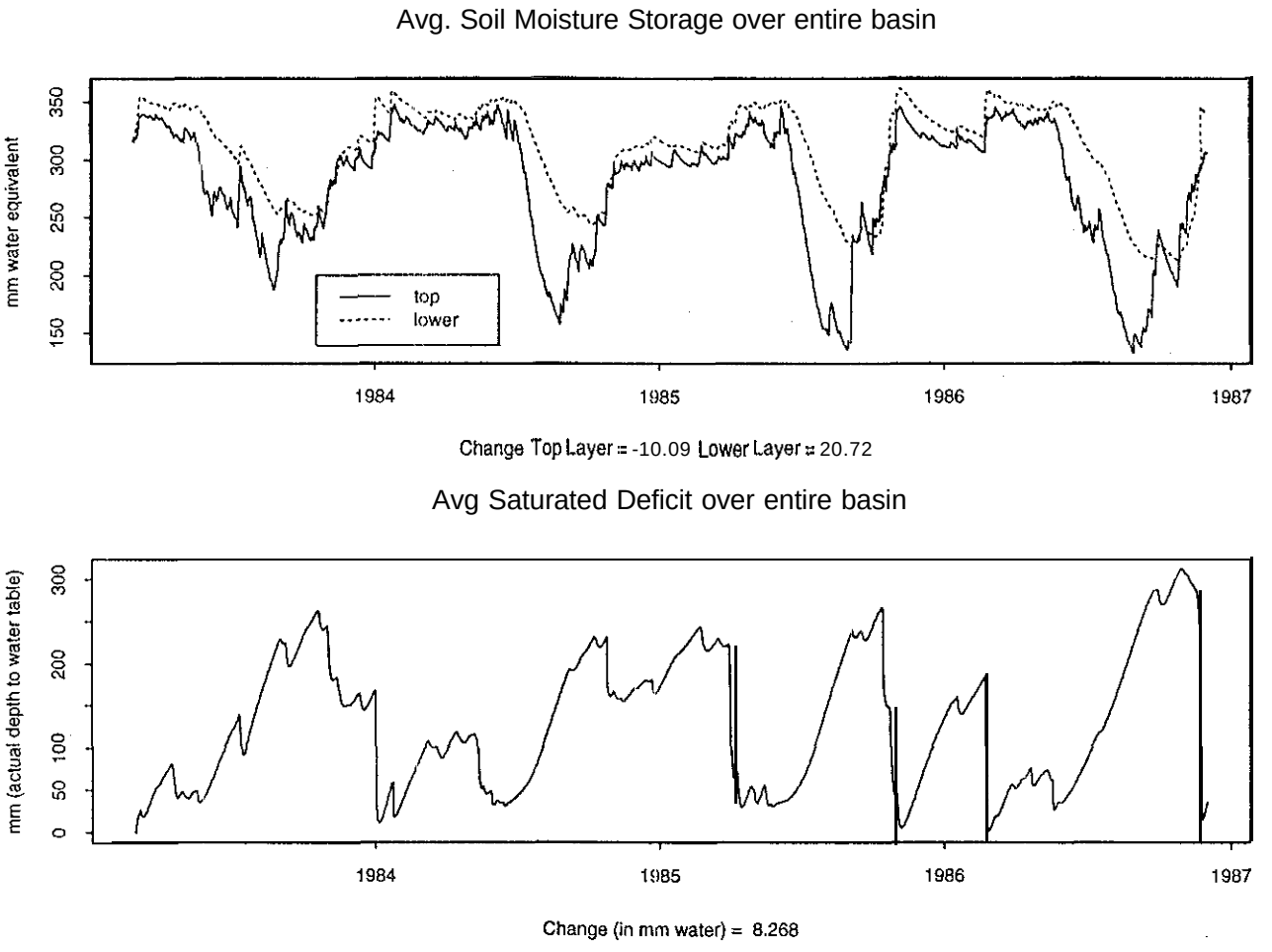

Figure 5.3. Predicted basinwide average soil moisture and saturated deficit during the calibration simulation with base parameters.

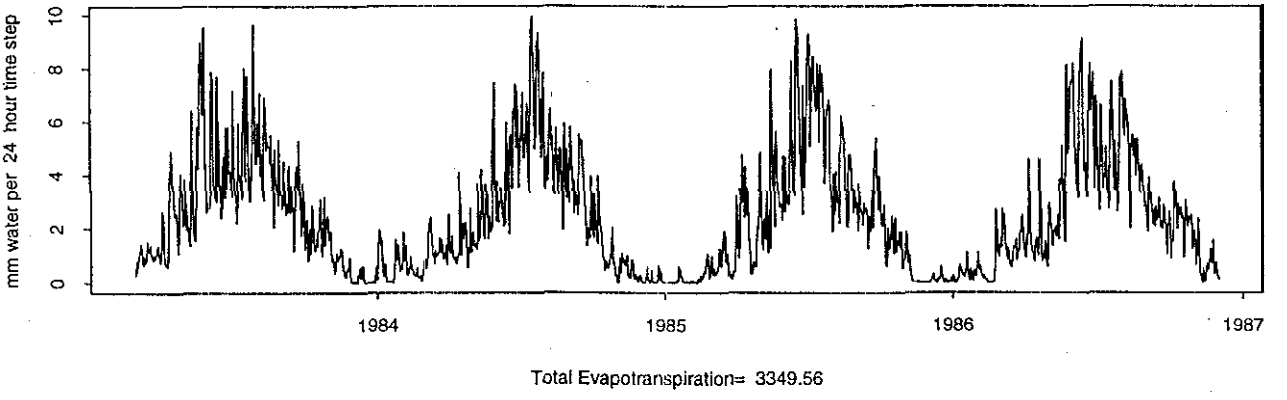

Figure 5.4. Predicted basinwide daily average evapotranspiration with base parameters.

agreement with the lower values discussed above, the two-sided base values of LAI were all multiplied by 2/3. This reduction, along with a reduction in the maximum stomata1 conductance of overstory from 10.8 to 5.4 (Monteith, 1976), reduced the average evapotranspiration over one season to 550 - 600 mm/year while reducing the maximum observed rates of evapotranspiration to a more realistic 5 - 6 mm/day,.

The orographic precipitation model was then calibrated (details presented in Chapter 3) such that the total predicted discharge matched that observed. This reduced the total predicted precipitation input for all subsequent calibration runs to 9668 mm.

Figure 5.5 presents a comparison of the observed and predicted discharges for the calibration period from DHSVM with the revised evapotranspiration parameters and updated precipitation models. Due to the decrease in predicted precipitation, the amount of overprediction during the January 1984 and February 1986 events has decreased while the amount of underprediction during the November 1986 event increased. One possible explanation for the over and under prediction is that for the events which are overpredicted, DHSVM is simply predicting more precipitation than actually occurred for the winter ROS events while underpredicting the precipitation for the November 1986 event. This possibility was ruled out by checking the observed precipitation at a number of stations around the basin (the same stations used in the orographic precipitation model calibration) and comparing those values to the predicted basinwide precipitation. In all cases, the predicted precipitation is an accurate reflection of the observed values.

5.4 Vertical Saturated Hydraulic Conductivity

Another explanation for these errors is that not enough infiltration is occurring. To check this possibility, the last simulation (shown in Figure 5.5) was repeated with all saturated vertical hydraulic conductivities (Kv) set to 0.1 m/hr. The observed vs. predicted discharges for this simulation are shown in Figure 5.6, and indicate that increasing the saturated vertical hydraulic conductivity has no noticeable effect on the predicted discharge. The errors in prediction are unchanged. This result is not surprising considering that Pacific Northwest soils are rarely infiltration limited. Therefore we would expect that increasing their vertical infiltration rates from realistic values by increasing Kv would not change the predicted discharges much.

5.5 Horizontal Saturated Hydraulic Conductivity

The saturated horizontal hydraulic conductivity (Kh) can greatly affect peak discharges.

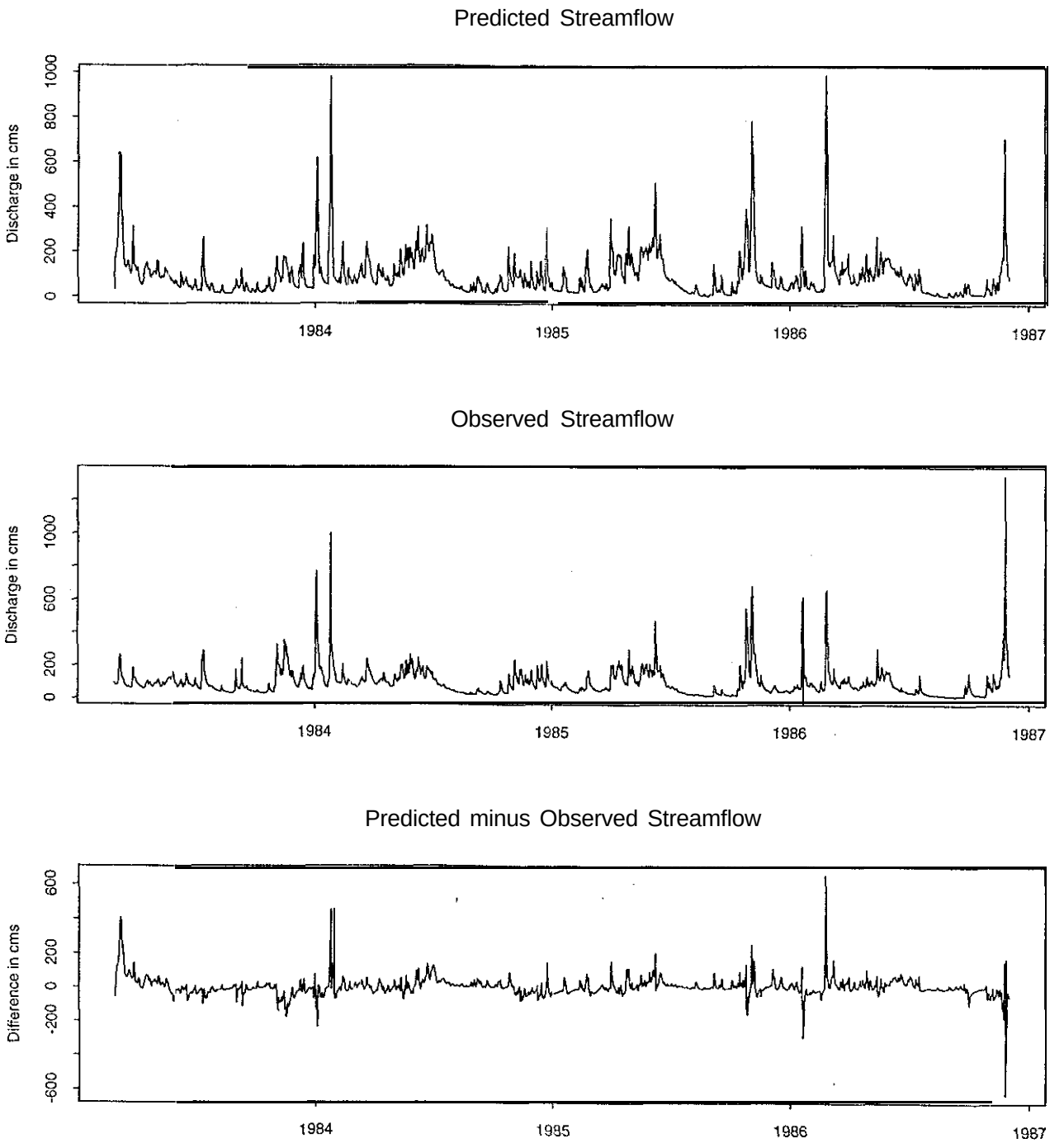

Figure 5.5. Comparison of observed vs. predicted discharge for DHSVM with revised LAI and stomata1 parameters.

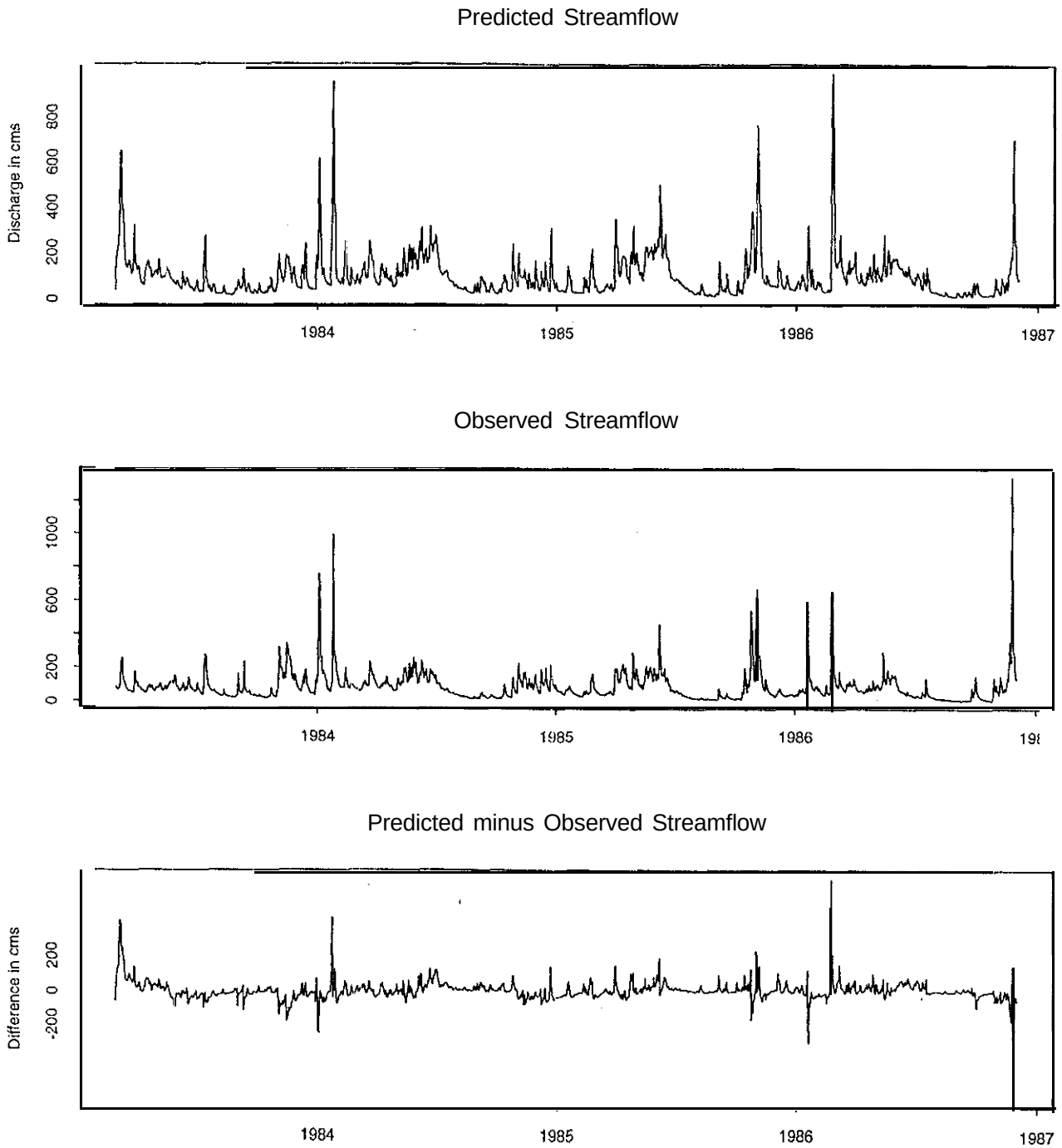

Figure 5.6. Comparison of observed vs. predicted discharge for DRSVM with revised vertical hydraulic conductivity.

This parameter directly controls the rate at which groundwater discharges to neighboring pixels. Increasing Kh will increase the flow of groundwater downslope and thus increase the level of baseflow into the river while accelerating the drydown of the watershed. A decrease in Kh will have the opposite effect. To illustrate these changes the simulation presented in Figure 5.5 (original vertical hydraulic conductivities) was repeated with Kh reduced from 0.1 to 0.01 m/hr. The results are shown in Figure 5.7. The impact on the predicted discharge is dramatic. The amount of overprediction for the two winter ROS events is increased by almost a factor of two while the previous error in prediction of the November 1986 event is unchanged in magnitude but reversed in direction. Also, the baseflow level in the summer months is significantly decreased as Kh is decreased.

From these result, we can conclude that the previous underprediction of the November 1986 event was mostly caused by excessively dry initial conditions. This conclusion is supported by the soil moisture distributions during the simulation period. Figure 5.8 compares the average soil moisture levels in both soil layers and the saturated deficit during the simulations with a Kh set to 0.1 m/hr and 0.01 m/hr, respectively. With a Kh set to 0.1 m/hr, the soil moisture levels in both the upper and lower rooting zones fluctuate from near saturation in the winter months to just below field capacity in the summer months while the saturated deficit cycles from near zero in the winter months to approximately 300 mm in the summer months. With a Kh of 0.01 m/hr, we observed almost no departure from saturation for the lower soil zone during the year. During the summer months, the upper soil zone does dry out to similar levels as seen with a Kh of 0.1 m/hr. However, during the winter months, the upper soil layer is nearly continuously at saturation, Also, with a Kh of 0.0 l m/hr, there is almost no increase of the saturated deficit from zero during the year. Since DHSVM represents infiltration as a one-dimensional process, an unrealistically wet subsurface will quickly translate any precipitation into runoff, thereby overpredicting discharge.

Another interesting note regarding the value of the horizontal saturated hydraulic conductivity is that our simulations show it has little effect on the amount of evapotranspiration. With a Kh of 0.1 m/hr DHSVM predicted 2507 mm of evapotranspiration while a Kh of 0.01 m/hr resulted in 254X mm. At first this might seem surprising since the decrease in Kh increased soil moisture levels., However, the summer values of soil moisture in the upper layer were equally low during both simulations while thu: summer values of soil moisture in the lower layer were not

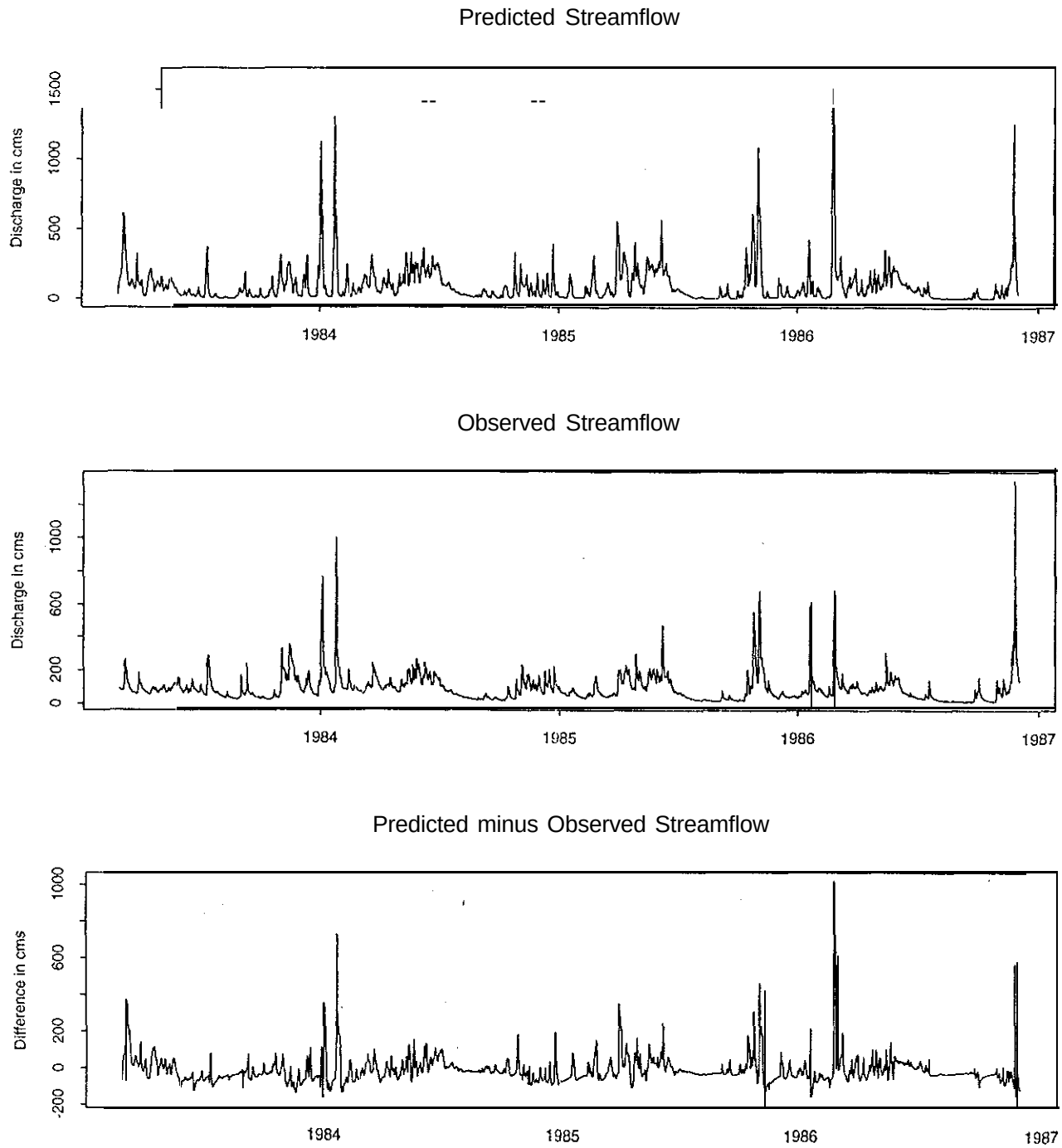

Figure 5.7. Comparison of observed vs. predicted discharge for DHSVM with revised hydraulic conductivity.

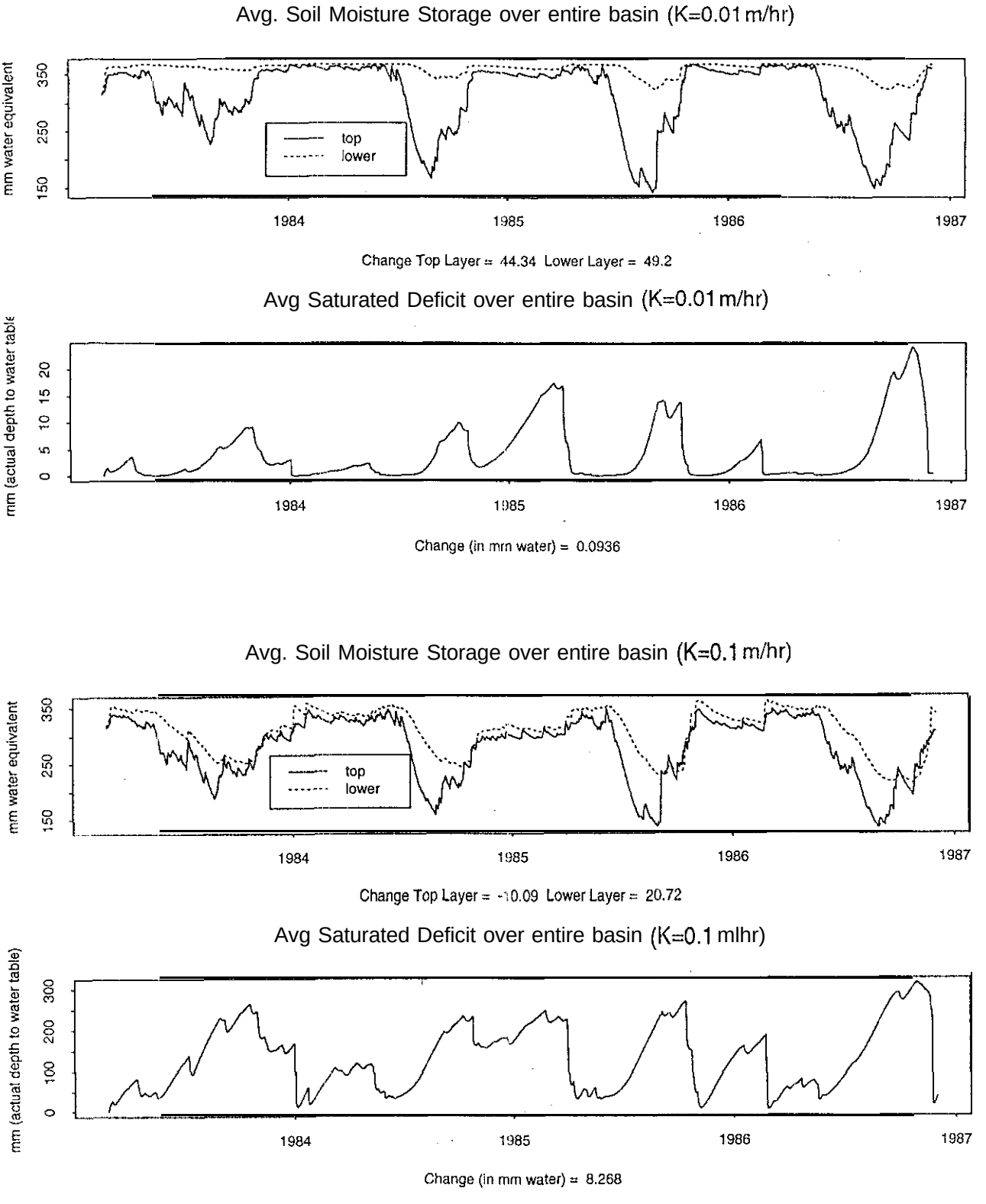

Figure 5.8. Comparison of soil moisture and saturated deficit predicted with horizontal hydraulic conductivities of 0.01 and 0.1 m/hr.

decreased enough so that available soil moisture began to limit evapotranspiration.

5.6 Depth of Upper Rooting Zone Soil Layer

Another parameter which can affect the translation of precipitation into runoff is the thickness of the soil layers. A thick soil layer will store more precipitation before producing runoff than a thin soil at identical soil moisture levels below saturation. This parameter was tested by decreasing the thickness of the upper soil layer from 0.75 to 0.25 meters, thereby decreasing the thickness of the: entire rooting soil layer from 1.5 to 1.0 meter (Kv and Kh remained at base values). This change is consistent with observations in the Snoqualmie watershed which report root development between 6 and 28 inches into the soil (USFS, 1973). The results are shown in Figure 5.9. Note that this change has little affect on the January 1984 and February 1986 event but does slightly improve the estimate of the November 1986 event. However, the November 1986 flood is still underestimated. Overall, changing the depth of the upper rooting zone soil layer has little impact on the performance of DHSVM for the Snoqualmie basin.

5.7 Additional Calibration

The results presented above reveal that the horizontal saturated hydraulic conductivity is the most sensitive parameter of those tested. Unfortunately, it can vary by orders of magnitude even in relatively homogenous subsurface materials. Even if point measurements of Kh were available, they most likely would not be directly applicable given the conceptualization of the downslope moisture redistribution used in DHSVM. Therefore, the value of Kh must be chosen with care. To this end, we performed a large number of simulations to find the 'best' value for this parameter in the range of 0.1 m/hr and 0.01 m/hr. Although increasing Kh above 0.1 m/hr improved the predictive capability of DHSVM for the January and February storms, it worsened simulation of the November 1986 unacceptably. Our objective in this stage of the calibration was to simulate the November 1986 event adequately while minimizing the remainder of the residual series especially the January 1984 and February 1986 events. This calibration requires a tradeoff between accuracy of ROS events with wet initial conditions and those with dry initial conditions. To aid in this calibration, DHSVM was run with a variable time step. The period from March 1, 1983 to September 30, 1986 was simulated at a daily time step while the period from October 1, 1986 until November 30, 1986 was simulated at a three-hour timestep. Simulating the November event at a three hour time step allows for detailed examination of the effect of Kh on the peak dis-

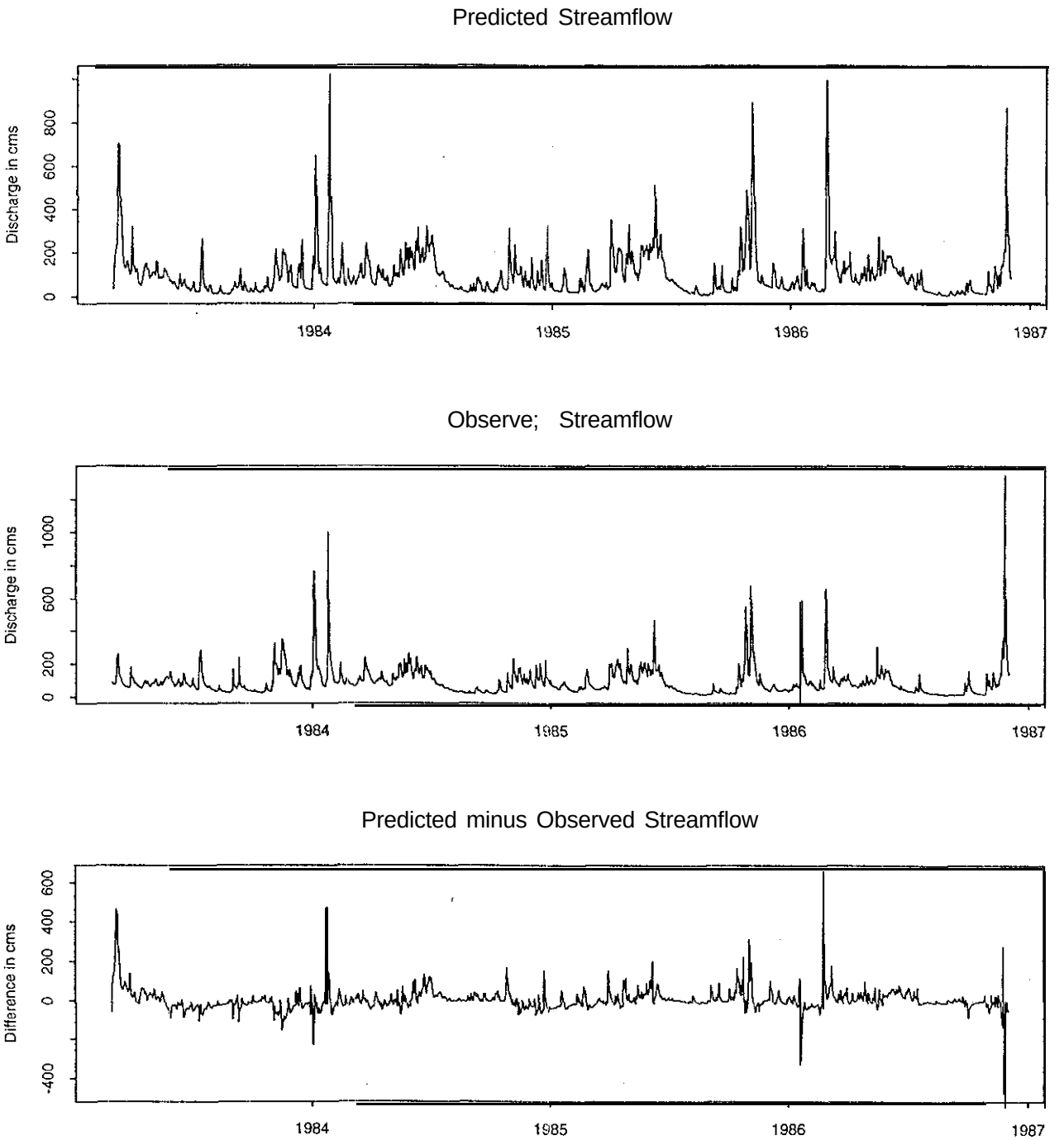

Figure 5.9. Comparison of observed vs. predicted discharge for DBSVM with revised upper rooting zone soil thickness.

charge and the timing of the predicted and observed hydrographs.

The results of this analysis suggested that a horizontal saturated hydraulic conductivity of 0.03 m/hr allows for an accurate simulation of the November 1986 while not significantly worsening the performance of the model during the January 1984 and February 1986 events. The final results with a K.h of 0.03 are shown in Figures 5.10 and 5.11. Figure 5.10 shows the predicted discharge with a three hour time step and the observed hourly discharge for the November, 1986 event. Note that the peak is slightly underestimated but the timing and duration of the event are well simulated. Although the peak could be better approximated by further decreasing Kh, this would have worsened the performance for the winter ROS events. The predicted and observed streamflow and the residual series for the simulation period from March, 1983 through September, 1986 is shown in Figure 5.11.

Table 5.1 compares the maximum mean daily predicted discharge for DHSVM simulations with Kh equal to 0.01, 0.03 and 0.1 m/hr to the observed peak daily discharge for the January 1984 and February 1986 events. Increasing Kh from 0.1 to 0.03 results in a small increase in the overprediction of the January 1983 event and a more modest increase in oveiprediction of the February 1986 event but yields a large improvement in the prediction of the November 1986 event, although it is still underestimated. Any further decrease in Kh results in unacceptably large overpredictions of the January and February events without any significant improvement in the

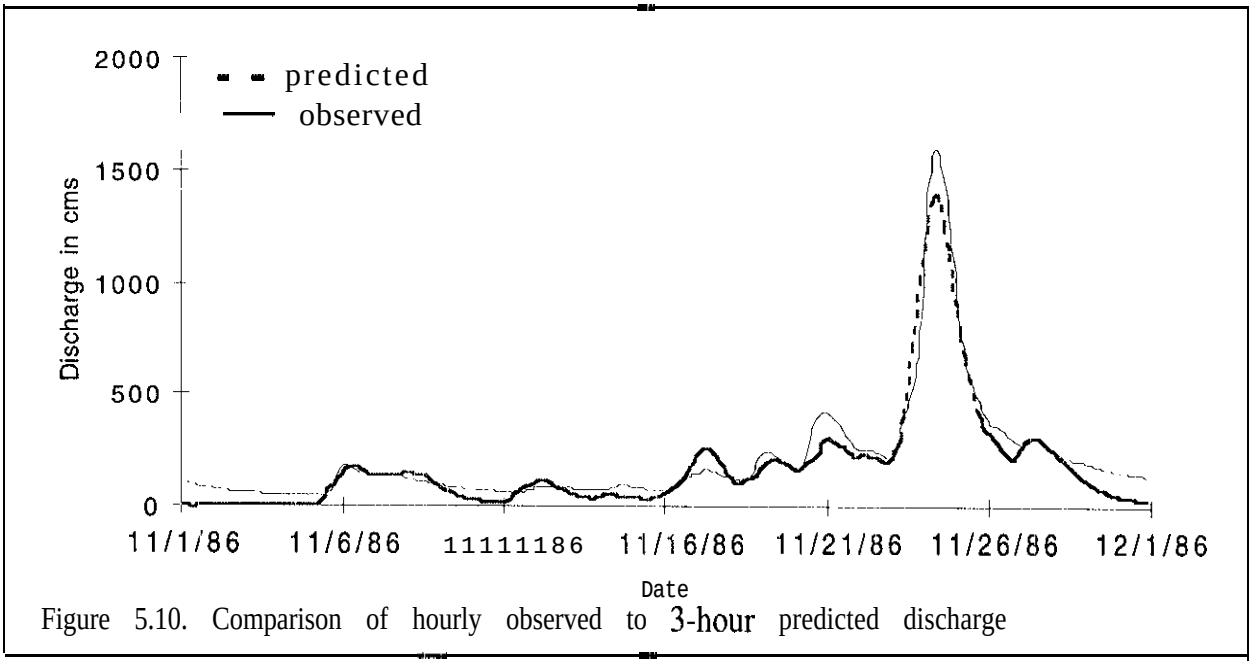

Figure 5.10. Comparison of hourly observed to 3-hour predicted discharge

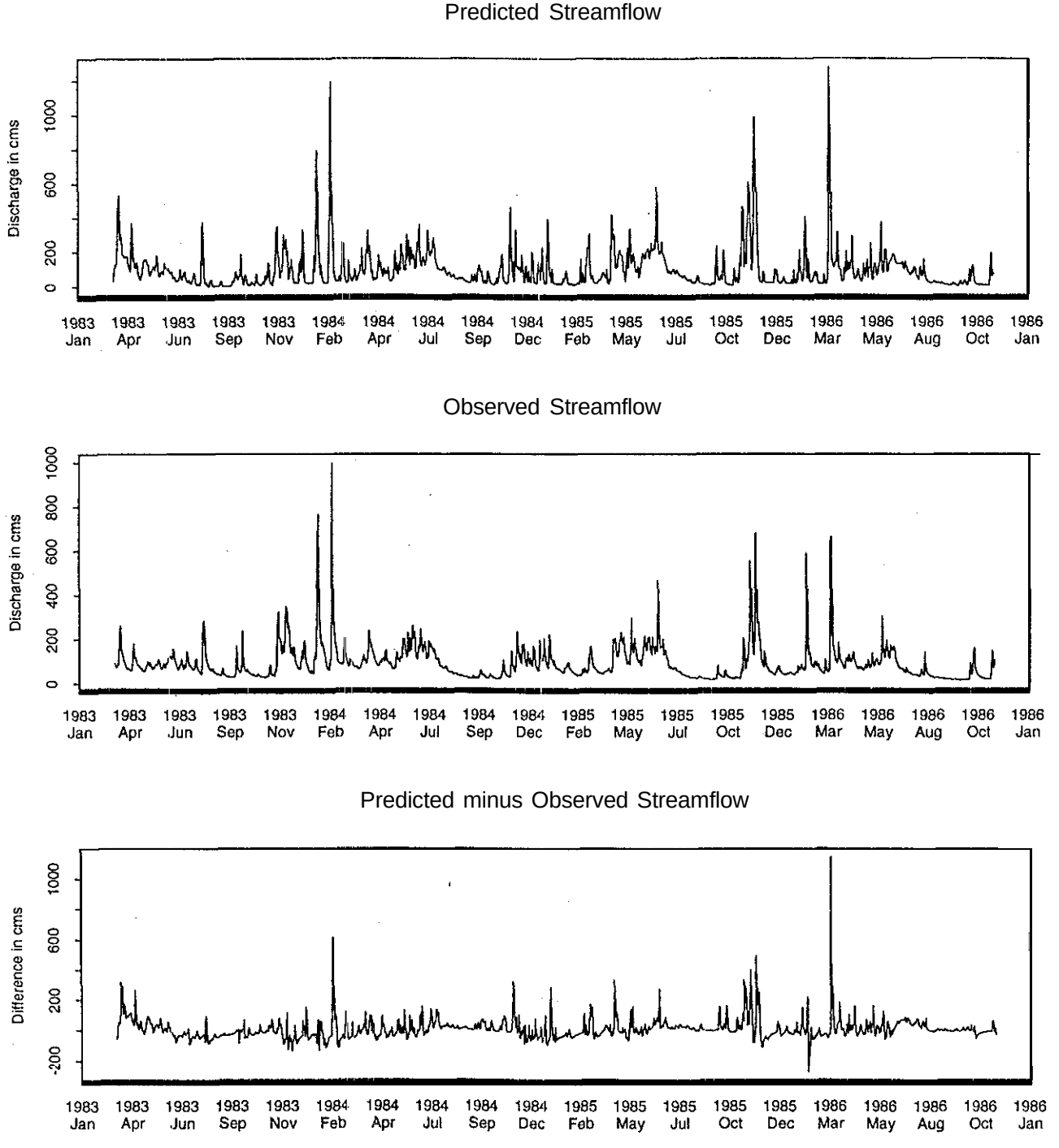

Figure 5.11. Comparison of mean daily observed vs. predicted discharge for calibrated DHSVM.

November event.

The calibrated DHSVM was then used to simulate the period between November 1, 1990 and November 30, 1990 during which the second largest recorded flood on the Snoqualmie river occurred. A three hour model time step was used for this simulation. Initial conditions for this event were obtained by simulating the period from the end of the calibration period (November 30, 1986) through October 31, 1990 at a daily time step. The final values of the initial variables on October 3 1, 1990 were used as the initial conditions. The observed and predicted streamflows for the November 25 event are shown in Figure 5.12. The magnitude, timing and duration of the peak flow are well predicted, especially considering the magnitude of the observed event.

Table 5.1 Comparison of predicted and observed maximum mean daily discharges for three ROS events

Simulation Parameters	January 1983 streamflow (cms)	February 1986 streamflow (cms)	November 1986 streamflow (cms)
observed	996	659	1345
Kh=0.1 m/hr	980	989	713
Kh=0.03 m/hr	1190	1272	1231
Kh=0.01 m/hr	1295	1583	1252

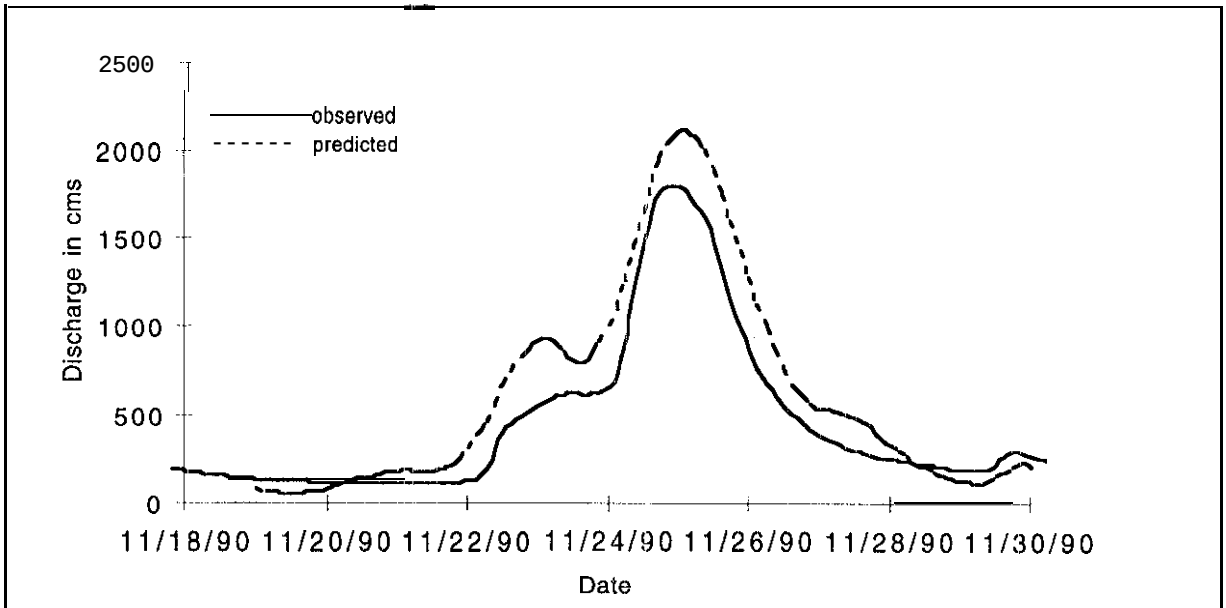

Figure 5.12. Verification of DHSVM model calibration on November 1990 ROS event

Chapter 6. Retrospective Analysis

The central hypothesis of our work is that forest harvesting can lead to changes in peak streamflows. One problem in evaluating whether or not changes have occurred is that trends related to vegetation changes can be confounded with those due to climatic variations. In this chapter, we perform a retrospective analysis of the historic streamflow record of the Snoqualmie River at Carnation using DHSVM to control for climate changes. Since DHSVM explicitly models the climatic record for the entire record with fixed land cover conditions, any trend in the predicted minus observed discharge (residual) time series can be attributed to land use changes. Our analysis focuses on simulating the annual maximum series (AMS) and peaks over threshold (POT) for the 46 year period 1948 through 1993 using 1989 land use conditions. If the cumulative effects of forest harvesting have increased peak streamflows over time then DHSVM should overpredict peak events early in the retrospective period and this level of overprediction should decrease as the simulation approaches the present.

6.1 Retrospective Analysis Implementation.

Simulation of the annual maximum series from 1948 until 1993 requires that DHSVM be run continuously for this entire period so that antecedent conditions are estimated properly. Simulation of the entire period at a 3 hour time step would require approximately 134,000 timesteps and nearly 70 days to complete on a Sun Sparc 20 workstation. To reduce the simulation time, we used a variable time step which simulated the majority of the record with a daily time step. Each annual maximum event was simulated with a three hour timestep for five days before and after the event. This approach reduces the total number of time steps to approximately 20,000, and the total run time to 10 days.

Initial conditions for January 1, 1948 were set identical to the initial conditions for the calibration period, i.e. fully saturated soils and groundwater levels with 0.5 meters of snow water equivalent over the basin and no intercepted snow. All pixels were assumed to contain an understory and forest cover conditions were set at constant 1989 values during the entire simulation.

All statistical tests for trend in this chapter used Kendall's tau test (Kendall and Gibbons, 1990) with a probability of type I error equal to 10 percent ($p=0.1$). Kendall's test is a nonparametric test which compares each observation in a series to all other observations and determines the presence of a trend based on rank and not actual difference measures. Thus the test is not sen-

sitive to the magnitude of an individual observation but only its rank.

6.2 Forest Harvesting History Of The Watershed.

An important factor affecting any trend in the residual series is the distribution of clearcuts and young tree stands in the watershed. If forest harvesting effects are important, an increase in the area of the watershed with young trees should result in a decreasing trend in the residual series while a decrease in area of young stands should lead to an increase in the residual series. The percentage of the Snoqualmie watershed (1561 km^2) supporting clear cuts and stands less than 5, 10 and 20 years old for 3 elevation bands is shown in Figure 6.1a. Of these three bands, 25% of the watershed's area is below 300 meters in elevation, 38% is between 300 and 900 meters, and 37% is above 900 meters. The information for these figures were obtained from harvest histories provided by Weyerhauser Co., Washington Department of Natural Resources, and the US. Forest Service. These data show that harvesting during the initial periods of the retrospective analysis was concentrated in the 300-900 meter elevation band and later shifted to elevations over 900 meters. The total percentage of the basin supporting trees less than 20 years old has been increasing steadily over the entire period of the retrospective analysis. This increase is predominately due to an increase in young stands above 900 meters in elevation. However, the percentage of the basin supporting trees less than 10 or 5 years old has shown a more cyclic nature with a peak occurring around 1975.

Figure 6.1 b shows the average age of the overstory during the retrospective period. Pixels which were considered either bare or agricultural by DHSVM were excluded from the average and those pixels which contained trees older than 80 years were set to an age of 80 for purposes of computing the average. The figure shows a significant decrease in the average age of the overstory over the retrospective period with the majority of the decrease occurring from 1960 to 1975 and the minimum at 1989.

6.3 Statistical Analysis Of Observed AMS And POT Data.

Connelly, et al. (1993) found no significant trend in the AMS for the Snoqualmie watershed from 1932, through 1989. However, the analysis in this chapter focuses on the period from 1948 through 1993 (for which climate data records are available in electronic form) and also includes the POT series. Therefore, we extend the analysis of Connelly, et al. to both the AMS and POT series for the 1948-93 time period.

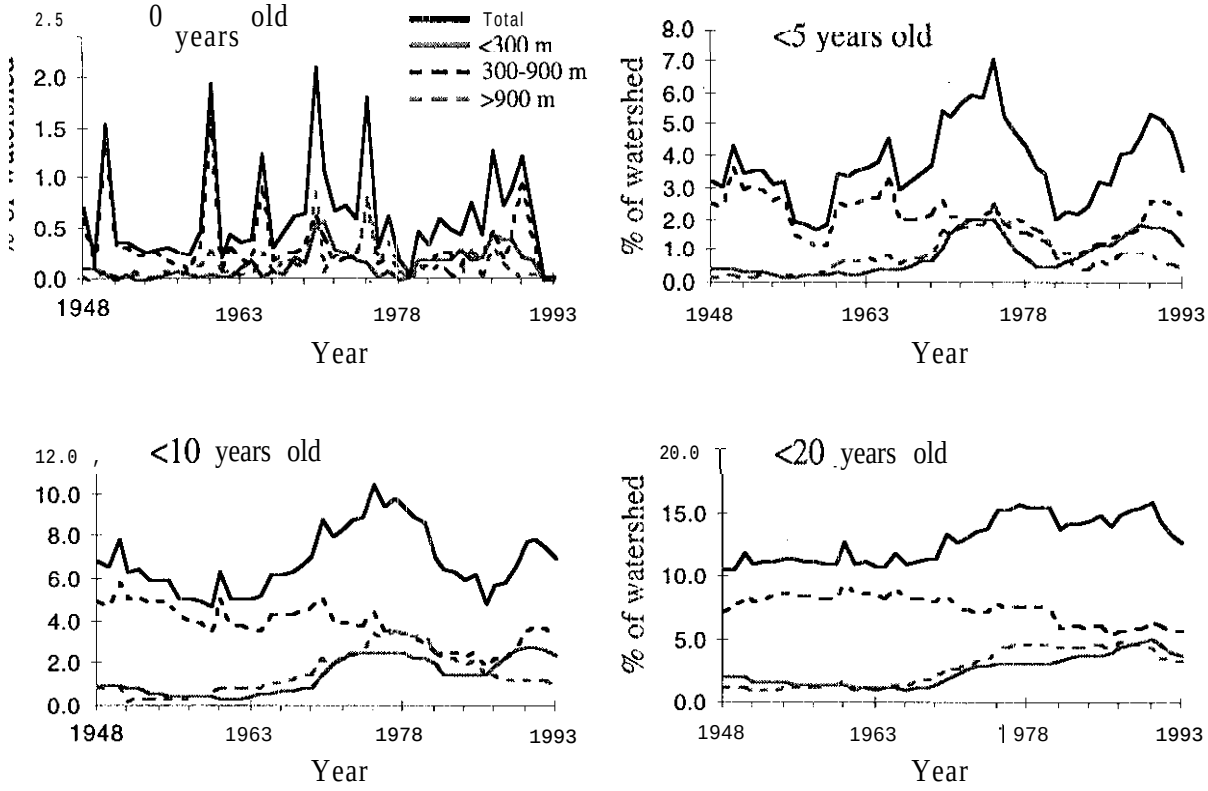

Figure 6. la. Area of watershed containing clearcuts or trees younger than 5, 10 or 20 years by elevation band (after Connelly et al., 1993).

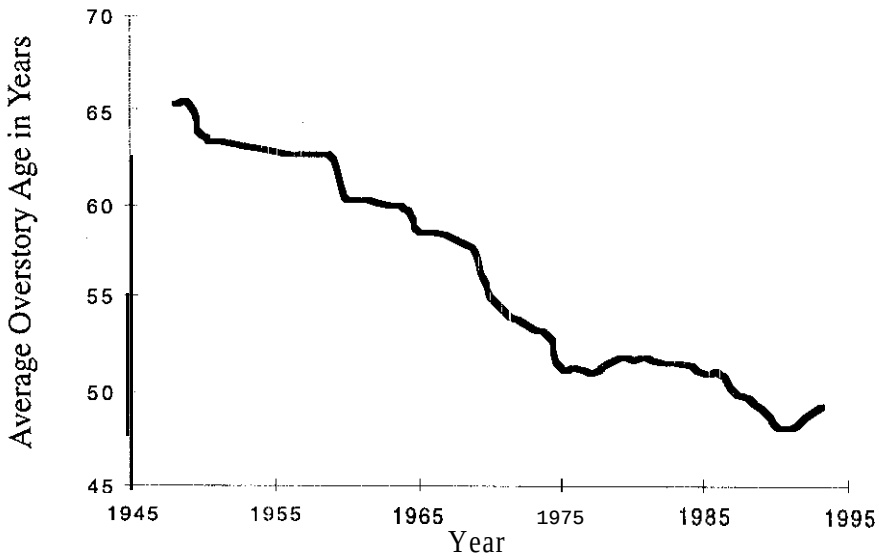

Figure 6. lb. Average overstory age of the watershed during the retrospective period. Agricultural and bare areas were excluded from the average and all pixels containing trees older than 80 years were assigned a:n age of 80.

Figure 6.2 shows the observed instantaneous AMS data for the retrospective analysis. No significant trend was found in this series. Figure 6.3 shows both the observed instantaneous peak and mean daily streamflow for each date in the POT series. Mean daily discharges were used for the statistical analysis of the POX series since the majority of the retrospective simulation used a daily timestep. Application of Kendall's test indicated significant increasing trends in both series with a more significant trend in the mean daily streamflows ($p=0.03$) than in the instantaneous peaks ($p=0.08$).

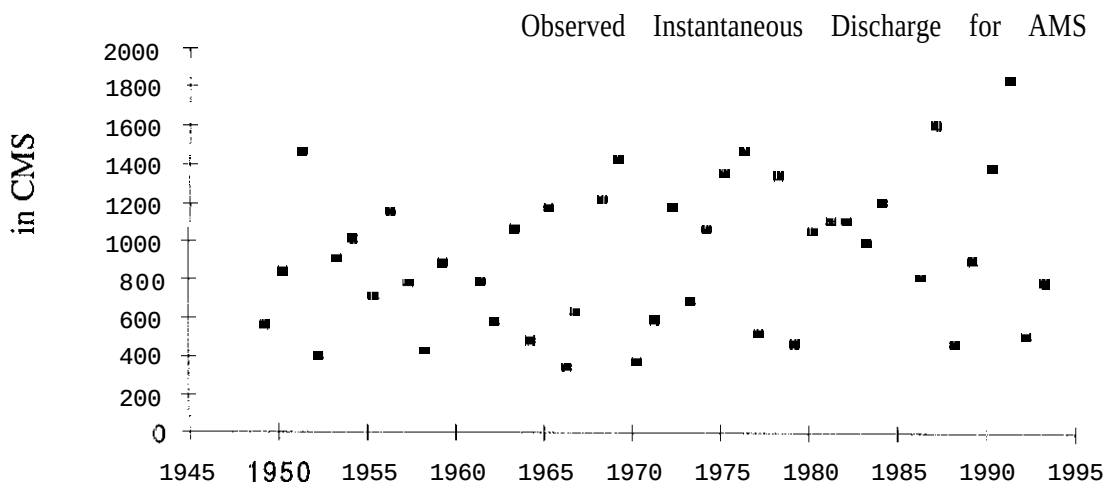

Figure 6.2. Observed AMS streamflows for the Snoqualmie River at Carnation between 1948 and 1993.

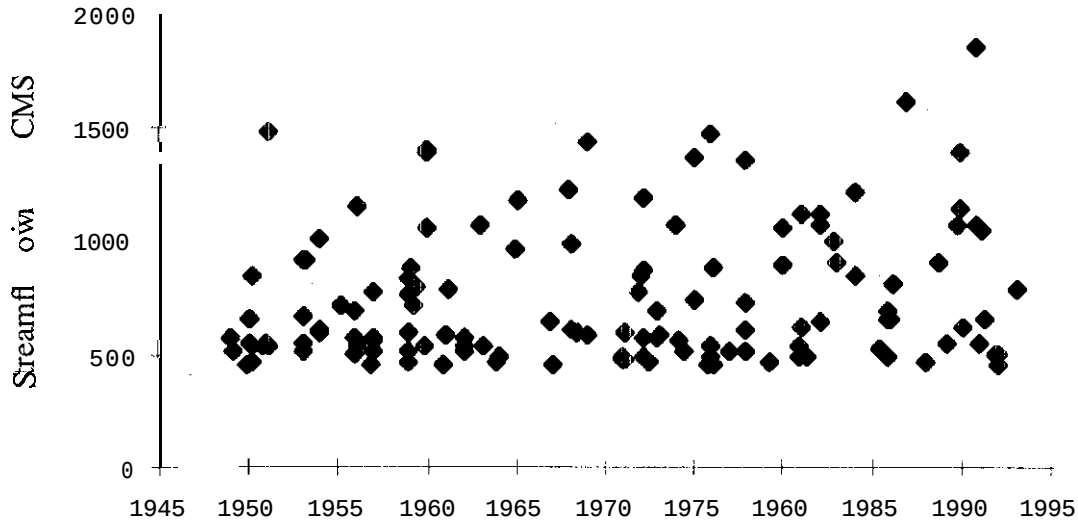

Figure 6.3a. Observed instantaneous maximum streamfows for USGS peaks over threshold series

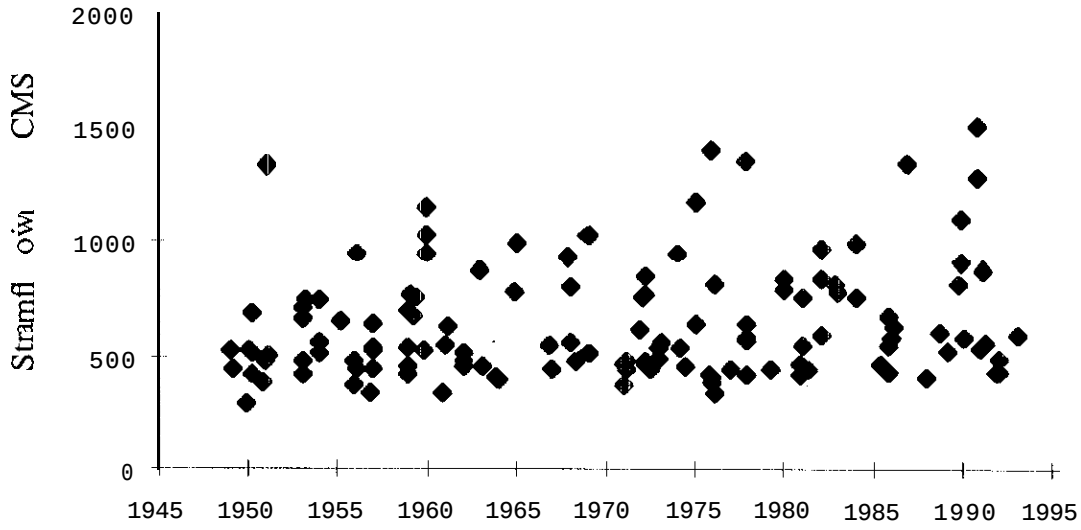

Figure 6.3b. Observed mean daily streamflows on USGS peaks over threshold dates.

6.4 Residual Series From Retrospective Analysis On Annual Peak Events

The results from the retrospective analysis of the 45 annual peak streamflow events are shown in Figure 6.4. The actual residual value (predicted minus observed instantaneous peak discharge) for each event is shown along with the residual series transformed to percent overprediction and the cumulative residual series. Perhaps the most remarkable feature of Figure 6.4 is that before 1964 and after 1975 the majority of the events are overpredicted (some by as much as 200

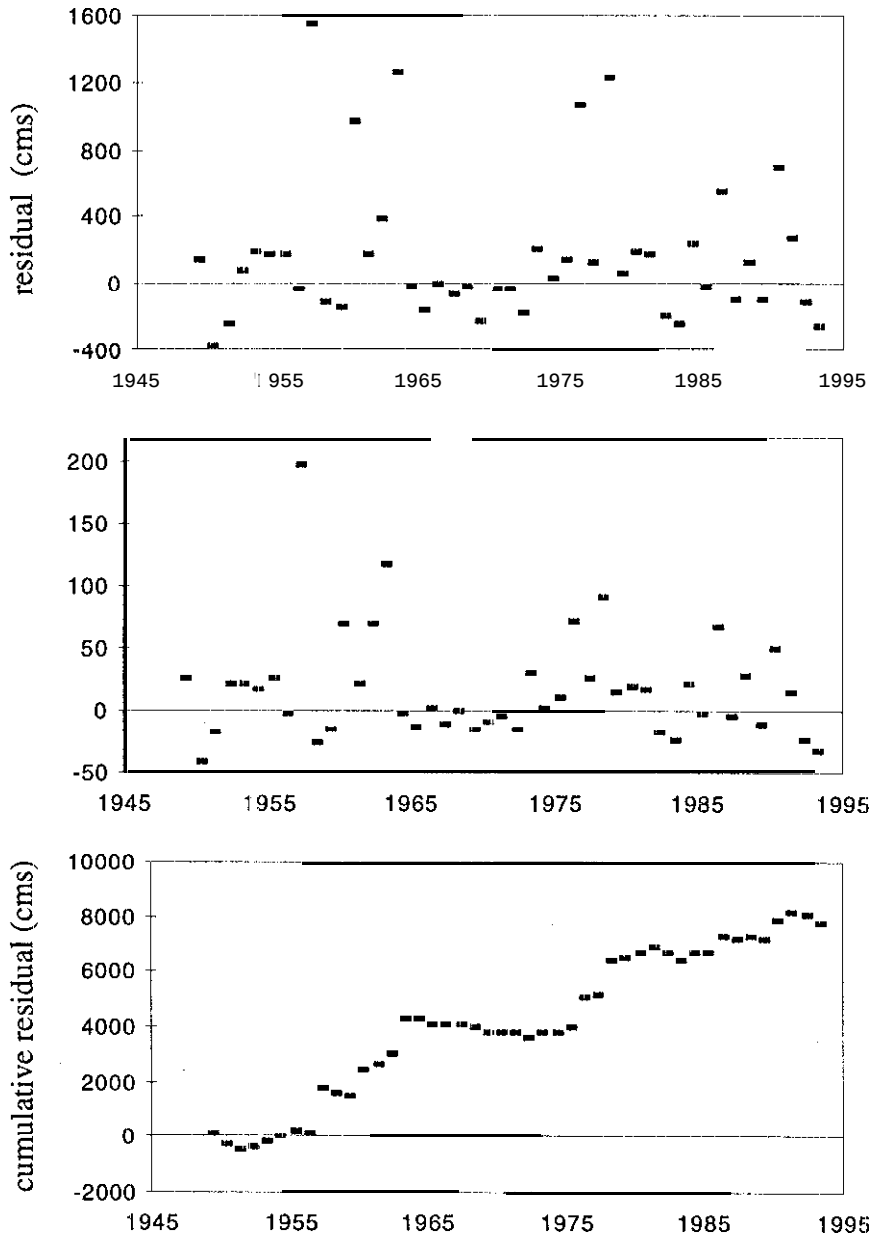

Figure 6.4. Residual series obtained from annual maximum streamflow events

percent), while the events between 1964 and 1975 are almost all underpredicted. Fortunately, the events which are overpredicted by large margins occur both early and late in the retrospective period and are not expected to bias the statistical test for trend since it is not sensitive to the absolute magnitude of the residual but only its relative rank.

Before proceeding with a statistical trend analysis of the residual series, it: is worthwhile to examine the behavior of DHSVM during a few of the events in the annual peak series which have large positive residuals (overpredictions). Figures 6.5a and 6.5b show the predicted precipitation, discharge, soil moisture, saturation deficit, snow water equivalent and snow melt averaged over three elevation bands for the 11 days before during and after the events of November 23, 1959 and November 20, 1962.

To explain the source of the overpredictions, we first compared the observed precipitation at selected stations to that predicted by the orographic sub-model in DHSVM. Table 6.1 shows the observed precipitation at five stations compared to the predicted basinwide average precipitation for four well approximated 'events and five events with large overpredictions. Data not available for a given event are marked 'NA'. For all nine events, the average predicted precipitation is huger than the observed precipitation at any of the stations and most closely matches that at Stampede Pass. However, as noted earlier, the average annual discharge of the Snoqualmie River at

Table 6.1.3 day reported precipitation in millimeters prior and during select storm events which produced peak streamflows over 1000 cms

	Event date	Snoqualmie Falls elev=134m	Cedar Lake elev=475m	Tolt reservoir elev=609m	Snoqualmie pass elev=920m	Stampede pass elev=1125m	Average predicted
Overpredicted Events	12-10-56	70	124	na	223	271	314
	11-23-59	124	134	na	265	226	270
	11-20-62	56	71	na	141	246	292
	12-3-75	173	254	106	na	337	372
	12-2-77	38	114	69	na	276	305
Well predicted events	12-12-55	105	117	na	175	145	163
	1-16-74	125	146	93	na	124	152
	12-15-79	153	164	117	na	154	185
	11-24-86	149	229	196	na	182	212

Carnation is roughly equal to the: annual observed precipitation at Stampede Pass. Therefore, the average precipitation over the basin must be, on average, greater than that observed at Stampede Pass.

The ratio of average predicted precipitation to observed precipitation at Stampede Pass is, on average, 1.16 for both well predicted and overpredicted events. However, for the overpredicted events, the ratio of predicted precipitation to observed precipitation is much higher than for the well predicted events. For example, the ratio at Cedar Lake is 1.12 for the well predicted events and 2.55 for the overpredicted events. The overpredicted events show a strong increase in observed precipitation with increasing elevation which the orographic sub-model can not duplicate. This leads to precipitation overprediction at low elevations and is the major cause of the large overpredictions in streamflow for these events.

This nature of this overprediction can be further observed in the event histories. Before the peak streamflow of the 1959 event (shown in Figure 6.5a), a maximum of 40 mm of precipitation fell in a three hour period and the entire snow pack below 900 meters, along with a significant fraction of that over 900 meters, melted, releasing as much as 15 mm of additional water over a three hour period. This influx of water, combined with almost saturated soil moisture and only small deficits in the groundwater table, produced a predicted peak streamflow of 2374 cms which far exceeded that observed (1399 cms).

Similar conditions prevailed during the 1962 event shown in Figure 6.5b. A short peak of over 40 mm of precipitation in 3 hours and up to 8 mm of snowmelt in the elevation band above 900 meters immediately preceded the peak streamflow. This precipitation plus melt quickly satisfied the remaining saturated zone and soil moisture deficit and lead to an extremely overpredicted peak discharge of 2327 cms compared to the observed peak discharge of 1070 cms.

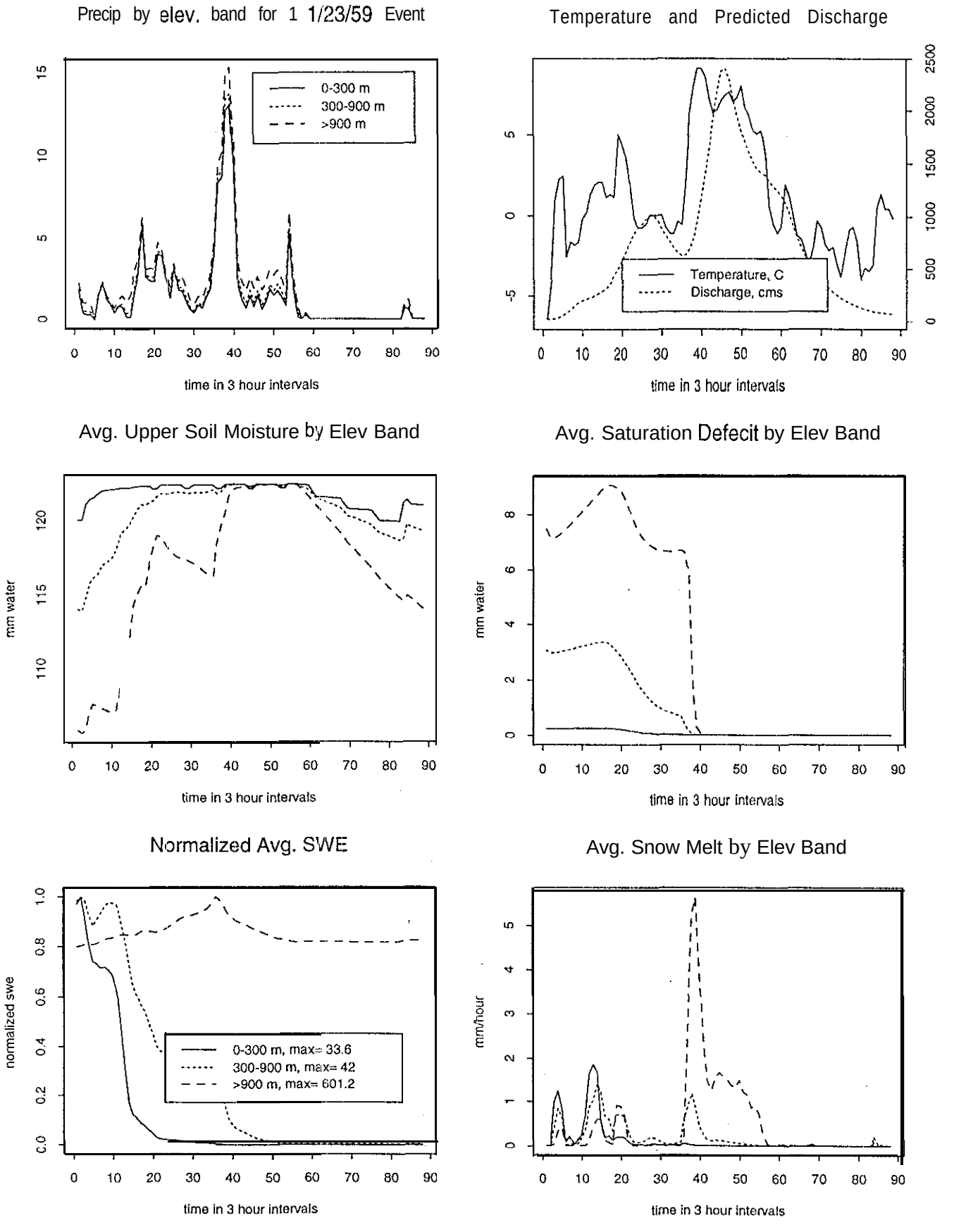

Figure 6.5a. DHSVM performance during 1 1/23/59 event.

Precip by elev. band for 1 1/20/62 Event

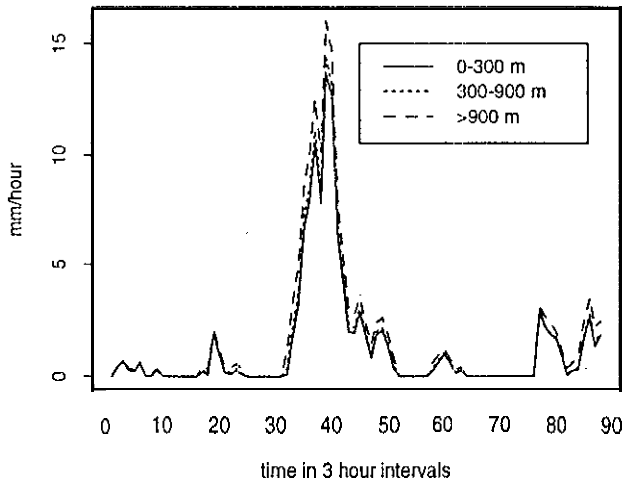

Temperature and Predicted Discharge

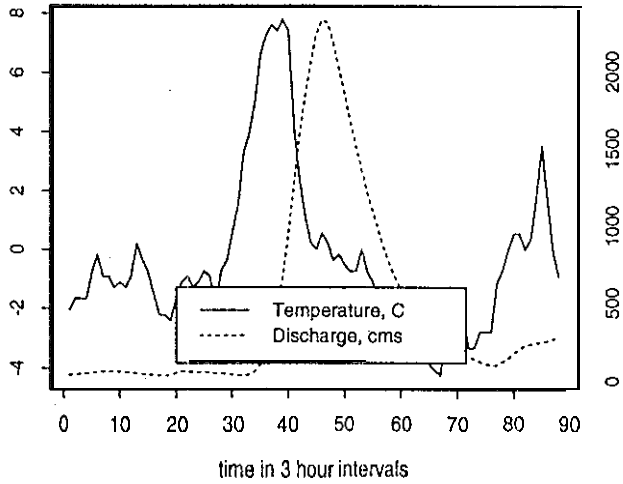

Avg. Upper Soil Moisture by Elev Band

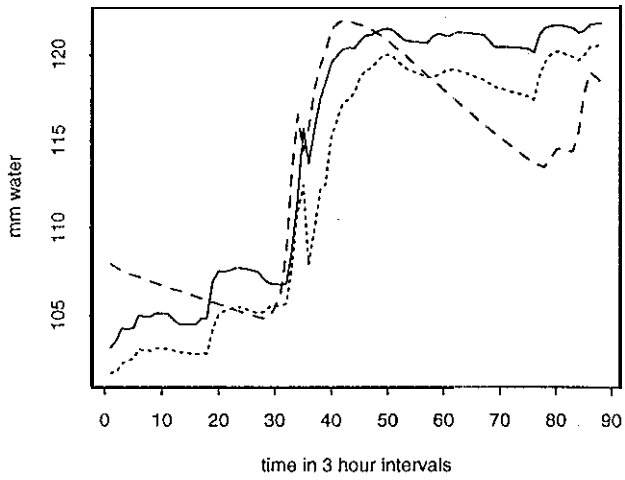

Avg. Saturation Defecit by Elev Band

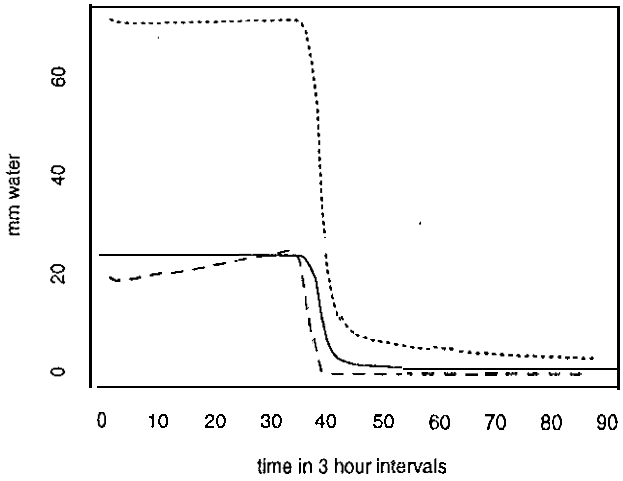

Normalized Avg. SWE

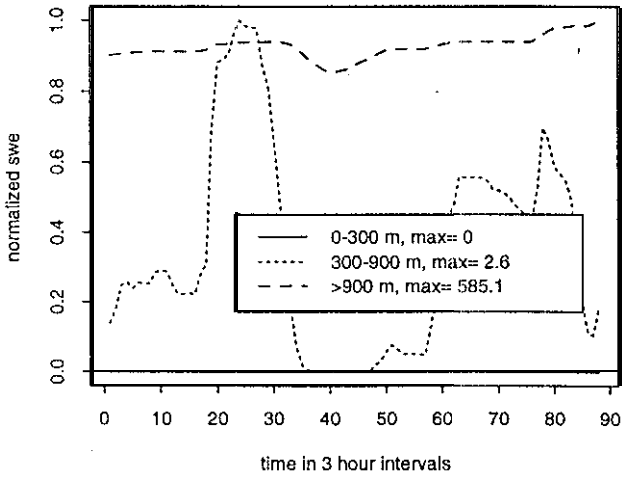

Avg. Snow Melt by Elev Band

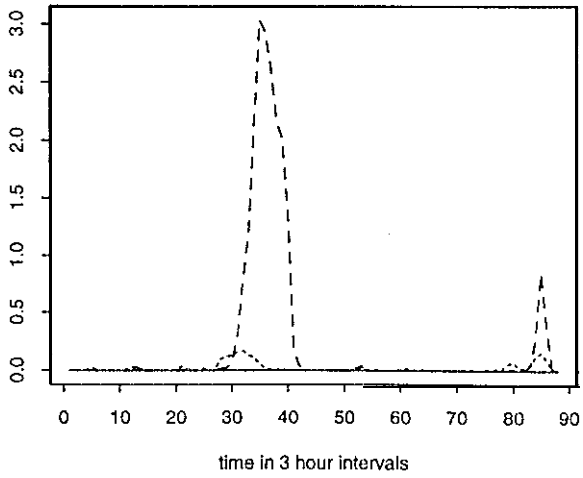

Figure 6.5b. DHSVM performance during 11/20/62 event

6.5 Statistical Test For Trend 'In The Residual Of Annual Peak Events

No trend was detected at the p=0.1 level when Kendall's test was applied to the 45 values of the raw or percent AMS residual series. This result suggests that there has not been a change in annual peak streamflows due to land use changes that DHSVM can detect. Furthermore, when the residual series from 1948 to 1975 were analyzed, no trend was found at the p=0. 1 level.

6.6 Residual Series For USGS Peaks Over Threshold.

It has been suggested that the greatest impact of land use changes is not on the largest floods but on the smaller events which occur, on average, several times each year (Jones and Grant, 1996). If true, this would explain the lack of trend in the residual series of the annual maximum events and suggests the focus of the analysis be shifted toward smaller events. As a basis for this broader analysis we used the USGS peaks over threshold series which records those peaks in excess of a specified value. There has been some concern that the USGS has changed the threshold for the peaks over threshold series at some gaging stations. However, we verified that the threshold value for the Snoqualmie River gage near Carnation has not been changed from the published value: of 16,000 cfs over the period of the retrospective analysis.

We compared the observed mean daily flow on each date in the USGS peaks over threshold series to the mean daily flow predicted by DHSVM on the same date. The difference between the predicted and observed values formed the threshold residual series. Mean daily flows were used instead of instantaneous flows because the majority of threshold events in the retrospective analysis were simulated at a dailly time step. Those events which were included in the annual maximum series were simulated, at a three hour time scale with predicted mean daily discharge values used to construct the POT series.

The POT residuals are plotted in Figures 6.6a and 6.6b which show the actual value of the residual and the residual expressed as a percentage of the observed mean daily discharge, respectively. Each figure is further partitioned into two series, those residuals with an observed daily mean flow above 650 cubic meters per second (49 events indicated with dark points) and those below 650 cms (83 events indicated with light points). The mean daily streamflow threshold of 650 cms was chosen to approximate the mean annual flood, i.e. one event per year in the analysis.

Application of Kendall's, test to the entire POT residual series (all 132 values) showed no significant trend in either the percent residual series or the raw residual series. Also, no trends were found in the POT series wiith observed mean daily discharges greater than 650 cms. This

. Observed mean daily discharge less than 650 cms

Observed mean daily discharge greater than 650 cms

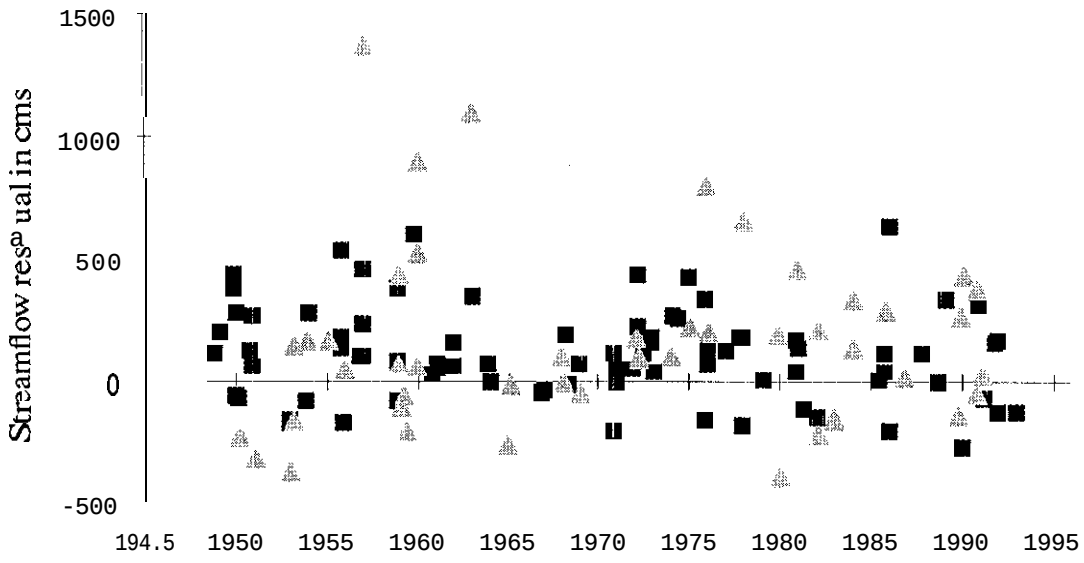

Figure 6.6a. Raw residuals from POT series

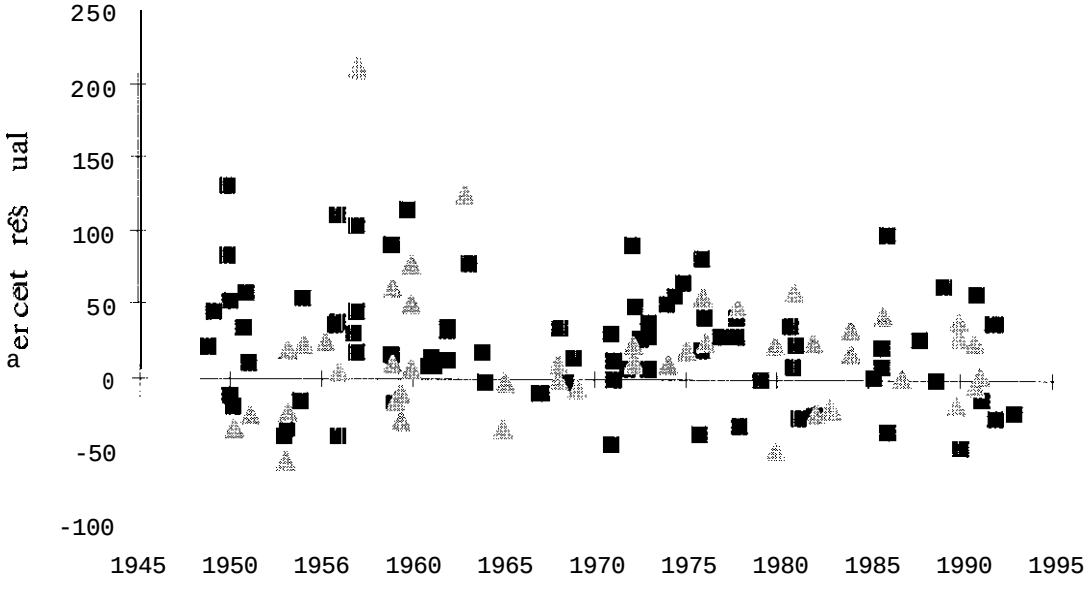

Figure 6.6b. Percent residuals from POT series

result agrees with the absence of trend observed in the AMS residuals. However, when Kendall's test was applied to the POT residuals with an observed mean daily discharge less than 650 cms, significant downward trends were observed (p=0.05) for both the raw and percent residuals.

These results suggest that. some factor other than climate (which is explicitly modeled by DHSVM over the period of the retrospective analysis) has contributed to increasing the magnitude of smaller events in the POT series but has not significantly influenced larger events in either the POT series or the AMS.

6.7 Segregation Of Pot Residuals By Snow Melt Volume.

To attempt to interpret the cause of the decreasing trend in the residual series for the small POT events, we segregated the entire POT series into four categories based on a snowmelt index. Two separate indices were used in which the total basinwide predicted snowmelt was divided by either the total basinwide predicted precipitation or the total predicted discharge during the event. Totals were calculated during the three days prior to and including the date of each POT event. Each of the two sets of segregated POT residuals was examined for trends in both the raw and percent residuals.

Our hypothesis is that for events of equal size (as indexed by total precipitation or discharge), those with small snowmelt contributions are less likely to increase due to forest harvesting. This hypothesis assumes that increased snowmelt volumes during ROS events are the cause of increases in peak streamflows and implies that there would be no trend in the residuals analysis for small snowmelt events and a significant decreasing trend in the residuals for larger snowmelt events of equal overall magnitude. Coffin and Harr (1992) have observed that the percent increase in snowpack outflow due to removal of forest canopy decreases as the size of the event (as indexed by total snowpack outflow) increases. Given that any increases in snowpack outflow for harvested relative to forested. sites are predominately due to increases in snowmelt volume, it follows that as the total amount of precipitation increases, the observed percent increase in snowpack outflow must decrease. However, the actual increase (expressed as a depth of water instead of a percentage) would not be expected to decrease. To account for this subtle distinction, we examined both the percent and raw residuals for trends.

To illustrate the magnitude of the trends o'bserved and to clarify the nature of the segregation, the results for the percent residual analysis of the snowmelt versus precipitation index are

presented in Figure 6.7 The results for the entire segregation analysis are presented in Table 6.2. Figure 6.7 shows the residuals of the POT series segregated into four categories: events in which the 3 day snowmelt was less than 6 %, between 6 and 15 %, between 15 and 25 %, and greater than 25 % of 3 day precipitation. Each of these categories was chosen with roughly the same number of events so that the power of the statistical test would be roughly comparable for each category.

The results were exactly opposite of what our hypothesis suggests. Results from all segregated series, summarized in Table 6.2, show that there are significant decreasing trends in the percent residuals for only those events in which snowmelt volumes were minor fractions of precipitation or discharge. As the amount of snowmelt increases, the significance of the trend disappears. Analysis of the raw residuals reveals that for the snowmelt vs. precipitation index, the trend remains for small snowmelt events but disappears in all categories for the snowmelt vs. dis-

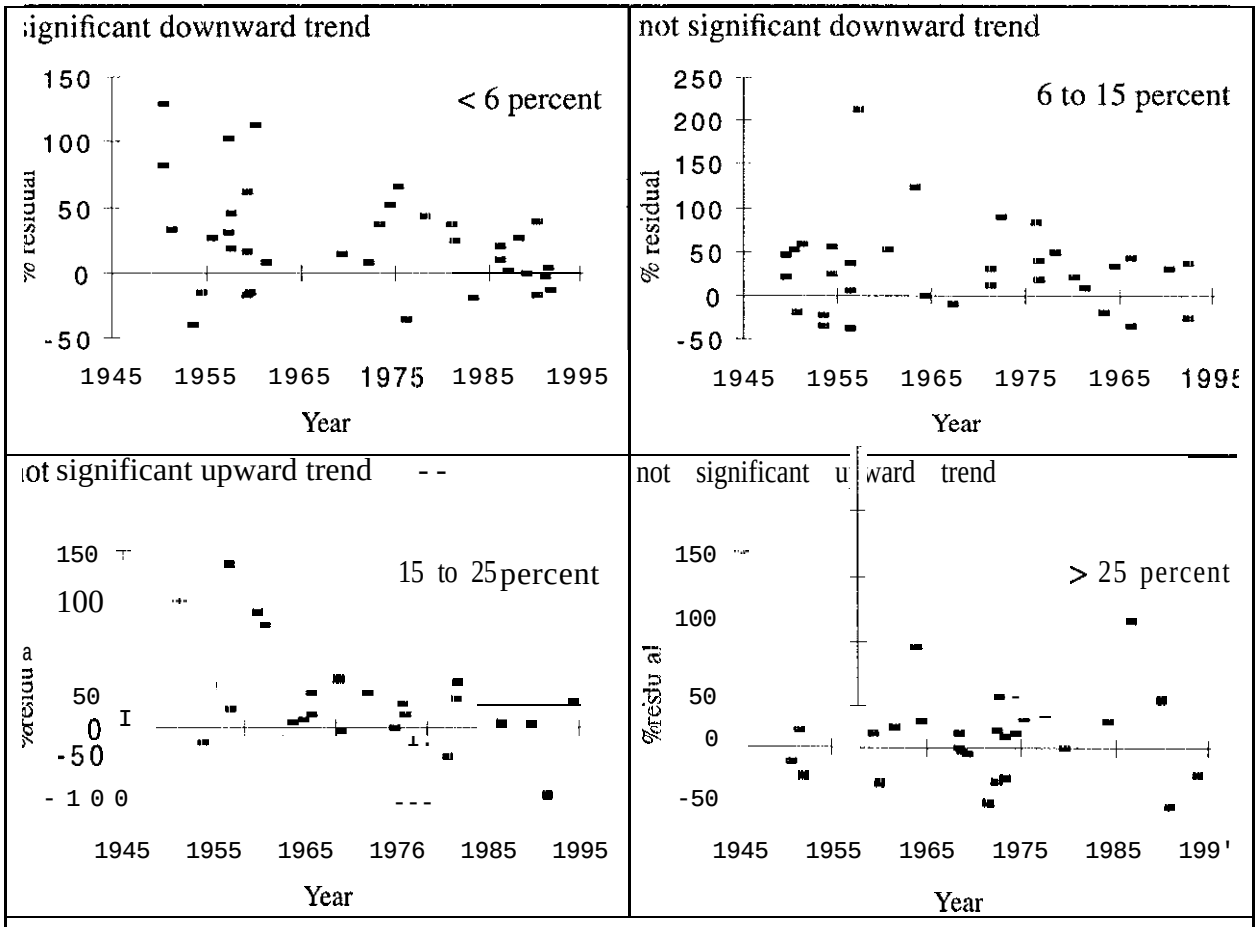

Figure 6.7. Threshold residual series segregated by 3 day snowmelt expressed as a percentage of 3 day event precipitation

Table 6.2. Results from analysis of POT residuals segregated by snowmelt volume

Snowmelt Index	Percent Interval	Percent residual trend	Raw residual trend	Average total snowmelt (mm)	Average total precip. (mm)	Average total discharge (mm)
snowmelt / precip.	< 6	down (p=0.04)	down (p=0.07)	4.5	134.7	248.0
	6-15	-	-	13.3	148.2	234.4
	15-25	-		24.7	131.0	279.7
	> 25	-	-	37.0	102.5	229.2
snowmelt / discharge	< 3	down (p=0.09)	-	3.7	126.7	270.1
	3 - 7	-	-	13.8	158.1	271.8
	7 - 12	-	-	22.1	119.7	243.9
	> 12	-	-	36.3	108.4	205.5

charge index. Even though smaller events (as indexed by discharge or outflow) are expected to show larger increases in streamflow due to forest harvesting (Coffin and Harr, 1992; Jones and Grant, 1996), the trends revealed in the small snowmelt events of the segregation analysis can not be explained by smaller total discharges or precipitation. In fact, the category with the smallest precipitation volumes and discharges had the largest snowmelt contributions and contained insignificant increasing trends. Theses results are in direct opposition to our initial hypothesis, and suggest that either the hypothesis is incorrect or the underlying assumption that ROS effects are driving increased peak streamflows is not valid. If the latter is true we would expect to see insignificant increases in peak discharges for given ROS events due to removal of forest cover.

6.8 Simulation Of Residual Series With Varying Forest Cover.

The analysis described above fixed forest cover at 1989 conditions. The results indicate that a trend does exist in the residual series for smaller peak streamflow events and not for larger events, however the importance of the ROS mechanism appears is questionable. One method by which we can further investigate the mechanism responsible for the trend in the residual series is to resimulate periods of the retrospective analysis with forest cover conditions set to 1948 and 1975 levels, which effectively brackets the range of effects. A direct comparison of the predicted

discharge series for the retrospective analysis can then be made with 1989, 1975, and 1948 forest cover.

Figure 6.8 compares the discharge predicted with 1948 forest conditions to that predicted with 1975 forest cover from January 1, 1948 until December 3 1, 1962. The maximum increase in predicted discharge is only 60 cms which occurred during an annual peak event and produced a percentage difference of only 6%. The largest percentage increase is approximately 30% but this occurs during relatively small events which are not included in the 'USGS peaks over threshold series. Examination of the actual values from the peaks over threshold series show a maximum actual difference of 40 cms for a. maximum percent increase of only 6%. The figure also shows a cyclic pattern of overprediction followed by underprediction during each year. This cyclic behavior occurs during the spring snowmelt season in which events are dominated by snowmelt, driven in large part by solar radiation. Removal of forest canopy exposes a larger portion of the snowpack to shortwave radiation thereby increasing early snowmelt events. Furthermore, because more of the snowpack melts rapidly during the early spring due to the removal of forest canopy, later events decrease in size.

Figure 6.9 shows a similar comparison of 1989 forest cover to 1948 forest cover for the same retrospective time period. The increases are even smaller than those resulting from comparing 1975 to 1948 forest cover. Comparison of the maximum predicted increase in discharge to the minimum detectable difference that would result in a trend in the residual suggests that it is not likely that the observed trend in the residual series seen in the smaller events of the peaks over threshold series is due to vegetation changes. Further investigation of the cause will require an extension of DHSVM to incorporate the effects of land use changes not currently modeled, such as the effects of roads on runoff generation and subsurface interception. These mechanisms have been suggested as significant contributors to increased peak streamflows in western Oregon basins (Jones and Grant, 1996).

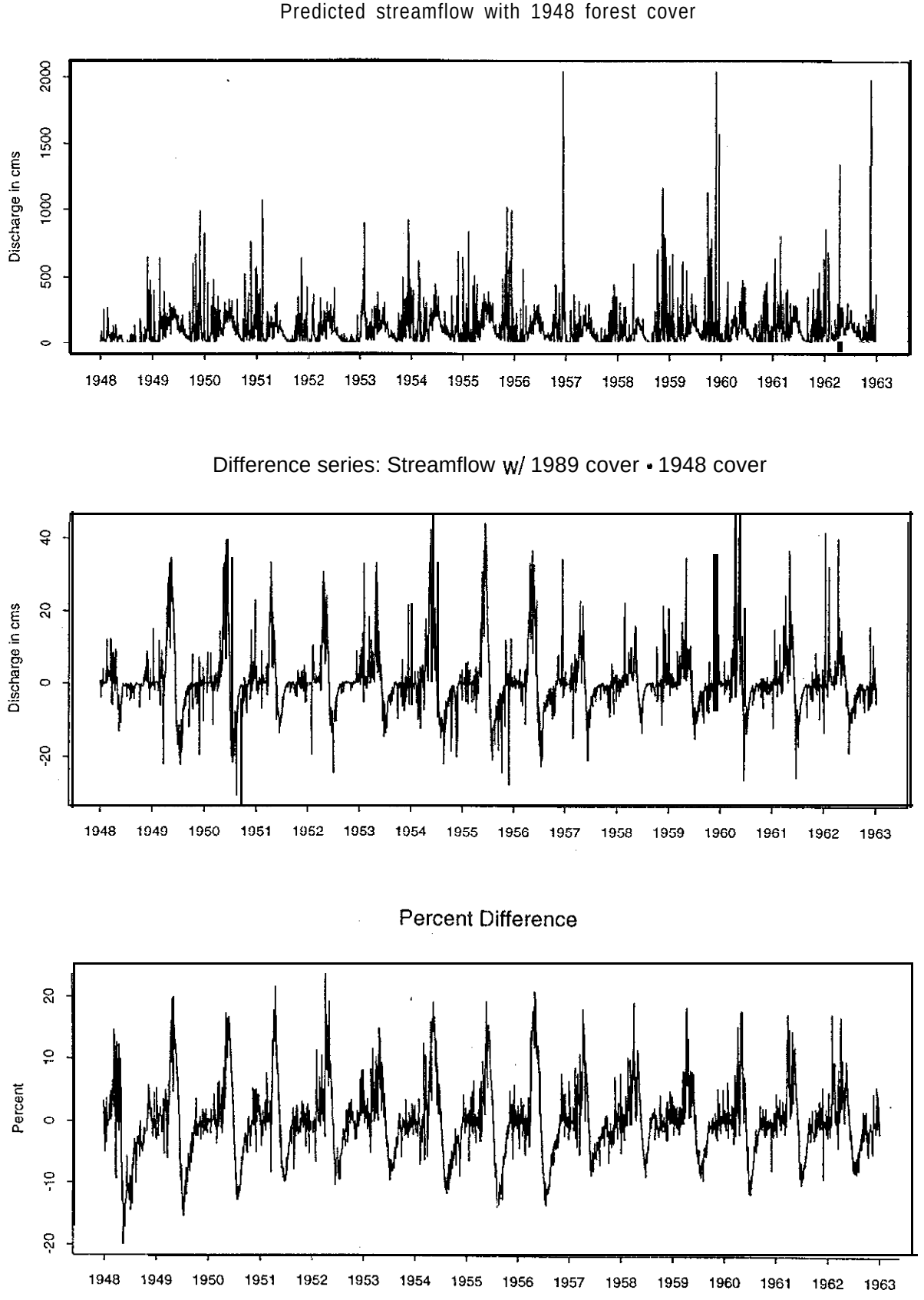

Figure 6.8,. Comparison of streamflow record with 1989 and 1948 forest cover.

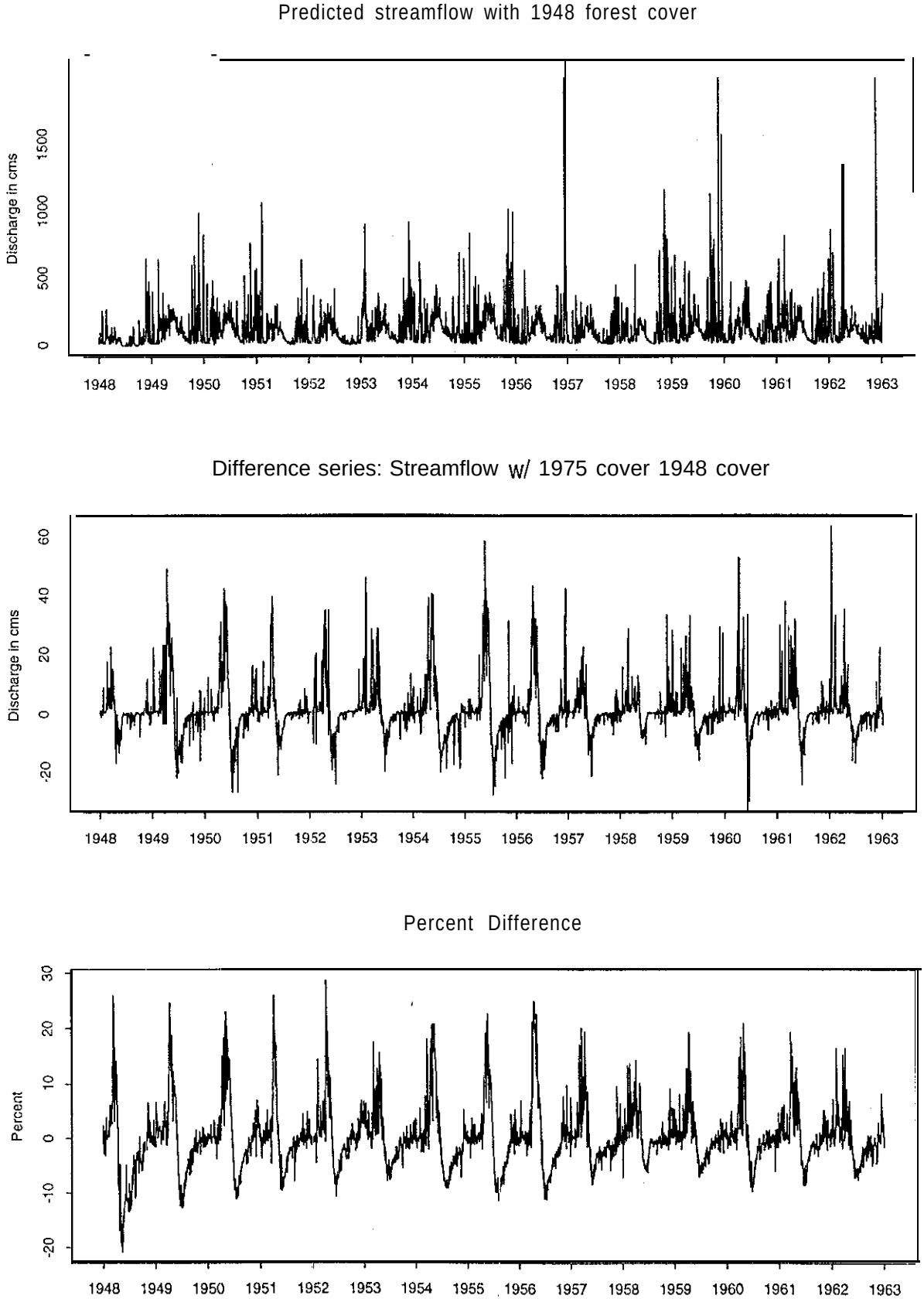

Figure 6.9. Comparison of streamflow record obtained with 197.5 and 1948 forest cover

Chapter 7. Sensitivity of Streamflow to Forest Harvesting Alternatives

The results of the retrospective analysis presented in Chapter 6 suggest that ROS mechanisms, which were specifically incorporated into DHSVM to account for the effects of forest harvesting on peak: streamflows, do increase peak streamflows but not to the degree needed to account for the observed trend in the residual series. This chapter extends the sensitivity analysis of Chapter 6, in which forest harvesting conditions were varied over historical levels, to include an analysis of several hypothetical harvest strategies. The sensitivity analysis focused on simulation of the continuous climatic record from January 1, 1948 through December 3 1, 1955 (the first eight years used in the retrospective analysis). This period is of sufficient length to evaluate the likely effects of alternative harvest strategies as it contains several of the largest peak flows of record (e.g. the floods of February 1951 and 1953). The simulations were structured as described for the retrospective analysis. However, for the purposes of this analysis, overstory vegetation classes were changed such that the entire watershed was assumed to be covered by the dominant species, Douglas fir. This change removes the individual variation among overstory species, thereby focusing the sensitivity analysis on overall forest harvesting effects and not on which specific species were cut. Manipulation of the year of origin input file (described in Chapter 4) allows for direct specification of the overstory age on each pixel from clearcut to old growth.

7.1 Effect Of Clearcutting The Entire Watershed

To provide an upper bound on the expected impact of forest harvesting as predicted by DHSVM, the most drastic of forest harvesting strategies was simulated, the complete clearcutting of the entire 1500 km^2 watershed. Acomparison between the hourly predicted streamflows with complete oldgrowth Douglas Fir coverage and complete clearcutting for the eight annual peak events between 1948 and 1955 is shown in Figure ‘7.1. The figure shows that for these annual events, all peaks would be increased by complete clearcutting of the watershed. However, the magnitude of the increase varies by event from as small as 20 cms for the event of December 1953 to over 300 cms for the event of February 1951. It should be emphasized that these results are for a limiting case and should not be used to infer trends in streamflow based on more realistic harvest strategies, which are presented later in this chapter. However, they are useful in suggesting an upper bound of forest effects on peak streamflow.

To explain the factors behind this variation among events, it is helpful to analyze the pre-

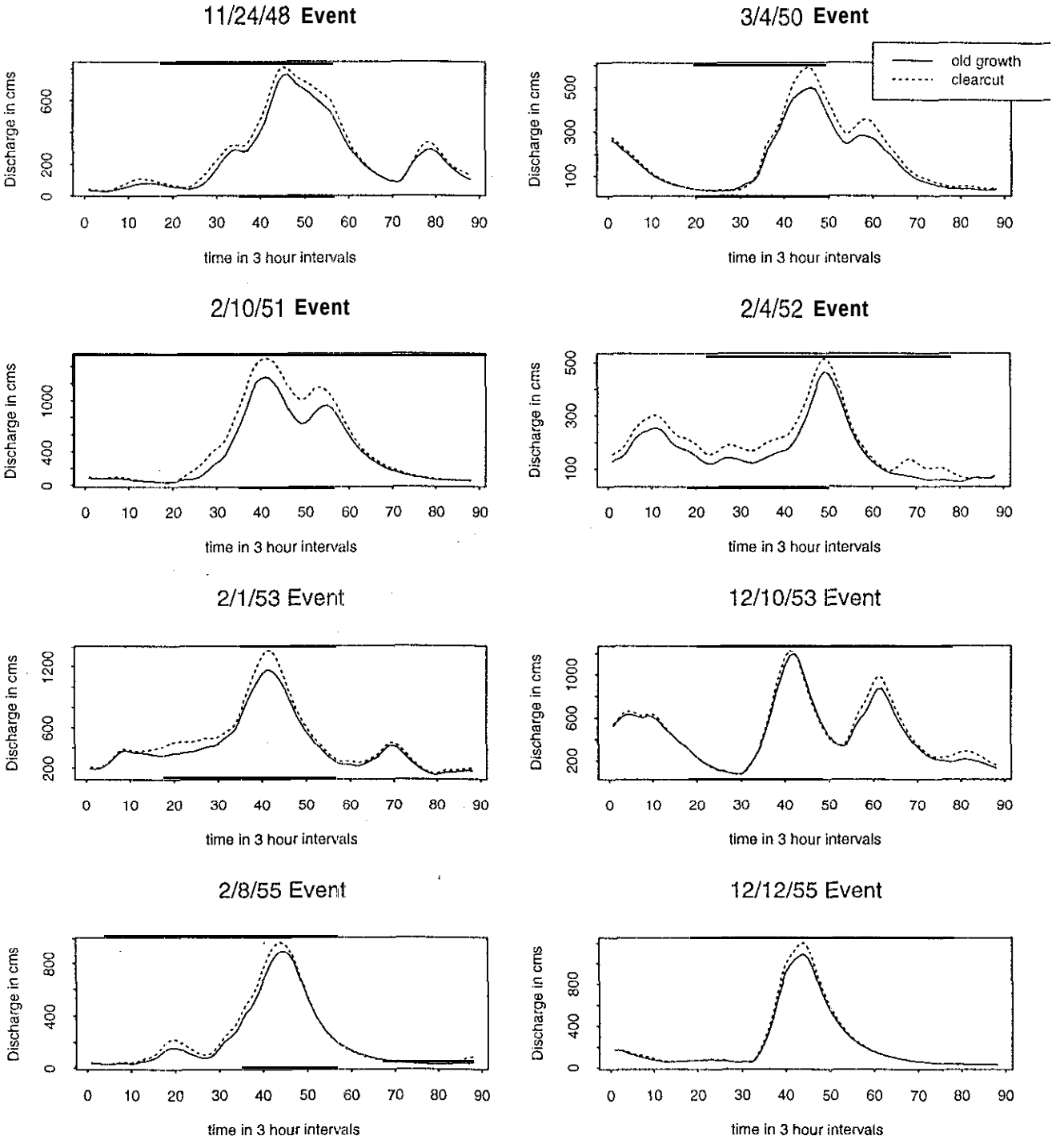

Figure 7.1. Annual peak streamflows simulated with all old growth Douglas fir and 100 percent clear cut.

dictions of DHSVM during two events: one in which a large increase in peak streamflow was observed (February 1951), and tlhe other which showed almost no increase in streamflow (December 1953).

Figure 7.2 shows predicted precipitation and observed temperature (at Stampede Pass) and compares the predicted distribution of snow water equivalent and snowmelt over three elevation bands (less than 300 m, between 300 and 900 m, and over 900 m) for the simulations with complete old growth coverage and complete clearcutting for the February 195 1 event. The legend of the normalized snow water equivalent plot indicates the maximum SWE (in mm) during the event in each elevation band.

Note that the two lower elevation bands contain less snow water equivalent in the old growth simulation than the clearcut simulation. However, the highest elevation band contains more snow water equivalent during the old growth simulation. This reversal in trend with increasing elevation was seen in all the annual peak events. It is indicative of the sheltering of the snowpack by the old growth forest during the rare snowmelt events above 900 meters and perhaps more importantly, the limited rolles snow interception and direct melt from the canopy play above 900 meters. (Wind redistribution of snow on the ground is not simulated by DHSVM.) Below 900 meters, in the transient snow zone, ROS occurs more frequently and snow interception and direct melt dictate the distribution of snow.

During this event, the observed temperature at Stampede Pass rose to over 6°C. In both simulations, the entire accumulated snowpack below 300 meters melted, producing an additional 21 mm of runoff due to the larger initial snow accumulation in the clearcut simulation. Furthermore, the elevation band above 900 meters produced significantly more snowmelt at the height of the storm during the clearcut simulation, even though it had less snow. This increase is due to the increased latent and sensible heat transfers caused by higher wind velocity over the snow in the clearcut areas. However, the main increase in snowmelt occurred in the transient snow zone. In the old growth simulation, roughly 30 percent of the initial accumulated snowpack of 250 mm melted at a maximum rate of up to 1.3 mm/hour. During the all clearcut simulation, roughly 50 percent of the initial accumulated snowpack of 318 mm melted at a rate of up to 2.7 mm/hour. This large increase in predicted snowmelt translates directly to the observed increases in peak discharge if the entire watershed were clearcut.

Precip by elev. band for 2/10/51 Event

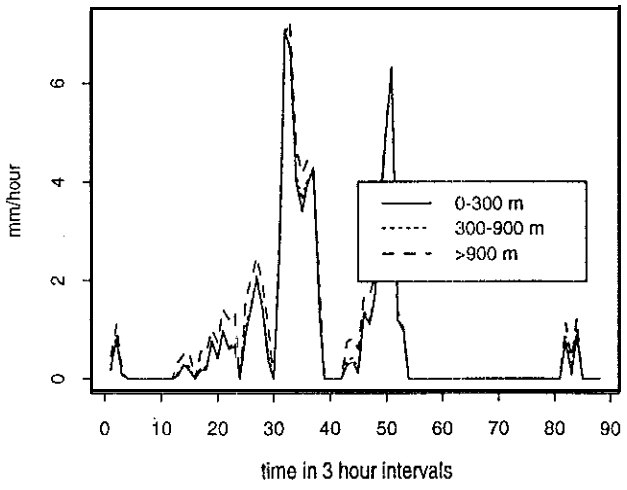

Temperature and Predicted Discharge

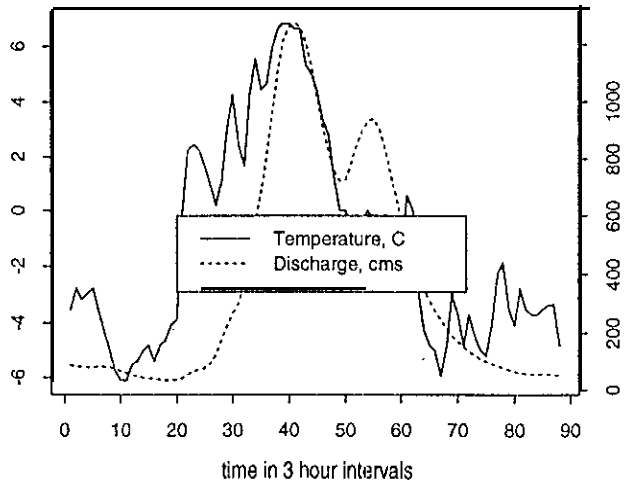

Normalized Avg. SWE w/old growth forest

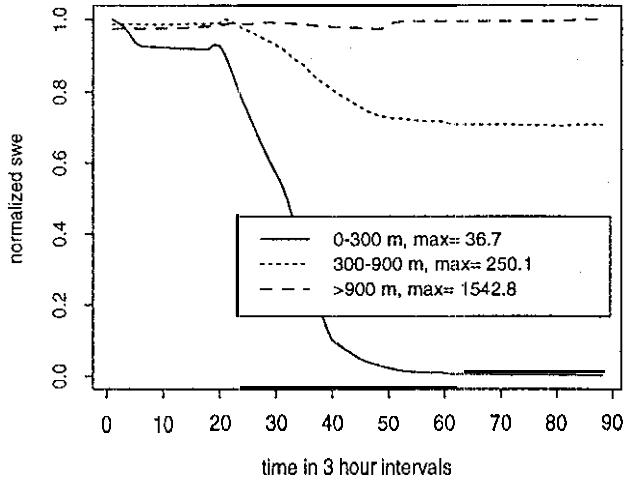

Avg. Snow Melt w/ old growth forest

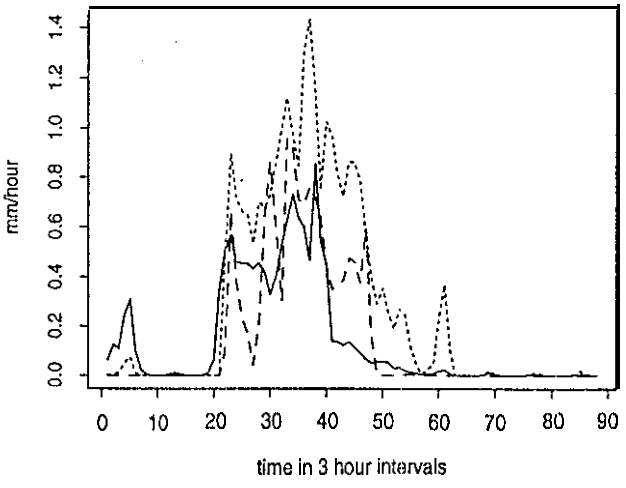

Normalized Avg. SWE under clearcut conditions

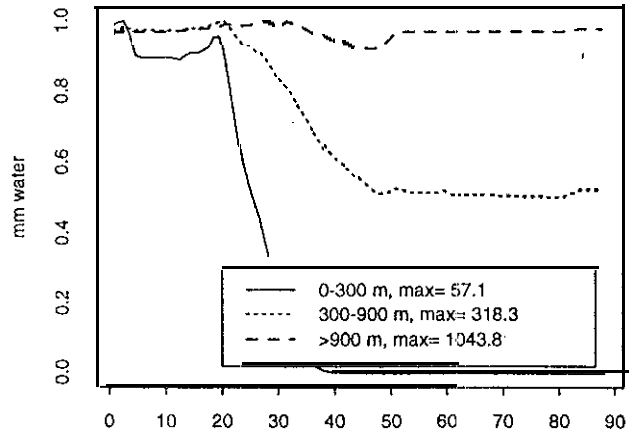

Avg. Snow Melt by Elev Band w/ clearcut

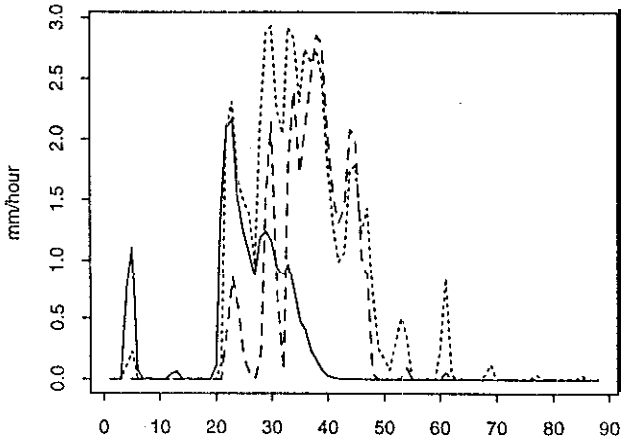

Figure 7.2. DHSVM predictions with varying forest cover for 2/10/51 event.

Figure 7.3 summarizes a similar analysis of the December 1953 event which produced relatively little additional extra streamflow if the entire watershed were clearcut. In this event, the observed temperature at Stampede Pass increased to approximately 3 degrees Centigrade during the peak precipitation period of the event. During the warm period of the event, the clearcut simulation produced only slightly more snowmelt than the old growth simulation. The only notable exception occurred during the period of maximum precipitation when the clear cut simulation predicted over 2.7 mm/hour of snowmelt in the transient snow zone while the old growth simulation predicted only 1 mm/hour of snowmelt. However, these increases were too short-lived to affect peak streamflow, due to low air temperatures before and after the storm.

Figure 7.3 also indicates the role snow interception and subsequent melt plays during ROS events. Below 300 meters, snow accumulation in the clearcut simulation reached 33 mm during the initial cold period of the event. However, in the old growth simulation, snow accumulation reached only 4.8 mm, even though the precipitation and temperature distributions over the watershed were identical for both simulations. In the old growth simulation, most of the snowfall below 300 meters was intercepted by the canopy, where it was exposed to higher latent and sensible heat transfer and melted.

We have already shown in Chapter 6 that the trend in the residual series of the retrospective analysis is more significant for smaller events. On this basis, we would expect to see larger percent increases in streamflow for the peaks over threshold series than for the annual peak series. Moreover, we should observe even larger increases for those events which are smaller than the threshold streamflow. Figure 7.4 shows the predicted streamflow record from January 1, 1948 through December 3 1, 1955 with all old growth, and a difference series in which the old growth streamflow is subtracted from the predicted streamflow record based on an entirely clearcut watershed. This difference is also expressed as a percent of the old growth streamflow.

With respect to the entire period of continuous simulation, vegetation removal over the entire basin leads to a maximum increase in streamflow of approximately 300 percent and a maximum decrease of almost 100 percent. In the entire series, those events which show the largest increase in streamflow occur during the early part of the spring melt season. Removal of the canopy exposes the snowpack to larger latent and sensible heat transfer, and more importantly, higher net shortwave radiation. Thus, during the early part of the snowmelt season, streamflow increases. The largest decrease occurs during the later part of the snowmelt season. Since the

Precip by elev. band for 12/1 0/53 Event

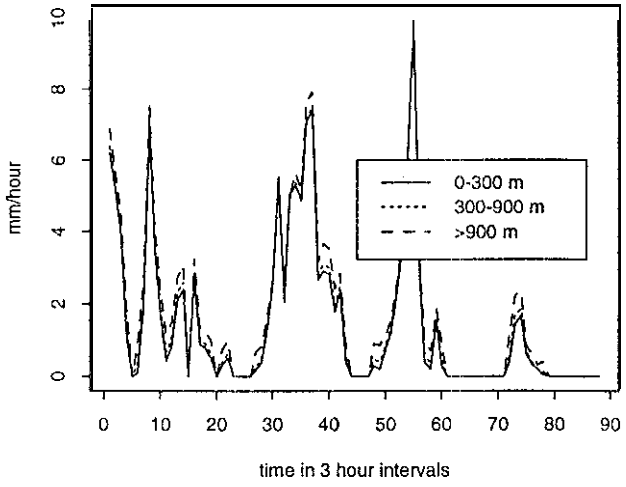

Temperature and Predicted Discharge

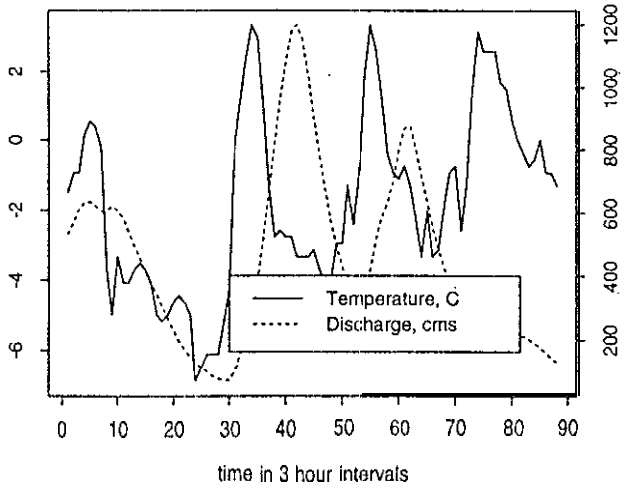

Normalized Avg. SWE w/old growth forest

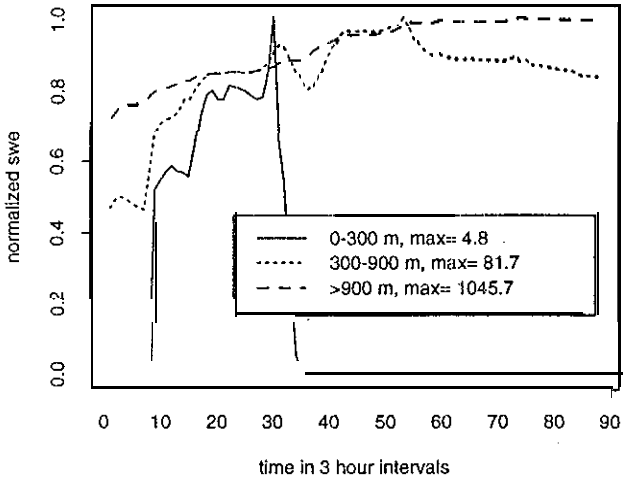

Avg. Snow Melt w/ old growth forest

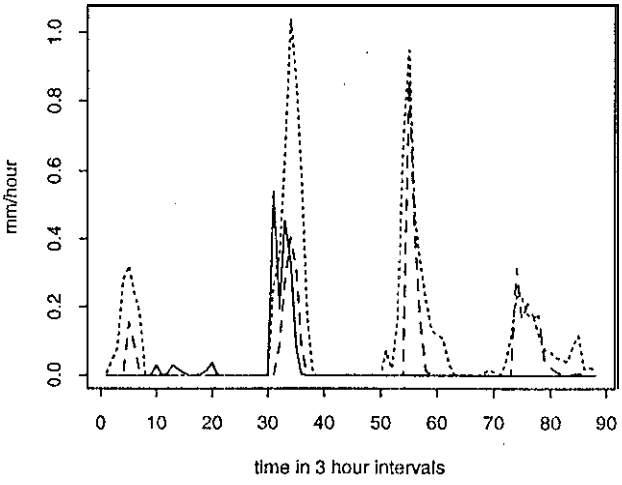

Normalized Avg. SWE under clearcut conditions

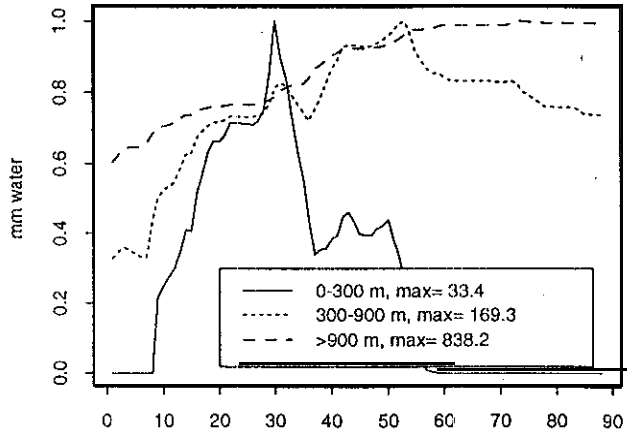

Avg. Snow Melt by Elev Band w/ clearcut

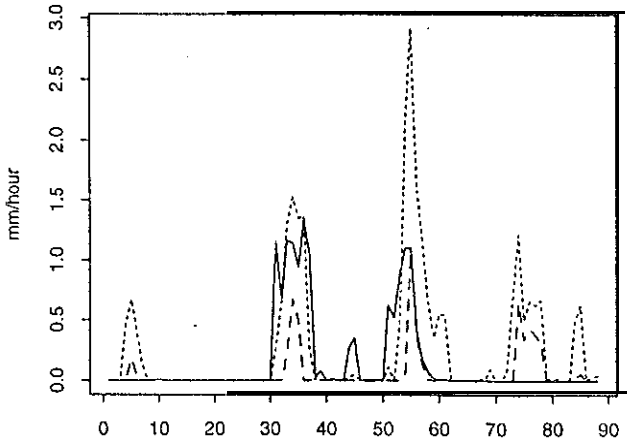

Figure 7.3. DHSVM predictions with varying forest cover for12/10/53 event,

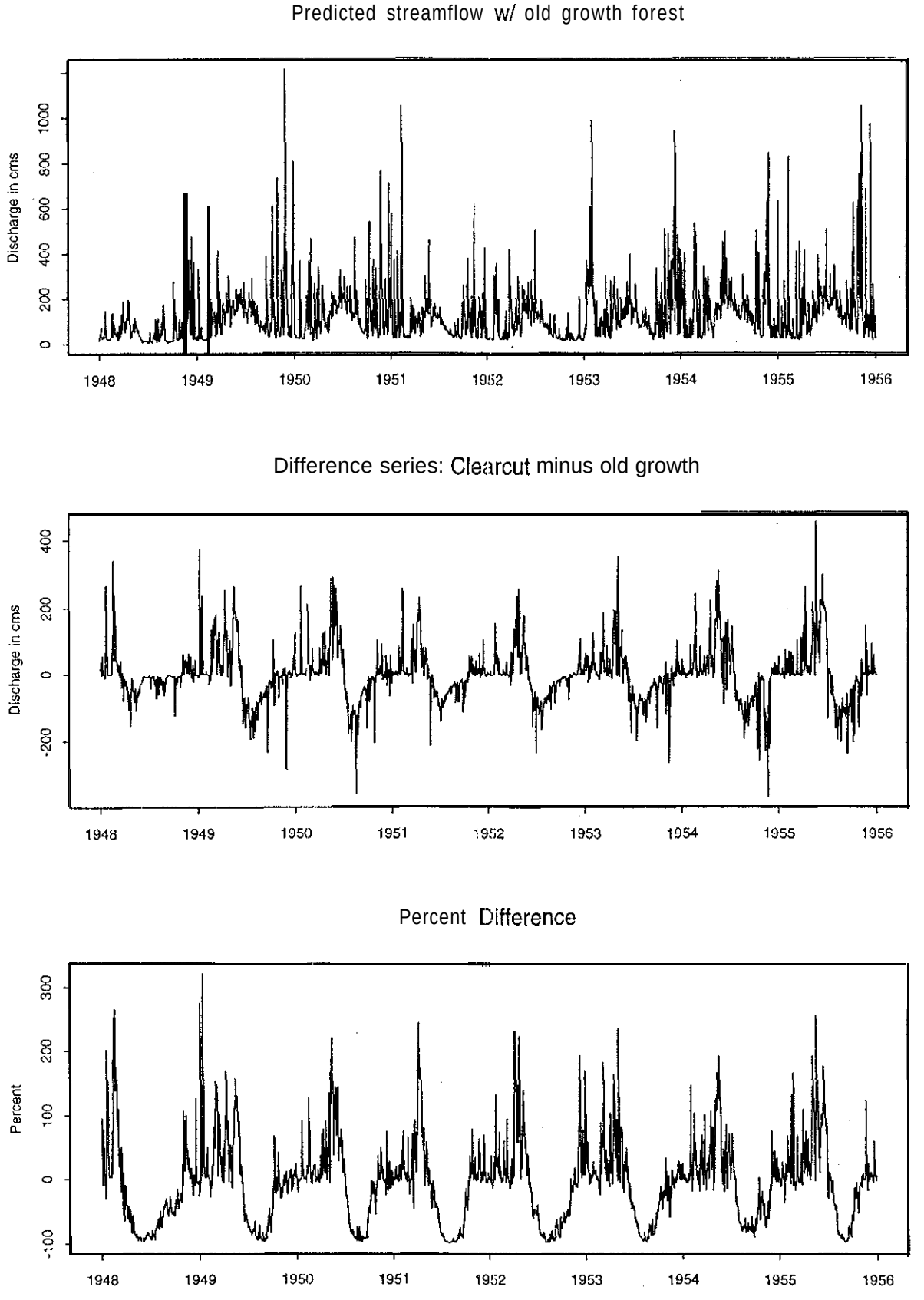

Figure 7.4. Continuous predicted streamflow from 1948 through 1955 as simulated with old growth Douglas Fir and compared to all clear cut conditions

snow melts at a faster rate after removal of the canopy, those snowmelt events which occurred later in the season with old growth coverage are effectively shifted earlier in the year.

Extracting those peaks from Figure 7.4 which belong to the peaks over threshold series show that they realize a more modest maximum increase of 72 percent if the entire basin were clearcut. Since the largest streamflows on the western slopes of the Cascades are not typically associated with spring snowmelt:, we would not expect those events which exhibit the largest increases in streamflow due to clearcutting to be present in the POT series. However, these results do have the potential implications for interior (i.e. Columbia basin) tributaries where spring snowmelt produces many flood peaks.

7.2 Effect of Alternative Harvest Strategies

Although removal of all overstory vegetation is predicted to lead to large increases in peak streamflows, these results are not directly applicable to the more modest harvest strategies that are of practical interest. Therefore, we evaluated the effects of alternative harvest strategies that are within the range of the historical basinwide harvest fractions. Each alternative strategy assumes clearcutting of 10 percent of the total watershed area (i.e. 157.7 km^2 out of 1577 km^2) in three elevation bands: (1) below 300 meters; (2) between 300 and 900 meters; and (3) above 900 meters. In each case, the DHSVM pixel (100 m by 100 m) represents the minimum scale at which cuts are made, i.e. each pixel is assumed to be either all old growth or entirely clearcut. The clearcut pixels are arranged to minimize visual impact on the landscape following the recommendations of Fridley et al. (1991), which are based on examination of computer rendered landscapes of potential clearcut strategies. They suggest that clearcuts be arranged to follow the natural contours of the land so that they mimic natural disturbances such as stream channels and landslides to the extent possible. To mimic these patterns, we developed a simple computer program which forces clearcut areas to: (1) remain inside the specified elevation bands, (2) follow regions of decreasing upgradient accumulation, (3) begin only in regions in which the accumulation value is less than a given threshold (i.e. focus clearcutting along the minor tributaries while avoiding larger ones), and (4) cut all pixels within a given distance from the central path of ascent while tapering the beginning and end of each clearcut (i.e. follow stream channels upgradient). The forest harvest patterns generated by this algorithm for the three elevation bands are shown in Figure 7.5 along with the DEM of the watershed for reference to the elevation boundaries. Each of the

three harvest alternatives was simulated over the period January 1, 1948 through December 31, 1955 and the predicted streamflows were compared to those predicted for the entire old growth case.

Results for the eight annual flood peaks assuming all harvest in the transient snow zone (300 - 900 m) are shown in Figure '7.6. The results of the analysis indicate that the eight predicted annual peak hydrographs for all three harvest strategies would be almost indistinguishable from those resulting from the old growth case. The relatively large increases predicted for the 100 percent harvest case are greatly reduced. Smaller differences were also seen for the entire continuous streamflow record including spring melt events, as compared to the complete overstory removal case.

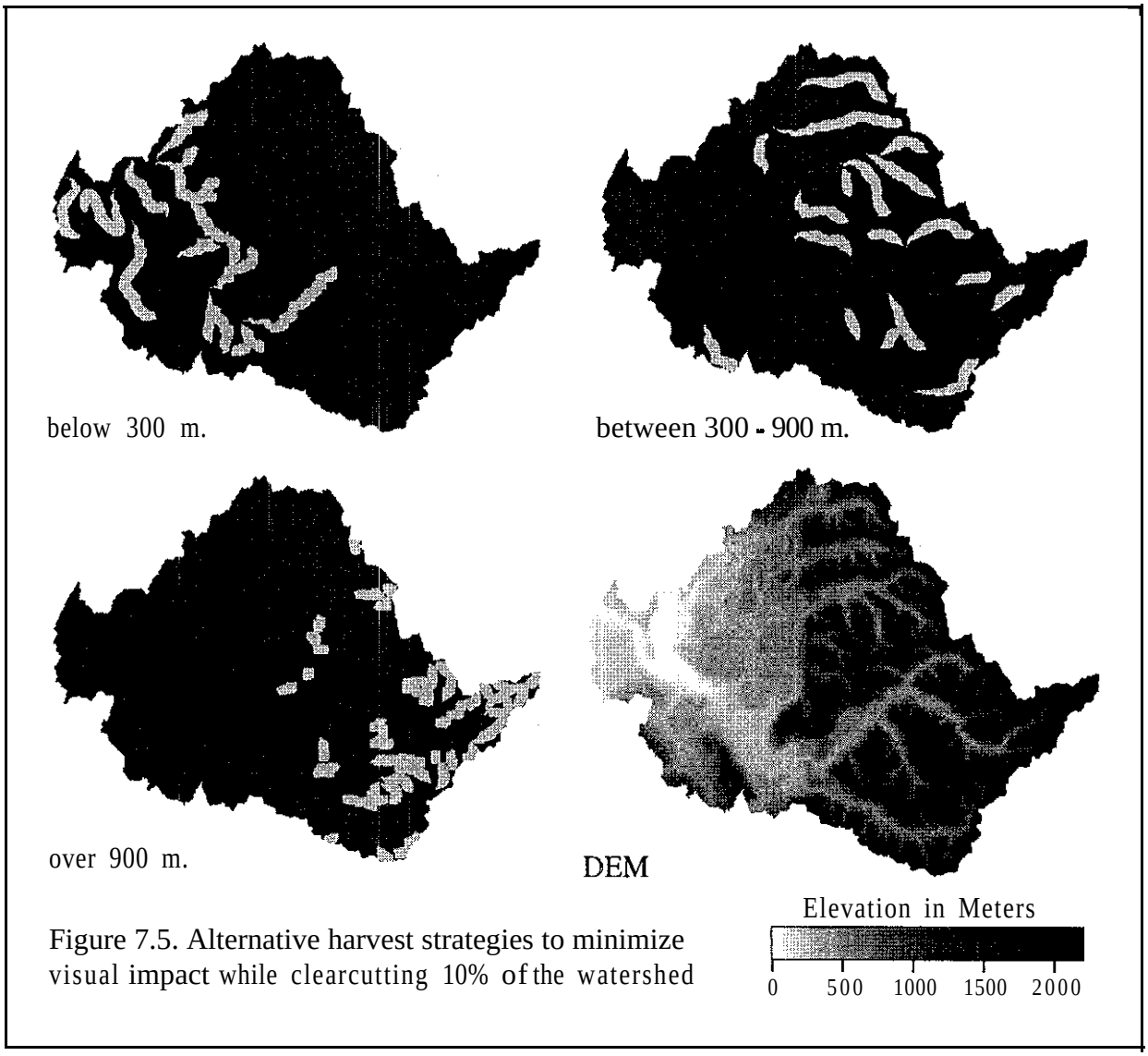

Figure 7.5. Alternative harvest strategies to minimize visual impact while clearcutting 10% of the watershed

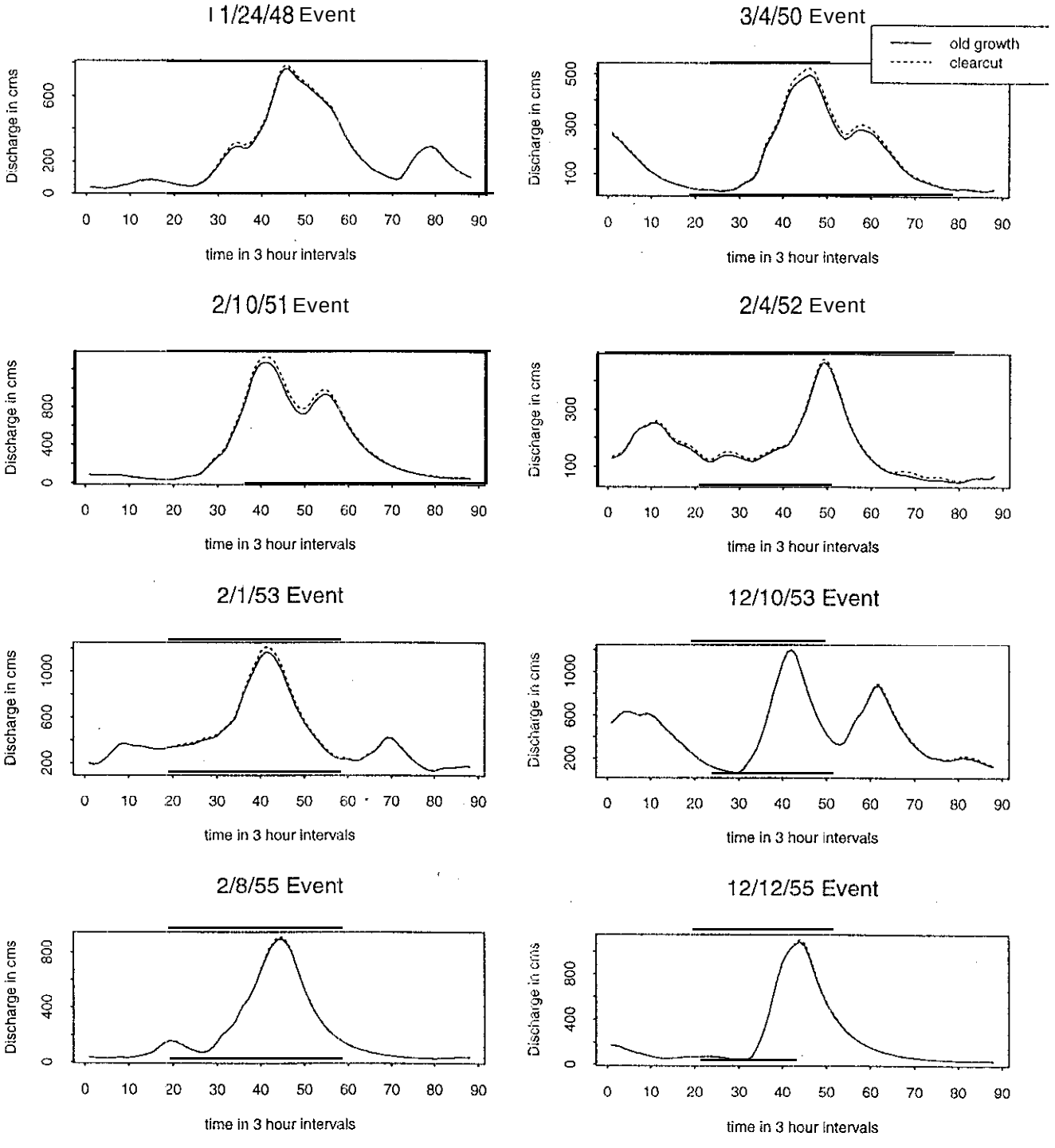

Figure 7.6. Annual peak streamflows simulated with 10% of basin cut between 300 and 900 meters and all old growth Douglas Fir.

Figure 7.7 presents the difference series for each harvest strategy when compared to streamflows obtained with all old growth. With 10 percent of the basin harvested below 300 meters, the maximum increase (40 cms) and percent increase (50 percent) occur during the same event which is not in the peaks over threshold series. The maximum percent increase in the peaks over threshold series is 10 percent while the average increase of the peaks over threshold values is only 2 percent.

With 10 percent of the basin harvested between 300 and 900 meters, the maximum observed increase (60 cms) occurs during an annual peak event and translates into an approximately 5 percent increase. The largest percent increase of approximately 45 percent occurs during an early spring snowmelt event which is not in the peaks over threshold series. The average increase in the peaks over threshold series is 2 percent. Similarly small increases are seen for the 10 percent harvest above 900 meters case.

The lack of increase in streamflow that result when realistic percentages of the watershed are cut support the conclusion first suggested in Chapter 6 that the observed trend in the residual series of the retrospective analysis is not solely caused by ROS mechanisms. In order to account for the observed trend with the ROS mechanism alone would require removal of mature forest from most of the watershed. Observed increases in the POT series are more likely to be related to other mechanisms not explicitly modeled by DHSVM, such as the effects of forest roads; although additional research will be required to test this hypothesis. However, the result that spring snowmelt events are most affected by forest harvesting does suggest that analyses, similar to those presented here, may yield useful insights into possible changes in the behavior of east-slope Cascade streams, for which most events in the peaks over threshold series occur during the spring snowmelt period.

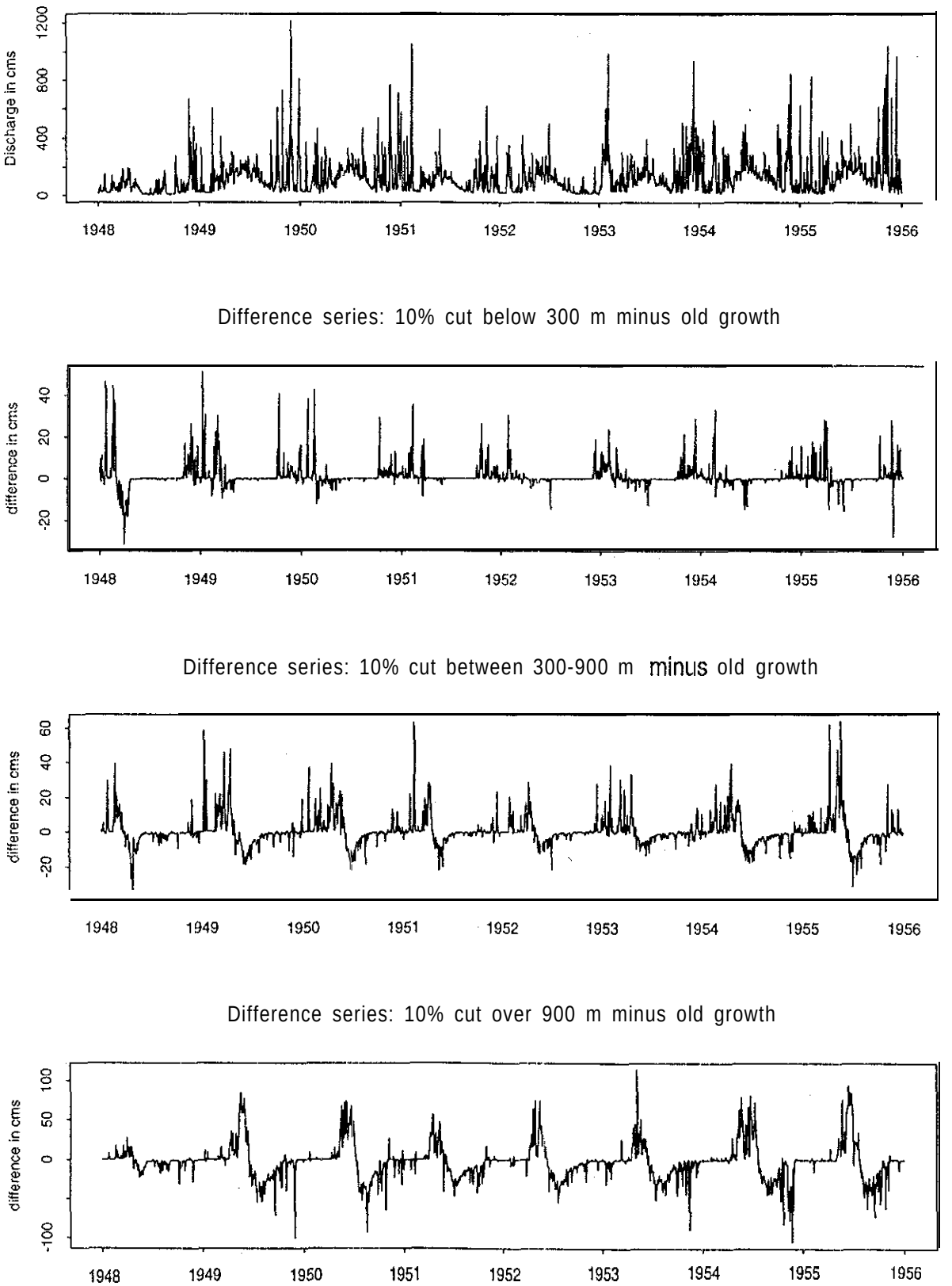

Figure 7.7. Predicted continuous streamflow from 1948 through 1955 with all old growth Douglas Fir as compared to streamflow with 10% of the basin cut (1) below 300 meters, (2) between 300 and 900 meters, and (3) above 900 meters.

Chapter 8. Conclusions

The central hypothesis of this work is that forest harvesting can result in increased flood peaks, particularly those resulting from rain-on-snow events. These changes are thought to result from differences in the accumulation and ablation of snow in the forest canopy, and changes in the accumulation and melt of snow on the forest floor, in mature as contrasted with young forest. To evaluate this hypothesis, the Distributed Hydrology-Soils-Vegetation Model (DHSVM) was used to predict explicitly the effects of soils, vegetation, terrain, and snow physics on runoff production. Several modifications to DHSVM were made for the purposes of evaluating the effects of forest harvesting on flooding, including: a) incorporation of a module to estimate the topographic effects on precipitation, b) modification of the original single-layer snow model to incorporate a thin surface layer, and c) inclusion of a channel routing scheme.

Initial testing of the modified DHSVM was performed using the period March 1, 1983 through November 30, 1986 using daily time steps. Particular attention was given to the flood of November 1986, which was the third largest flood of record at the USGS Carnation gage. This period also included large ROS floods in January 1984 and February 1986, as well as a spring snowmelt event: during June 1985. A range of initial conditions and event timing provided a robust testing series for DHSVM. The flood of November 1990 was used to verify DHSVM. Following calibration, primarily of the lateral hydraulic conductivity, along with specification of more realistic leaf area index values, good model performance was achieved for the calibration and verification periods.

A 46 year simulation (19481993) of the Snoqualmie River at Carnation was performed using DHSVM with fixed vegetation at 1989 conditions and the residuals (difference between simulated and observed peak flows) were analyzed for trends. Insofar as the residual series is adjusted for climatic variability (which should be reflected in both the model predictions and observations), any trends should be the result of land use changes - either due to forest harvesting, forest road development, urbanization or some combination of these.

Based on the residuals analysis, the major conclusions of the study are:

1) No significant trend has (occurred in the largest flood events, as evidenced by the absence of trend in the residuals for the annual flood peaks and larger events in the peaks-over-threshold series (> 650 cms).

2) There has been a significant increase in smaller events (< 650 cms) of the peaks-over-threshold series. For the reasons indicated above, this trend can be attributed to changes in land use.

3) Comparisons of DHSVM simulations for portions of the 46 year retrospective analysis with 1989 land use (minimum average overstory age), and the land use that existed at the time of selected floods, shows that the arnount of forest harvesting that has actually occurred in the Snoqualmie River basin is not enough to explain the observed trend in peak streamflows. Since DHSVM specifically incorporates the effects of harvest on ROS mechanisms, we conclude that these mechanisms, at least as represented by DHSVM, are not solely responsible for the observed increase in peaks streamflows. A sensitivity analysis of the same selected floods which prescribed vegetation removal for 10 percent of the entire basin likewise resulted in changes in peak flows smaller than those observed.

4) The largest changes in peak streamflows were found to occur for spring peak flows, most of which are significantly smaller than bankfull capacity. This result many have: important implication for changes in flood peaks that may have resulted form forest harvesting in some eastside catchments, where spring snowmelt peaks dominate the flood series.

5) The fact that observed changes in smaller floods in the peaks-over-threshold series are much larger than those predicted, given the magnitude of historical land use changes, suggests that some mechanism other than changes in ROS runoff is the cause. One possible explanation is the development of the forest road network accompanying logging activities. Runoff from forest roads is not accounted for in the current version of DHSVM. Extension of the residuals analysis using a version of DHSVM that includes road runoff and subsurface flow interception should help resolve the relative contributions of ROS and forest road mechanisms on increases in peak streamflows.

References:

Anderson, E. A., Development and testing of snowpack energy balance equations, ***Water Resources Research,*** 4(1), 19-37, 1968

Arola, A., Effects of subgrid scale spatial variability on mesoscale snow modeling, MS. thesis, Department of Civil Engineering, University of Washington, Seattle, 1993.

Berg, N., R. Osterhuber, J. Bergman, Rain-induced outflow form deep snowpacks in the central Sierra Nevada, California, ***Hydrological Sciences Journal,*** 36(6), pp. 61 l-629, 1991.

Berris, S. N., Comparative snow accumulation and melt during rainfall in forest and clearcut plots in western Oregon, M.S. thesis, Oregon State Univ., 1984

Berris, S. N., and R. D. Harr, Comparative snow accumulation and melt during rainfall in forested and clear-cut plots in the western Cascades of Oregon, ***Water Resources Research,*** 23(1), 135-142, 1987.

Brown, H. E., The status of pilot watershed studies in Arizona, American Society of Civil Engineers National Meeting in water resources engineering, Feb., 1969.

Bunnel, F. L., R. S. McNay, C. C. Shank, ***Trees and snow: the deposition of snow on the ground- a review and quantitative synthesis,*** Research Branch, Ministries of Environment and Forests, IWIFR-17, Victoria, B.C., Canada, 1985

Calder, ***I.*** R., ***Evaporation in the Uplands,*** John Wiley and Sons, Chichester, 14X pp., 1990

Coffin, B. A., and R. D. Harr, Effects of forest cover on volume of water delivery to soil during rain-on-snow. Final report for Project SH-1 (Rain-on-snow study) submitted to Sediment, Hydrology and Mass Wasting Steering Committee, July 30, 1992.

Connelly, B. A., T. W. Cundy, D. P. Lettenmaier, R. D. Harr, Implications of forest practices on downstream flooding: Phase I Interim Report, Washington Forest Protection Association, 1993.

Costa-Cabral, M. C., and S. J. Burges, Digital elevation model networks (DEMON): A model of flow over hillslopes for computation of contributing and dispersal areas, ***Water Resources Research,*** 30(6), 1681-1692, 1994.

Dubayah, R., J. Dozier, and F. W. Davis, Topographic distribution of clear-sky radiation over the Konza Prairie, Kansas, ***Water Resources Research,*** vol. 26, pp 679-690, 1990

Entekhabi, D., and P. S. Eagleson, ***Land surface hydrologyparumeterization for atmospheric general circulation models: Inclusion of subgrid scale spatial variability and screening with a simple climate model,*** Rep. 325, Ralph M. Parsons Lab., 195 pp., Mass. Inst. of Technology, Cambridge, 1989

Franklin, J. F. and R. H. Waring, Distinctive features of the northwest coniferous forest: development, structure and function, in Forests: Fresh Perspectives from Ecosystem Analysis, pp 59.86, 1980

Forest Ecosystem management Assessment Team (FEMAT), *Forest Ecosystem Management: An Ecological, Economic, and* Social *Assessment, Report of the Forest Ecosystem Management Assessment Team,* U.S. Govemrnent Printing Office 1993-793-071, Washington, DC, 1993

Frew, J. E., Tha image processing workbench, Ph.D. thesis, 382 pp., Department of Geography, University of California, Santa Barbara, 1990

Fritschen, L. J., L. Cox, and R. Kinerson, A 28 meter Douglas Fir in a weighing lysimeter, *Forest Science*, vol 19. pp 256-261, 1973

Gholz, H. L., Environmental limits on aboveground net primary production, leaf area, and biomass in vegetation zones of the Pacific Northwest, *Ecology,* vol 63, pp. 469-481, 1982

Gholz, H. L., Limits on aboveground net primary production, Leaf Area and Biomass in vegetational zones of the Pacific: Northwest, Oregon State University, Ph.D. dissertation, 61 pp., 1979

Gholz, H. L., F. K. Fitz, R. H. Waring, Leaf area differences associated with old growth forest communities in the western Oregon cascades, *Canadian Journal of Forestry Research,* (6), pp. 49-57. 1976

Grier, C. C., and S. W. Running, Leaf Area of Mature Northwestern coniferous forests: Relation to site water balance, *Ecology, 58,* pp. 893-899, 1977

Han:, R. D., Effects of clear-cut logging on rain-on-snow runoff in western Oregon: A new look at old studies, *Water Resources Research,* 22(7), *1095-I* 100, 1986.

Hoover, M. D., Vegetation management for water yield, Symposium on water balance in North America, pp. 191-195, Proceedings Series 7, American Water Research Association, Urbana, Illinois, 1967.

Jones, J.A., and G.E. Grant, Peak flow responses to clear-cutting and roads in small and large basins, western Cascades, Oregon, *Water Resources Research,* 32(4), *959-974,* 1996.

Kattelmann, R., Water release from a forested snowpack during rainfall, Forest Hydrology and Range Management, IAHS Publication *No.* 187, *International Association of Hydrological Sciences,* Washington, D.C., pp. 265-272, 1987.

Kendall, M. and J. D. Gibbons, *Rank Correlation Methods,* Edward Arnold, London, 260 pp., 1990

Klein, S. A., Calculation of Monthly Average Insolation on Tilted Surfaces, *Solar Energy,* 19, 325. 1977

Kobayashi, D., Snow accumulation on a narrow board, *Cold Regions Science and Technology,* (13), pp 239-245, 1986

Longley, K., D. Jacobsen, and D. Marks, Supplement to the image processing workbench (IPW), report, Environmental Research Lab., U.S. Environmental Protection Agency, Corvallis, Oregon, 1992

Maidment, D. R., J. F. Olivera, A. Calver, A. Eatherall and W. Fraczeck, A unit hydrograph derived from a spatially distributed velocity field, *Hydrological Processes,* 10(6), 1996.

Marshall, J. D., and R. H. Waring, Comparison of methods of estimating leaf area index in old growth Douglas Fir, Ecology 67(4), pp. 975-979, 1986

Monteith, J. L., *Vegetation and the atmosphere Vol 2,* Academic Press, San Francisco, 439 pp. 1976

Montgomery, D. R., G. E. Grant, and K. Sullivan, Watershed analysis as a framework for implementing ecosystem management, *Water Resources Bulletin, 3* l(3), 369-386, 1995

O'Callaghan, J. F. and D. M. Mark, The extraction of drainage networks from digital elevation data, *Computer Vision Graphics Image Process., 28,* pp. 323-334, 1984

Peck, E. L., and J. C. Schaake, Network design for water supply forecasting in the west, *Water Resources Bulletin,* American Water Resources Association, February, 1990

Peterson, D. L., M. A. Spanner, S. W. Running, and K. B. Teuber, Relationship of thematic mapper simulator data to leaf area index of temperate coniferous forests, *Remote Sensing of the Environment,* (22), 1987

Rhea, J. O., Orographic precipitation model for hydrometeorolgical use, Atmospheric Science Paper No. 287, Colorado State Univ., 1978

Schmidt, R. A., and C. A. Troendle, Sublimation of intercepted snow as a global source of water vapor, Proceedings, 60th Western Snow Conference, 1992

Staubitz, W. W., National water,-quality assessment program- Puget Sound Basin, Washington, USGS open file: report 94- 108, 1994

U.S.. Army Corps of Engineers, *Snow Hydrology,* North Pacific Division, Portland, Oregon, 1956

Waring, R. H., W. H. Emmington, H. L. Gholz, and C. C. Grier, Variations in maximum leaf area of coniferous forests in Oregon and its ecological significance, *Forest Science,* 24(1), pp. 131-140. 1978

Waring, R. H., K. Newman, and J. Bell, Efficiency of tree crowns and stemwood production at different canopy leaf densities, *Forestry*, vol. 54, pp. 129-137, 1981

Waring, R. H., 'W. G. Thies, and D. Muscato, Stem growth per unit of leaf area: a measure of tree vigor, *Forest Science, vol.* 26, pp. 112-l 17, 1980

Wetherbee, P. M.S. thesis, Department of Forest Resources, University of Washington, Seattle, 1995

Washington Forest Practice Board (WFPB), Standard Methodology for Conducting Watershed Analysis, Washington Forest Practice Act Board Manual, Version 2.0, 85 pp.

Wigmosta, M. S., D. P. Lettenmaier, and L. W. Vail, A distributed hydrology-vegetation model for complex terrain, *Water Resources Research,* 30(6), 1994